TR-131
1984

Texas Water Resources Institute
make every drop count

Relationship Between Soil Moisture Storage and Deep Percolation and Subsurface Return Flow

J.L. Nieber

Texas Water Resources Institute

Texas A&M University

RESEARCH PROJECT COMPLETION REPORT

Project Number B-248-TEX

October 1, 1980 - December 31, 1983

Agreement Number

14-34-0001-1269

RELATIONSHIP BETWEEN SOIL MOISTURE STORAGE AND DEEP PERCOLATION AND SUBSURFACE RETURN FLOW

By

John L. Nieber

Submitted to

Bureau of Reclamation
U.S. Department of the Interior
Washington, DC 20242

The work on which this publication is based was supported in part by funds provided by the U.S. Department of the Interior, Washington, DC, as authorized by the Water Research and Development Act of 1978 and The Texas Agricultural Experiment Station.

TR-131
Texas Water Resources Institute
Texas A&M University

February 1984

DISCLAIMER

Contents of this publication do not necessarily reflect the views and policies of the Office of Water Research and Technology, of the Bureau of Reclamation, U.S. Department of the Interior, nor does mention of trade names or commercial products constitute their endorsement or recommendation for use by the Texas Agricultural Experiment Station or the U.S. Government.

All programs and information of the Texas Water Resource Institute are available to everyone without regard to race, ethnic origin, religion, sex or age.

ABSTRACT

A simulation study was performed to analyze the relationship between the volume of moisture stored in a soil profile and the rate of percolation and subsurface return flow. The simulation study was derived on the basis of the Richards equation. The one-dimensional form of the Richards equation was used for the percolation process and the two-dimensional form of the Richards equation was used for the subsurface return flow process. In each case the Richards equation was transformed to a set of nonlinear algebraic equations using the finite element method to transform the space derivatives and the finite difference method to transform the time derivatives. The system of nonlinear algebraic equations were solved using the Gaussian elimination procedure and an under-relaxation procedure.

To characterize the percolation and subsurface return flow processes a sensitivity analysis was performed by varying parameters of the soil systems. It was found that the relationships between stored soil moisture and deep percolation and between stored soil moisture and subsurface return flow each form hysteresis loops. The percolation loops were most sensitive to soil texture class, and water application rate. Soil layering, soil evaporation, water table depth, and evapotranspiration did not greatly influence the percolation loop. The subsurface return flow loops were sensitive to soil texture, soil slope angle, length of the soil slope relative to soil depth, and water application rate. The subsurface return flow loops were not greatly influenced by soil layering.

The resulting percolation and subsurface return flow characteristics suggest the possibility of utilizing the derived characteristics in the physical representation of these processes in comprehensive hydrologic models.

TABLE OF CONTENTS

LIST OF TABLES

LIST OF FIGURES

Chapter 1

INTRODUCTION

There is significant value in the endeavor to improve the capability to predict or forecast phenomena of the hydrologic cycle. This value is quantifiable in terms of improved designs of water control and water supply systems, improved flood warning capability, improved water management in the agricultural, range and forestry sector, improved land management capability and enhanced capabilities to analyze and understand ecosystems. Much of the past improvement in hydrologic modeling capabilities lies in the fact that statistical models of hydrologic variables are continually evolving and with time the data base for statistical analysis continues to broaden. Other improvements in modeling lie in the development of models that simulate components of the hydrologic cycle. Improvements in this capability are very important because it is this category of hydrologic model that is useful in the assessment of the hydrologic input of land use changes, in the analysis of forecasting of floods (or droughts), and in the analysis of ecosystems.

A multitude of detailed studies have been performed and are currently being performed to increase the knowledge regarding the land phase components of the hydrologic cycle. Example studies include those reported by Woolhiser and Liggett(1967) on overland flow, Philip(1969) on infiltration, Freeze (1972a,b) on subsurface flow and baseflow,

Liggett and Cunge (1975) on flood routing, Freeze (1969) on groundwater recharge, Colbeck (1978) on snowmelt, Gupta(1973) on precipitation, and Brutsaert (1982) on evapotranspiration. Each of these studies utilized to some degree high level mathematical methods to represent each process.

Comprehensive models for simulating hydrologic phenomena on catchments generally use empirical relationships to represent each component of the hydrologic cycle included in the model (Soorooshian, 1983). It would be ideal if thorough mathematical descriptions, like those used in many single component hydrologic studies, could be employed in the comprehensive hydrologic models. The problem though is that the information to determine the parameters of the detailed mathematical models is not available on a routine basis and one generally must work with rainfall and watershed discharge to calibrate the model. Thus there appears to be an advantage to using simplified models of the hydrologic components since then the unknown hydrologic information can be "lumped" into a few empirical parameters.

The fact that information is not generally available to determine parameters for mechanistic hydrologic modeling does not preclude the value of hydrologic studies that are mechanistic in nature. Rather, it should be possible to derive from these mechanistic studies the information that could improve the physical representativeness of the empirical relationships currently employed in comprehensive hydrologic models.

The objective of the present study is to develop relationships between the moisture stored in a soil profile and the fluxes of deep percolation and interflow. These relationships will be developed based on a sensitivity analysis using mathematical models of one-dimensional and two-dimensional flow in porous media. Since comprehensive hydrologic models generally use stored soil moisture as a state variable the information derived from this study should be useful in calibrating the deep percolation and interflow parameters in comprehensive hydrologic models.

Chapter 2

MATHEMATICAL FORMULATION

The description of the flow of moisture in a rigid porous media as a mathematical boundary value problem can be expressed in general by the Richards equation,

$$C\ \partial\phi/\partial t = \nabla(K\nabla\phi) \qquad (1)$$

where; $\phi = \phi(x,y,z,t) = h+e$ = hydraulic head [L],

h = pressure head [L],

e = elevation head [L],

$K = K(\theta)$ = hydraulic conductivity [L/T],

$C = C(h) = d\theta/dh$ = specific moisture capacity [1/L],

t = time [T],

x,y,z = Cartesian coordinates [L], and

∇ = "del" operator [1/L].

The Richards equation is an expression for the law of conservation of mass (moisture) with Darcy's law (generalized for unsaturated flow conditions) substituted for the flux components in the conservation equation. Equation (1) applies only to incompressible fluid and incompressible porous media conditions, but it does allow for anisotropic as well as nonhomogeneous conditions.

Expressions for the coefficients C(h) and K(θ) adopted from Verma and Brutsaert (1971) are given by

$$C(h) = m\ \beta\ h^{(\beta-1)}\ A/(A+h^{\beta})^2 \qquad (2a)$$

$$K(\theta) = K_s\ ((\theta-\theta_r)/(\theta_s-\theta_r))^N \qquad (2b)$$

where; $m = \theta_s-\theta_r$ = drainable porosity,

θ_s = saturated moisture content,

θ_r = residual moisture content, and

A,β,N = soil related constants.

The solution of equation (1) for a specific problem depends upon the particular boundary conditions and initial conditions specified for the problem. For example, the character of the boundary conditions and the initial conditions will depend upon whether the problem being solved is one-dimensional, two-dimensional, three-dimensional, steady-state, or transient-state. Since the conditions considered in this study are for one-dimensional and two-dimensional transient flow the boundary conditions and initial for each case will be presented separately. The actual solution procedure for both cases will be presented in the next section.

2.1 ONE-DIMENSIONAL CASE

The one-dimensional case concerns the vertical flow of soil moisture in an essentially horizontal soil profile as illustrated in Figure 1. The soil profile is generally composed of layers of different texture. The upper boundary of the region is the soil surface and the bottom boundary is the water table at a depth D.

The equation governing the moisture flow in the soil mass above the water table boundary is derived by simplication of equation (1) to the one-dimensional case to yield,

$$C\ \partial\phi/\partial t = \partial/\partial z\ (K\ \partial\phi/\partial z) \qquad (3)$$

with the boundary conditions

1) $K(\theta)\ \partial\phi/\partial z = -q\ ,\ h \leq 0$ $\qquad z=D$

2) $\phi = D+d,\ h = d$ $\qquad z=D$

3) $\phi = 0,\ h = 0$ $\qquad z=0$

where q is the specified flux rate at the soil surface and d is the depth of ponding. The specified flux rate can be either rainfall intensity or evaporation. The boundary condition at the surface is one of specified flux unless the surface becomes ponded by a flux application rate in excess of the infiltration rate in which case the surface becomes ponded to a depth of d. At the bottom boundary the water table is maintained at a constant level by assuming that flow in the groundwater body is sufficiently high to remove all moisture percolating to the water table.

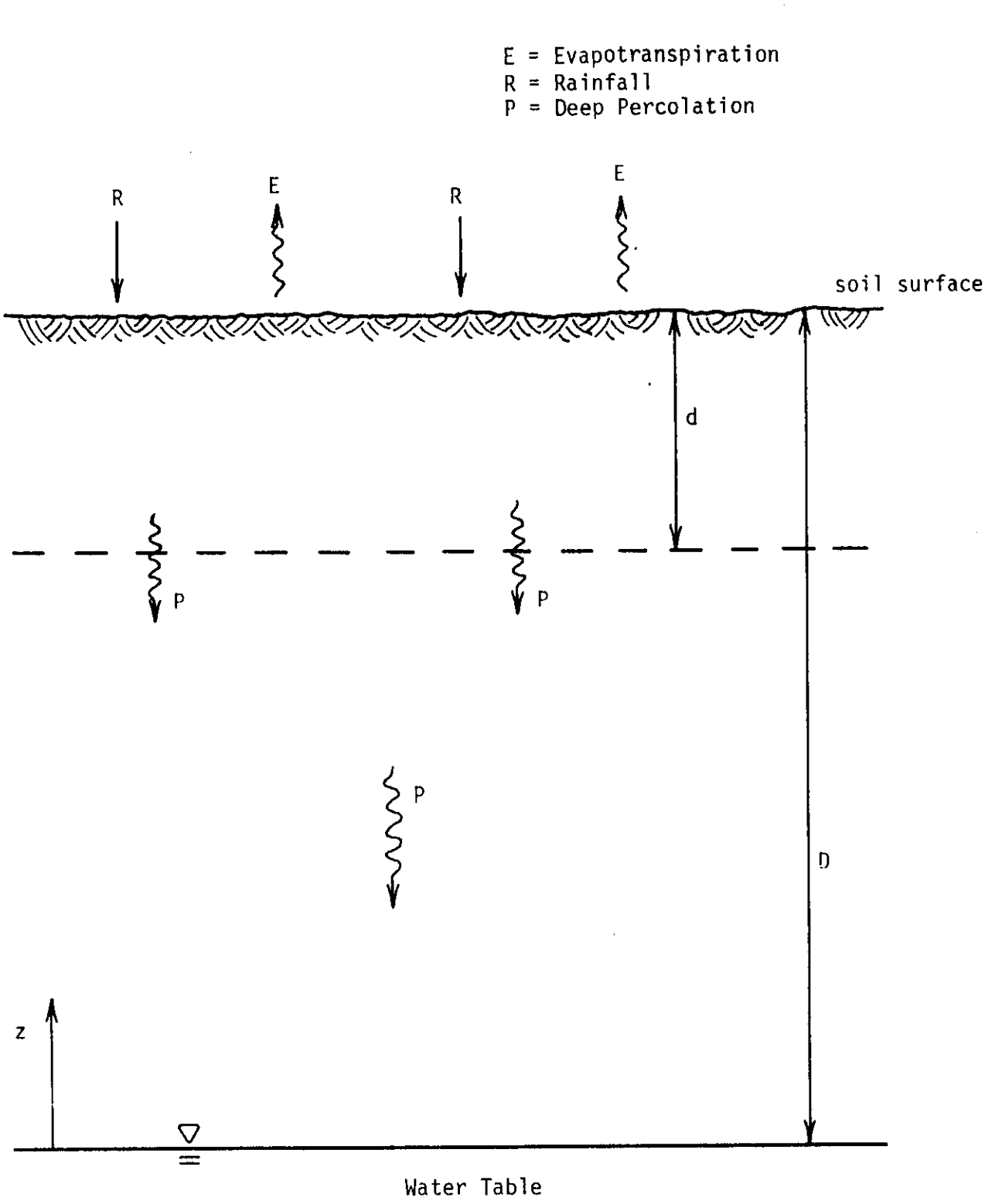

Figure 1. Illustration of the moisture flow domain for the one-dimensional analysis of deep percolation.

2.2 TWO-DIMENSIONAL CASE

To derive the flow region of interest for the two-dimensional case consider the watershed catchment area illustrated in Figure 2. Taking a vertical cross-section of the soil mass along a "flow-line" of the topographic surface produces the two-dimensional region to be examined in this study. The soil profile is assumed to be underlain by an impervious horizon such as a fragipan, hardpan, or bedrock. A further simplication for this study is to make the slope profile and soil depth uniform for the entire length of the slope. The resulting region of flow is illustrated in Figure 3.

The governing equation for this case is derived by simplication of equation (1) to the two-dimensional case to yield,

$$C\ \partial\phi/\partial t = \partial/\partial x\ (K\ \partial\phi/\partial x) + \partial/\partial y\ (K\ \partial\phi/\partial y) \qquad (4)$$

The boundary conditions for equation (4) for the conditions illustrated in Figure 3 are:

1.Boundary AB.

$-K\partial\phi/\partial n=q_n \qquad 0\leq x\leq x_1; x_2\leq x\leq L\cos\gamma$

$z=x\tan\gamma + d/\cos\gamma$

$h=0,\ \phi=e \qquad x_1\leq x\leq x_2$

$z=x\tan\gamma + d/\cos\gamma$

2. Boundary BC.

$-K\ \partial\phi/\partial n=0 \qquad x=0$

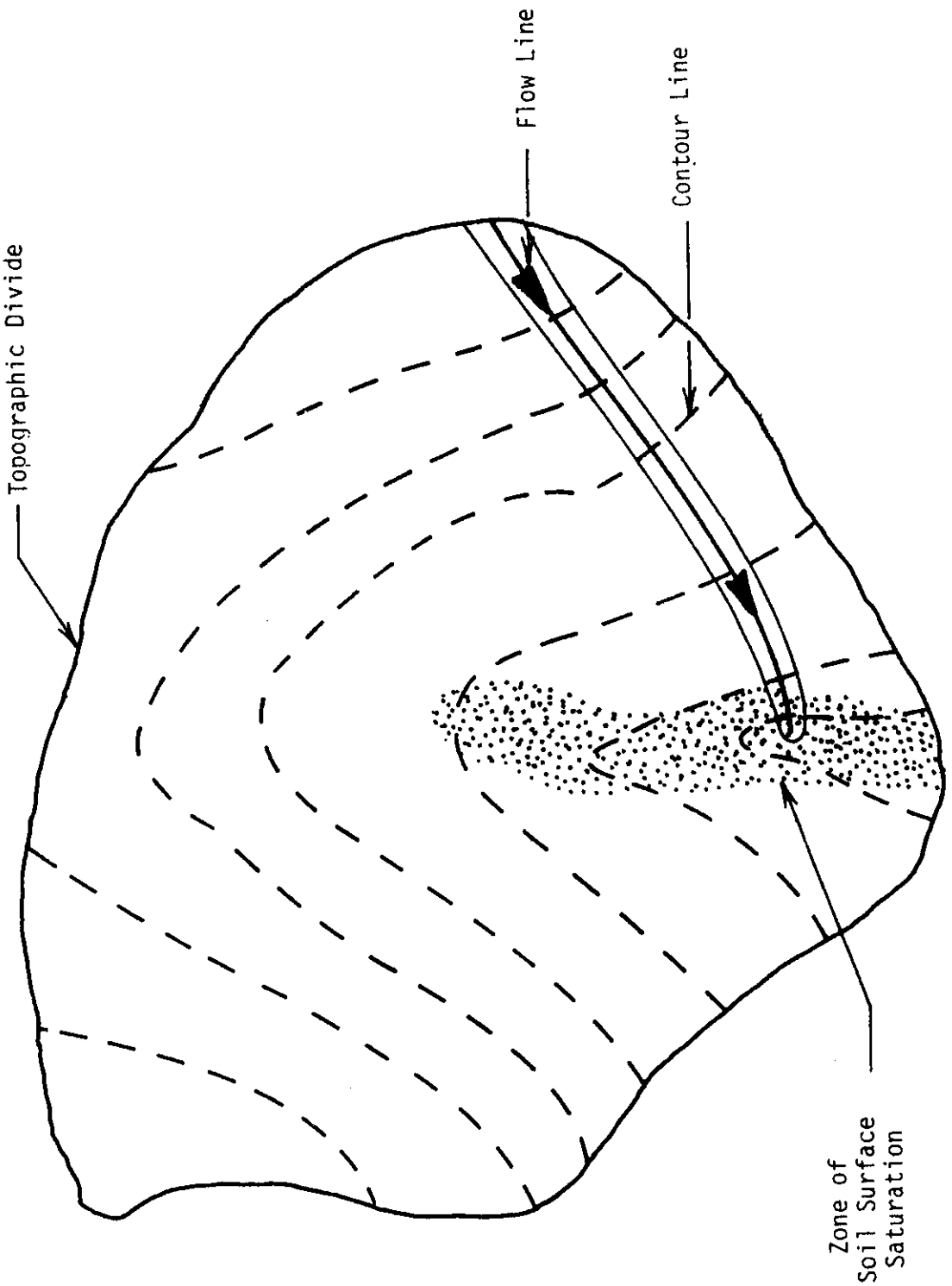

Figure 2. Plan view illustration of the flow conditions in a first-order valley basin.

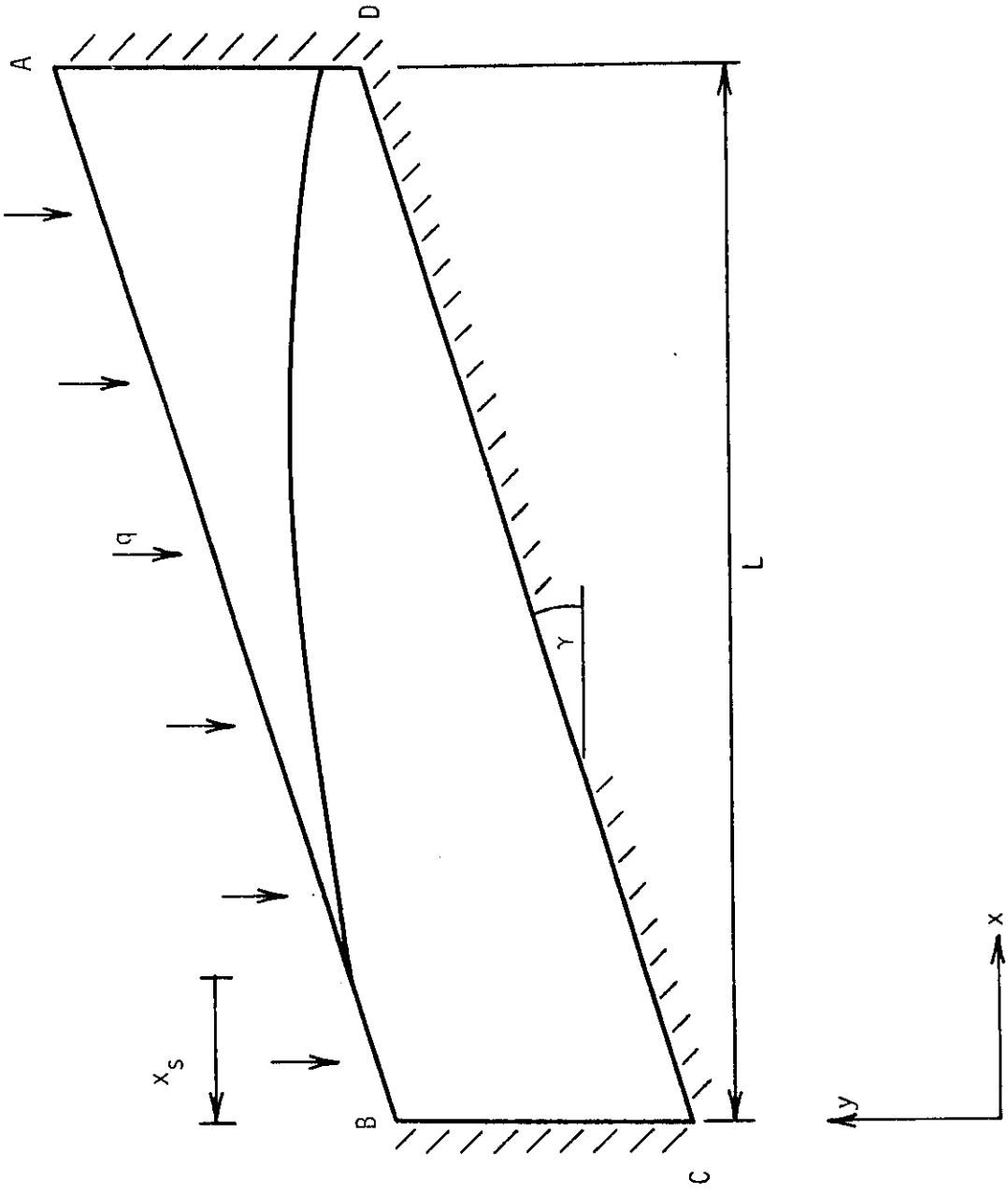

Figure 3. Illustration of the moisture flow region for the two-dimensional analysis of subsurface return flow.

3. Boundary CD.

$-K\ \partial\phi/\partial n=0 \qquad 0 \leq x \leq L\ \cos\gamma$

$z=x\ \tan\gamma$

4. Boundary DA.

$-K\ \partial\phi/\partial n=0 \qquad x=L\ \cos\gamma$

$L\ \sin\gamma \leq z \leq \sin\gamma + d/\cos\gamma$

where q_n is the flux normal to the boundary, d is the soil depth, and n is the unit normal vector.

The initial condition can be one of static equilibrium, steady-state flow,or transient flow. This condition is expressed in general terms by

$$\phi(x,z,t=0)=\phi_0(x,z)$$

Boundary AB is the boundary of potential seepage, it is the rainfall infiltration boundary, and it is also the boundary across which the evapotranspiration flux occurs. Boundary BC at the base of the slope is an impermeable boundary because the hillslope considered in this study belongs to the first-order valley basin class (Huggett, 1975) and for this hillslope type there is no incised stream channel at the base of the slope. It is assumed that the hillslope opposing the hillslope considered is identical in character so that boundary BC becomes a line of symmetry and therefore an impermeable boundary.

Boundary CD is an impermeable boundary because of the impermeable soil condition at the base of the soil profile and boundary DA is an impermeable boundary since it corresponds to the topographic divide of the catchment.

Chapter 3

NUMERICAL SOLUTION

The solution of equations (3) and (4) with the corresponding boundary conditions and initial conditions cannot be achieved by analytical means except for a narrow range of idealized problems. For the problems considered in this research it is not possible to derive analytical solutions and so numerical solutions are resorted to. The particular numerical method chosen to derive the numerical solutions is the finite element method in combination with the finite difference method. The derivations of the finite element equations for the one-dimensional and the two-dimensional cases are presented in detail in the Appendix.

The finite element equations for both the one-dimensional flow case and the two-dimensional flow case are represented by the matrix equations

$$\Sigma_j D_{ij}\, \Phi_j^k = \Sigma_j E_{ij}\, \Phi_j^{k-1} + Q_i \Delta t \quad \text{for} \quad i=1,2,\ldots,M \qquad (5)$$

where; Φ_j^k, Φ_j^{k-1} = hydraulic head at node j at time levels k and k-1, respectively,

Q_i = net flux rate at node i during time interval Δt,

Δt = time step,

D_{ij}, E_{ij} = coefficient matrices evaluated at time level k+1/2, and

M = the number of node points.

Particular attention should be paid to the detailed mathematical definitions of D_{ij}, E_{ij}, and Q_i given in the Appendix. The definitions will be different for the one-dimensional case and the two-dimensional case.

The system of equations represented by equations (5) is nonlinear because the coefficients appearing in the coefficient matrices are known at the beginning of a given time step but are not known for the end of the time step until the correct solution is known. To solve the system of equations for the vector of values Φ_j^k the Gaussian elimination procedure is employed. To do this though, it is necessary to have values for the coefficient matrices which are not available since the coefficients are unknown a priori. The under-relaxation iterative procedure described below is used to resolve this problem.

For any given time step the hydraulic heads Φ^{k-1}_j and the corresponding coefficients C and K are known for the beginning of the time step, but the hydraulic heads Φ_j^k and the corresponding coefficients C and K for the end of the time step are not known. So for the first iteration an estimate is made for the values of Φ_j^k (call it $\Phi_j^k(0)$) and the coefficient matrices are evaluated based on the hydraulic head values

$$(\Phi_j^k(0) + \Phi^{k-1}_j)/2$$

With the coefficient matrices evaluated the equations (5) are solved by Gaussian elimination to yield an improved estimate for Φ_j^k, that is $\Phi_j^k(1)$. This new estimate is then averaged with Φ^{k-1}_j in the same manner and an improved set of coefficient matrices derived. Equations (5) are again solved to yield an improved Φ_j^k, that is $\Phi_j^k(2)$. The process of iteration continues in this fashion until the following criterion is met,

$$\Phi_j^k(n) - \Phi_j^k(n-1) \leq \epsilon$$

where n is the iteration level,and ϵ is an arbitrarily small numerical constant.

The investigation of the control of soil moisture levels over deep percolation and subsurface return flow requires a sensitivity analysis of the numerical solution to the various parameters of the system. The characteristics of the sensitivity analyses for the one-dimensional and two-dimensional cases will be presented separately in the following subsections.

3.1 ONE-DIMENSIONAL CASE

The objective of investigating the one-dimensional case of soil moisture flow is to quantify the relationship between the percolation of soil moisture below a specific depth of the soil profile and the volume of moisture stored in the soil lying above that depth. In this study a one meter soil profile depth was chosen since the one meter depth is most representative of the depth used in comprehensive hydrologic models. A sensitivity analysis was performed to assess the

influence of soil properties, depth to the water table, rainfall intensity, evapotranspirative flux, and soil layering on this relationship. The soil properties considered are represented by sand, loam, and clay textures. The constants in equations (2) used to represent these soil textures are presented in Table 1. The characteristic parameters used to produce each simulation in the sensitivity analysis are presented in Table 2.

TABLE 1

Constants in equations (2a) and (2b) for sand, loam and clay textures

	Parameter					
Texture	θ_s	θ_r	K_s (m/min)	A	β	N
Sand	0.46	0.02	0.0018	1.43	1.32	4.89
Loam	0.50	0.05	0.0006	2.04	0.89	5.23
Clay	0.55	0.07	0.0003	3.40	0.63	5.47

To provide broadly applicable conclusions the results presented in the next chapter are presented in dimensionless form. The dimensionless variables are $Q_p^* = Q_p/K_s^e$ and $V^* = V/V_{sat}$, where Q_p is the percolation rate through the one meter depth, K_s^e is the equivalent saturated hydraulic conductivity, and V and V_{sat} are respectively the volume and saturated volume of moisture stored in the one meter profile. The dimensionless application rate parameter is $q^* = q/K_s^e$. For all simulations the depth to the water table was taken as 10 meters except for one simulation where the depth was taken as 1 meter.

TABLE 2

Parameter, values used in the sensitivity analysis of the percolation problem

Simulation Number	Parameter D(meters)	Parameter q^*	Parameter Soil Texture	Comments
1	10	1.0	loam	homogeneous
2	10	1.0	sand	homogeneous
3	10	1.0	clay	homogeneous
4	10	2.0	loam	homogeneous
5	10	0.5	loam	homogeneous
6	10	2.0	sand	homogeneous
7	10	2.0	clay	homogeneous
8	10	1.0	loam	soil evaporation at 12 mm/day
9	10	1.0	loam	evapotranspiration at 12 mm/day
10	1	1.0	loam	homogeneous
11	10	1.0	loam/clay	5 cm thick clay layer
12	10	1.0	loam/clay	10 cm thick clay layer
13	10	1.0	loam/clay	four 5 cm thick clay layers
14	10	1.0	loam/clay/sand	10 cm clay layer 25 cm sand layer
15	10	2.0	loam/clay/sand	10 cm clay layer 25 cm sand layer

3.2 TWO-DIMENSIONAL CASE

Of interest in the two-dimensional case is the subsurface return flow that occurs at the base of the slope. Conditions examined in the sensitivity analysis were soil characteristics, slope angle, soil depth, slope length, and rainfall intensity. The results from the calculations of subsurface return flow were analyzed on the basis of non-dimensional parameters. The set of parameters chosen for the analysis are presented below.

$$L^* = L/d,\ \gamma,\ \alpha = A^{\beta}/d,\ \beta,\ N,\ q^* = q/K_s,$$

$$Q^* = Q/Q_{max},\ \text{and}\ V^* = V/V_{max}$$

where; Q = the flux of subsurface return flow,

Q_{max} = the rate of subsurface return flow that exists when the entire slope is saturated,

V = the volume of moisture stored in the slope corresponding to the rate Q, and

V_{max} = the volume of moisture stored in the slope at complete saturation of the slope.

All other parameters have been defined previously. It is of interest to note briefly that the parameter $\alpha^{1/\beta}$ is a measure of the ratio between the magnitudes of the capillary fringe and the soil depth. This same parameter was used by Verma and Brutsaert (1971) in an analysis of the recession characteristics for shallow aquifers deeply incised by streams.

The parameter values used in the sensitivity analysis for the two-dimensional case are tabulated in Table 3. The simulations with layered soils were performed by allowing the soil parameter A to increase linearly into the soil profile while β and N remained constant. This increase in A essentially causes a decrease in soil hydraulic conductivity for increasingly deeper layers of the soil profile. Three of these layered simulations were run with the parameter A varying at a 10%, 20% and 40% rates.

TABLE 3

Parameter values used in the sensitivity analysis of the subsurface return flow problem

Simulation Number	Parameters						
	L^*	γ (degrees)	$\alpha^{1/\beta}$	β	N	q^*	Comments
1	20	15	0.233	3.0	3.0	0.10	homogeneous
2	20	15	0.233	5.0	3.0	0.10	homogeneous
3	20	15	0.233	3.0	3.0	0.50	homogeneous
4	20	15	0.233	3.0	3.0	1.00	homogeneous
5	10	15	0.233	3.0	3.0	0.10	homogeneous
6	30	15	0.233	3.0	3.0	0.10	homogeneous
7	50	15	0.233	3.0	3.0	0.10	homogeneous
8	20	15	0.464	3.0	3.0	0.10	homogeneous
9	20	15	1.00	3.0	3.0	0.10	homogeneous
10	20	15	1.71	3.0	3.0	0.10	homogeneous
11	20	5	0.233	3.0	3.0	0.10	homogeneous
12	20	20	0.233	3.0	3.0	0.10	homogeneous
13	20	30	0.233	3.0	3.0	0.10	homogeneous
14	20	20	1.71	3.0	3.0	0.10	homogeneous
15	20	30	1.71	3.0	3.0	0.10	homogeneous
16	30	20	1.71	3.0	3.0	0.10	homogeneous
17	50	20	1.71	3.0	3.0	0.10	homogeneous
18	30	30	1.71	3.0	3.0	0.10	homogeneous
19	50	30	1.71	3.0	3.0	0.10	homogeneous
20	20	15	--	3.0	3.0	0.10	layered - 10%
21	20	15	--	3.0	3.0	0.10	homogeneous - 10%
22	20	15	--	3.0	3.0	0.10	layered - 20%
23	20	15	--	3.0	3.0	0.10	homogeneous - 20%
24	20	15	--	3.0	3.0	0.10	layered - 40%
25	20	15	--	3.0	3.0	0.10	homogeneous - 40%

Simulations were run with homogeneous soils having a hydraulic conductivity equivalent to the apparent anisotropic hydraulic conductivity of the layered soil profiles. The equivalent hydraulic conductivity K_e was calculated by the formula,

$$K_e = (K_n \, K_p)^{1/2}$$

where; $K_n = 1/D \; \Sigma \; (K_i/L_i)$,

$K_p = 1/D \; \Sigma \; K_i \; L_i$,

K_i = hydraulic conductivity of soil layer i, and

L_i = thickness of soil layer i.

K_n is the equivalent hydraulic conductivity in the direction normal to the layers and K_p is the equivalent hydraulic conductivity in the direction parallel to the layers.

Chapter 4

RESULTS AND DISCUSSION

4.1 ONE-DIMENSIONAL CASE

The typical form of the relationship between Q_p^* and V^* for the one-dimensional case is illustrated in Figure 4. The relationship shown in Figure 4 was derived from simulation 1. It is observed that the Q_p^* vs. V^* relationship is not unique but is instead hysteretic. In all of the simulations performed in this analysis the wetting curve lies below the drying curve. The results produced for the different simulations differ because of the influence of the various parameter sets used in each simulation.

The influence of the soil type is illustrated by the results of simulations 1-3 (Figures 4-6). The soil types considered were sand, loam, and clay. These three types include the range of soil moisture characteristics expected. It is observed that the Q_p^* vs. V^* loop is broadest for the sand, narrowest for the clay, and intermediate in width for the loam. The Q_p^* vs. V^* loop is quite nonlinear for both the sand and the loam, but for the clay the relationship is quite close to being linear. There is also an apparent tendency for the percolation to continue at a lower level of saturation as the texture of the soil increases in coarseness (i.e., going from clay to sand). The results observed can be interpreted in terms of the pore size distribution of a

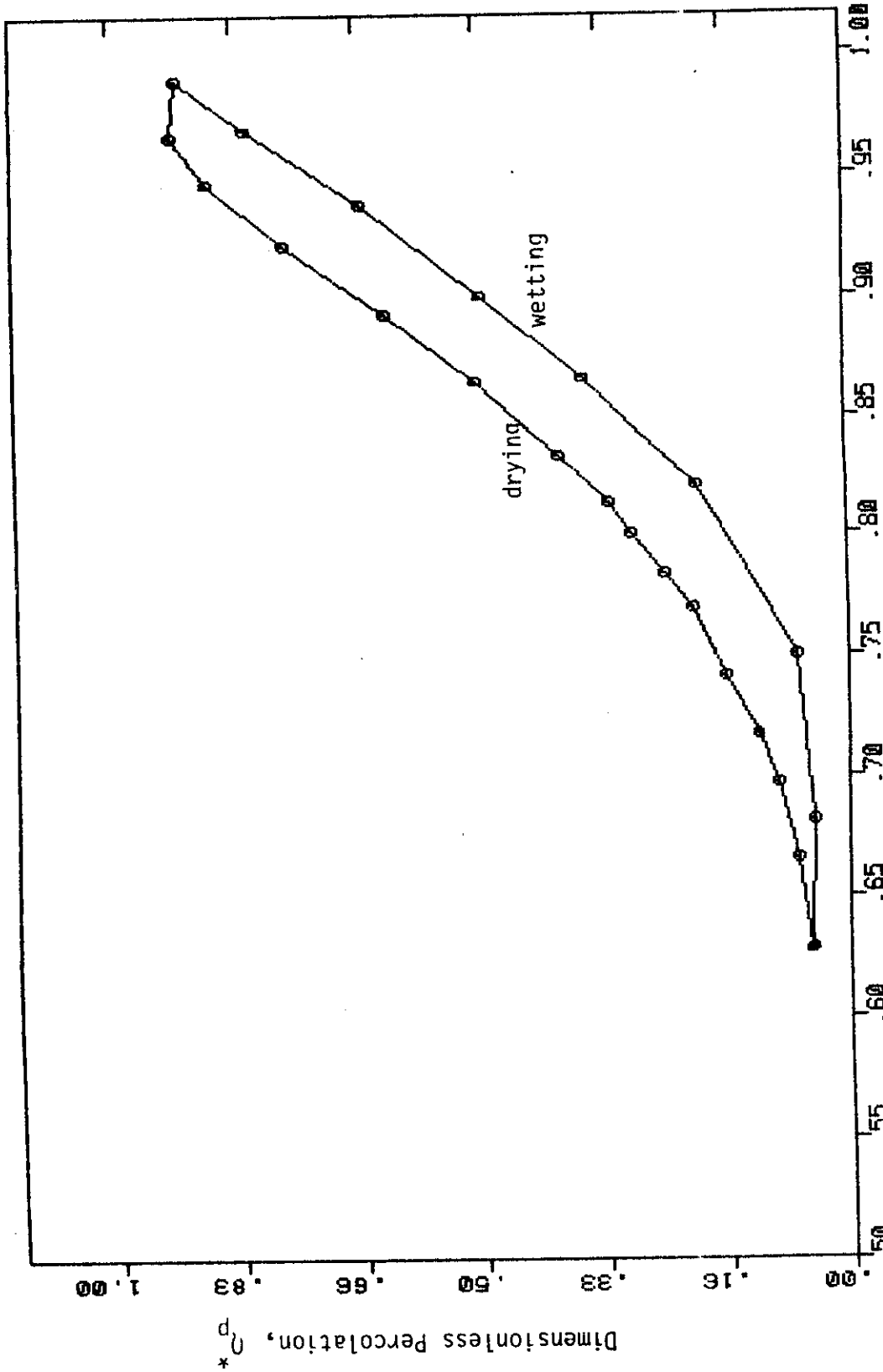

Figure 4. Relationship between Q_p^* and V^* for simulation 1: D=10m, $q=K_{loam}$, uniform loam profile.

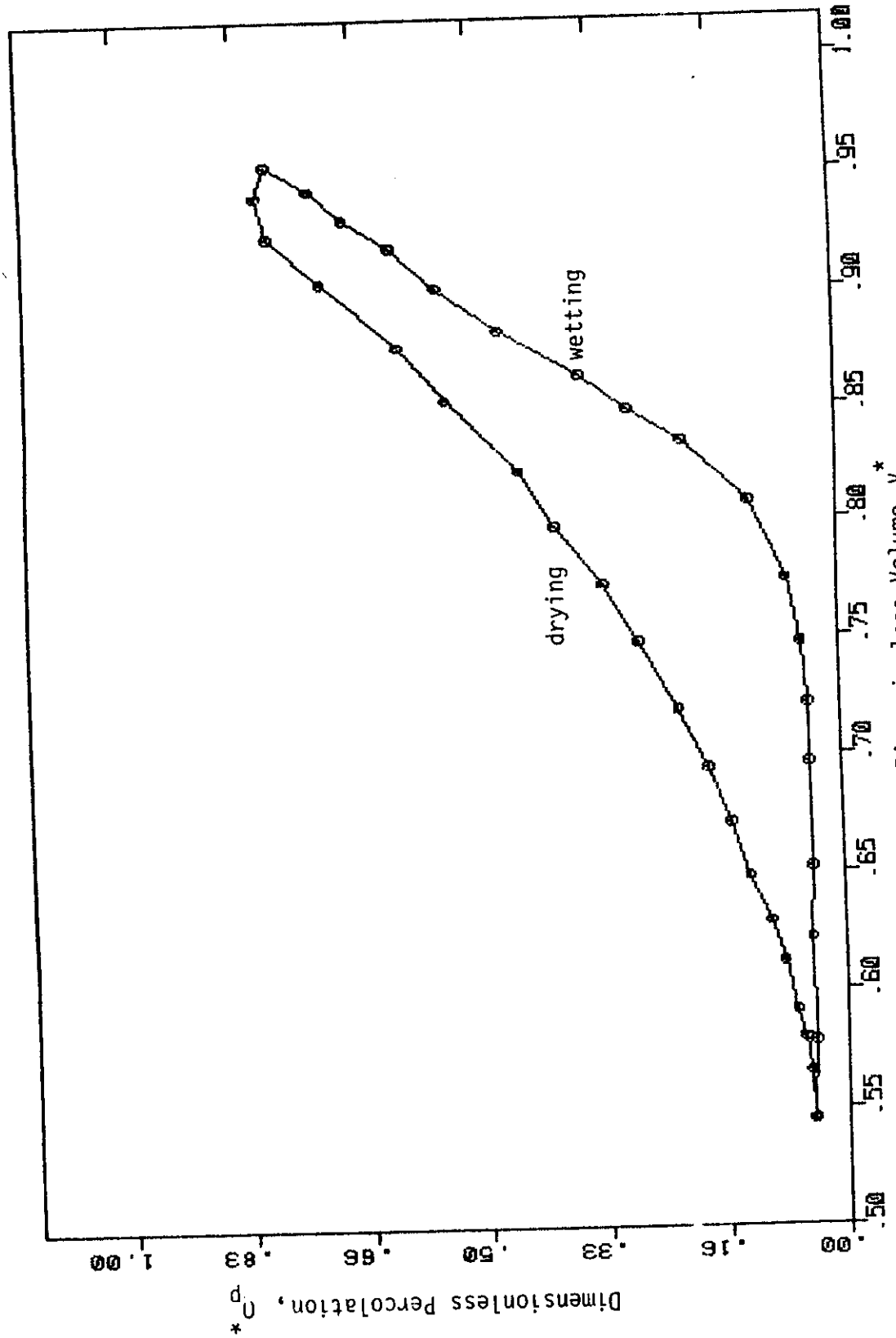

Figure 5. Relationship between Q_p^* and V^* for simulation 2: D=10m, $q=K_{sand}$, uniform sand profile.

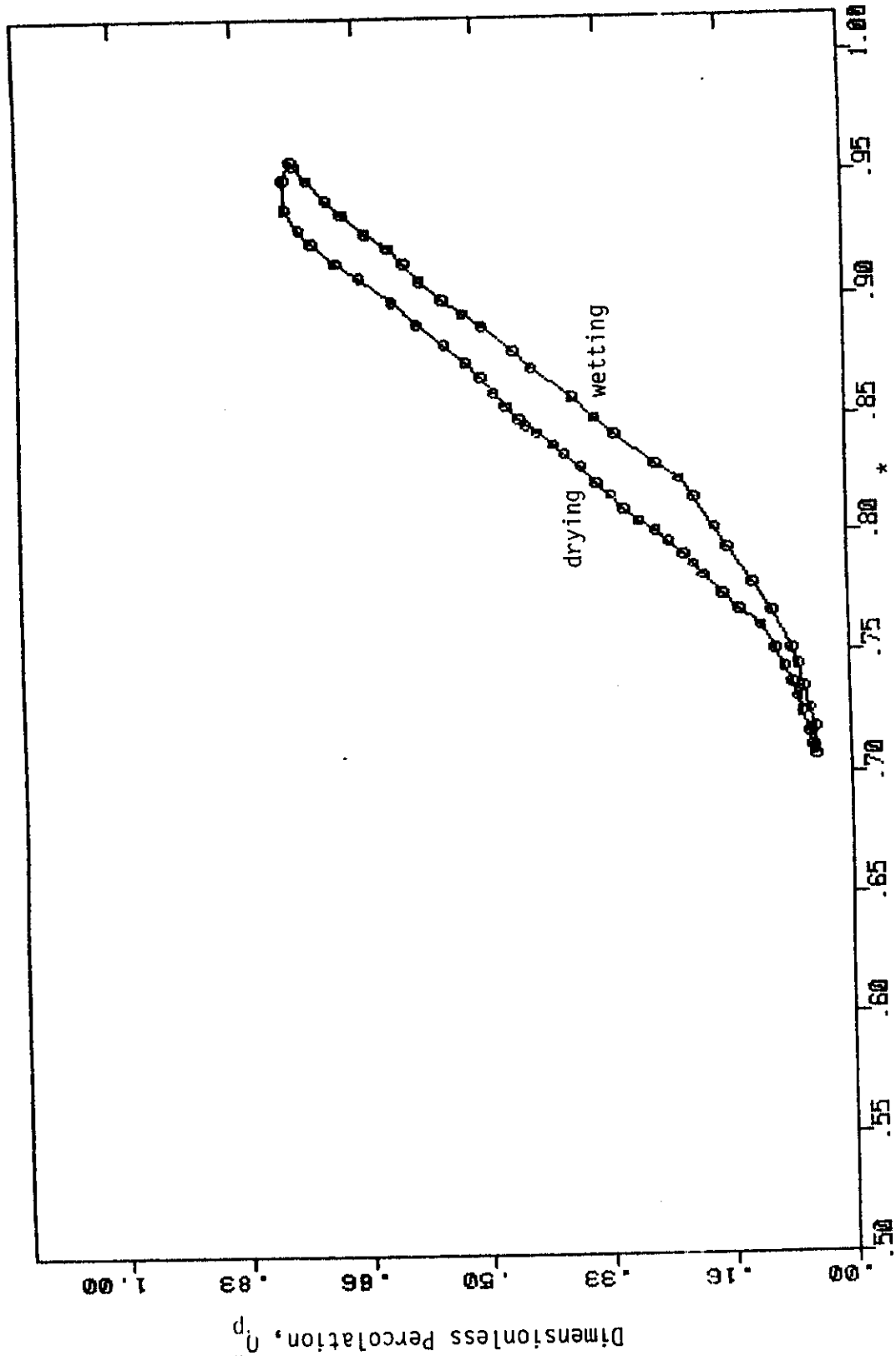

Figure 6. Relationship between Q_p^* and V^* for simulation 3: D=10m, $q=K_{clay}$, uniform clay profile.

soil and the maximum pore size. The sand will have a larger fraction of pore sizes than the loam or clay. The capillary forces will then be stronger in the loam and clay than in the sand. Thus it will be possible to release a greater fraction of the available soil moisture from the sand than from either the loam or the clay. Thus the Q_p^* on the drying boundary curve will tend to be higher for the sand than for the loam and in turn the loam Q_p^* drying boundary curve will be higher than that for the clay.

The influence of the relative application rate on the Q_p^* vs. V^* curve for the loam soil is illustrated in simulations 1 and 4 (Figures 4 and 7). In simulation 1 the application rate was equal to the saturated hydraulic conductivity and in simulation 4 the application rate was twice the saturated hydraulic conductivity. It is observed that the boundary drying curves are essentially the same for both simulations. The major difference between the Q_p^* vs. V^* relationships for the two simulations is in the lower portion of the boundary wetting curve. The boundary wetting curve for the simulation with the higher application rate lies to the right of the boundary wetting curve for simulation with the lower application rate. The same observation can be made for the sand profile in simulations 2 and 6 (Figures 5 and 9) and for the clay profile in simulations 3 and 7 (Figures 6 and 10). The explanation for this result for all soils is simply that the higher application rate produces a steeper wetting front in the soil profile. The influences of the steeper wetting front is not felt by the deep percolation process until a higher degree of saturation is reached. A lower relative application rate for the loam soil is illustrated by

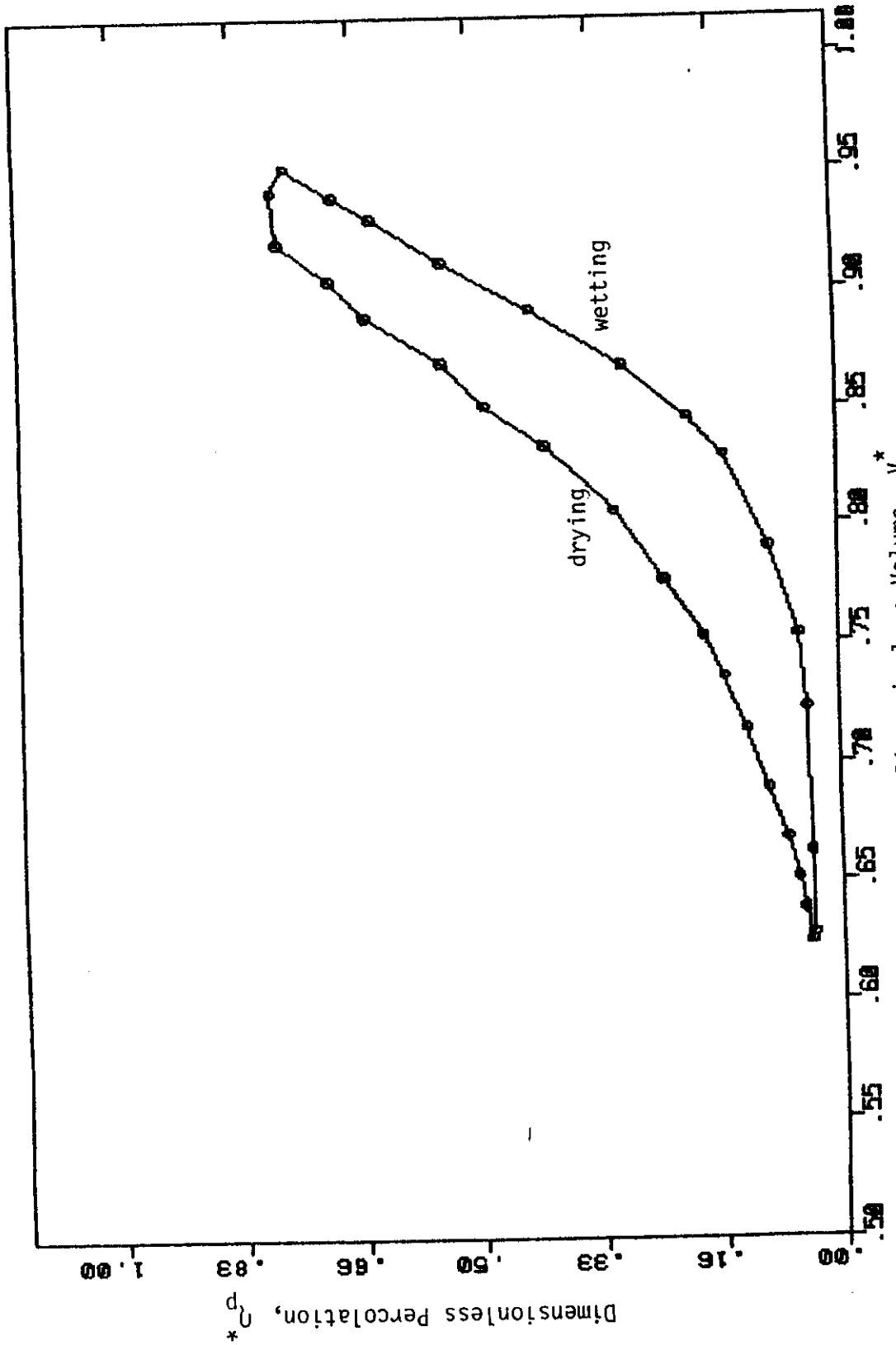

Figure 7. Relationship between Q_p^* and V^* for simulation 4: D=10m, $q=2K_{loam}$, uniform loam profile.

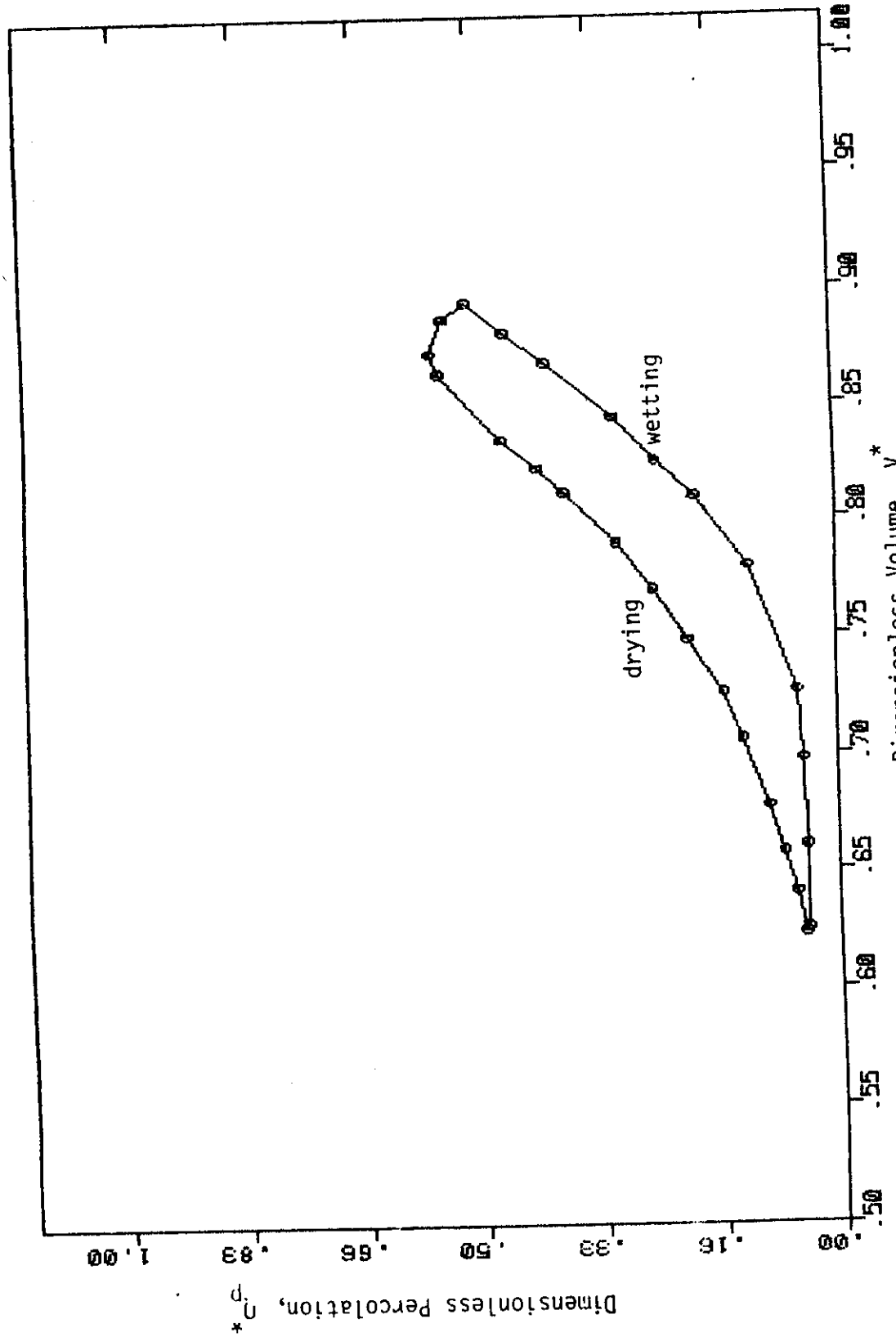

Figure 8. Relationship between Q_p^* and V^* for simulation 5: D=10m, q=0.5K_{loam}, uniform loam profile.

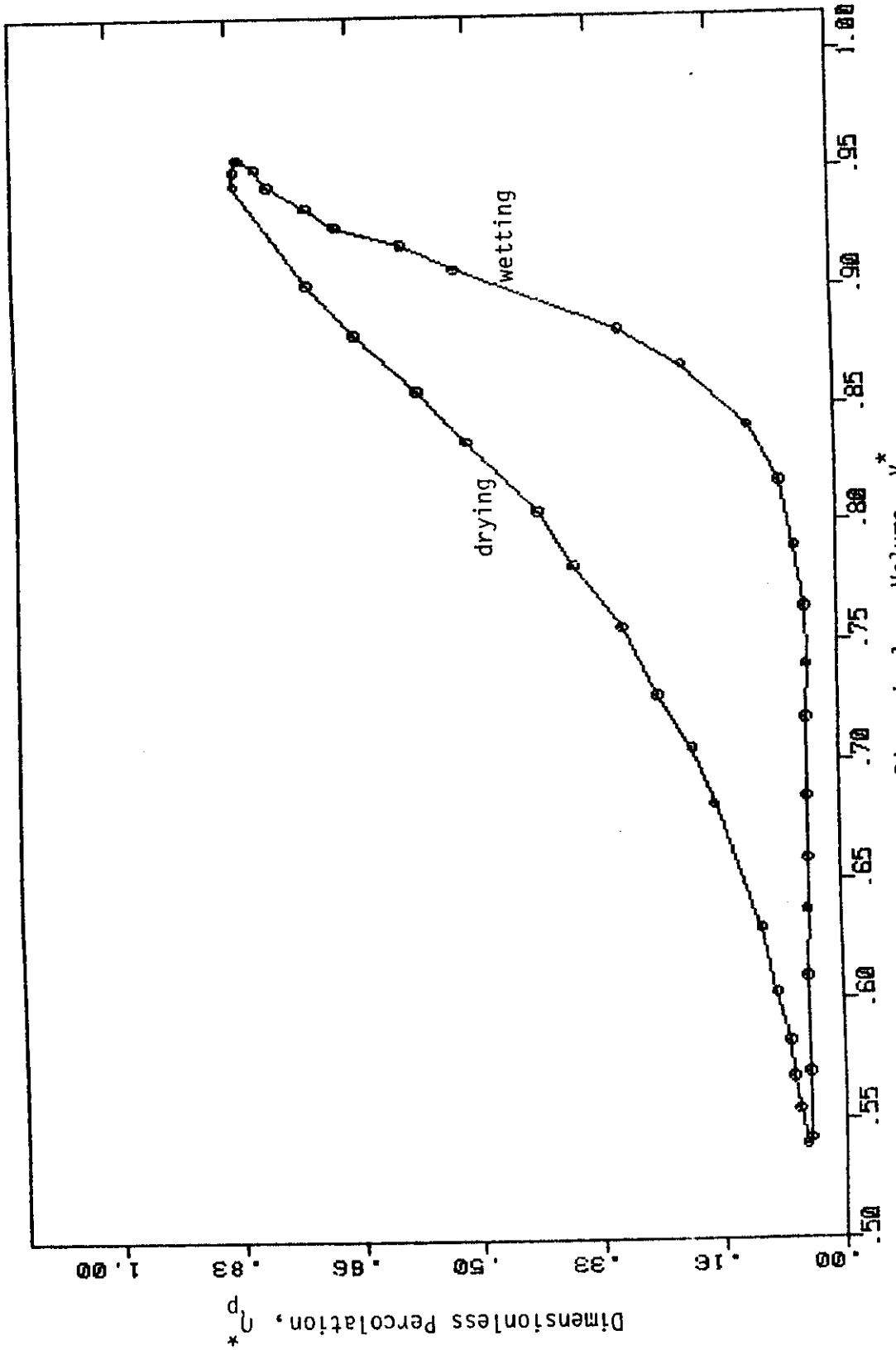

Figure 9. Relationship between Q_p^* and V^* for simulation 6: D=10m, $q=2K_{sand}$, uniform sand profile.

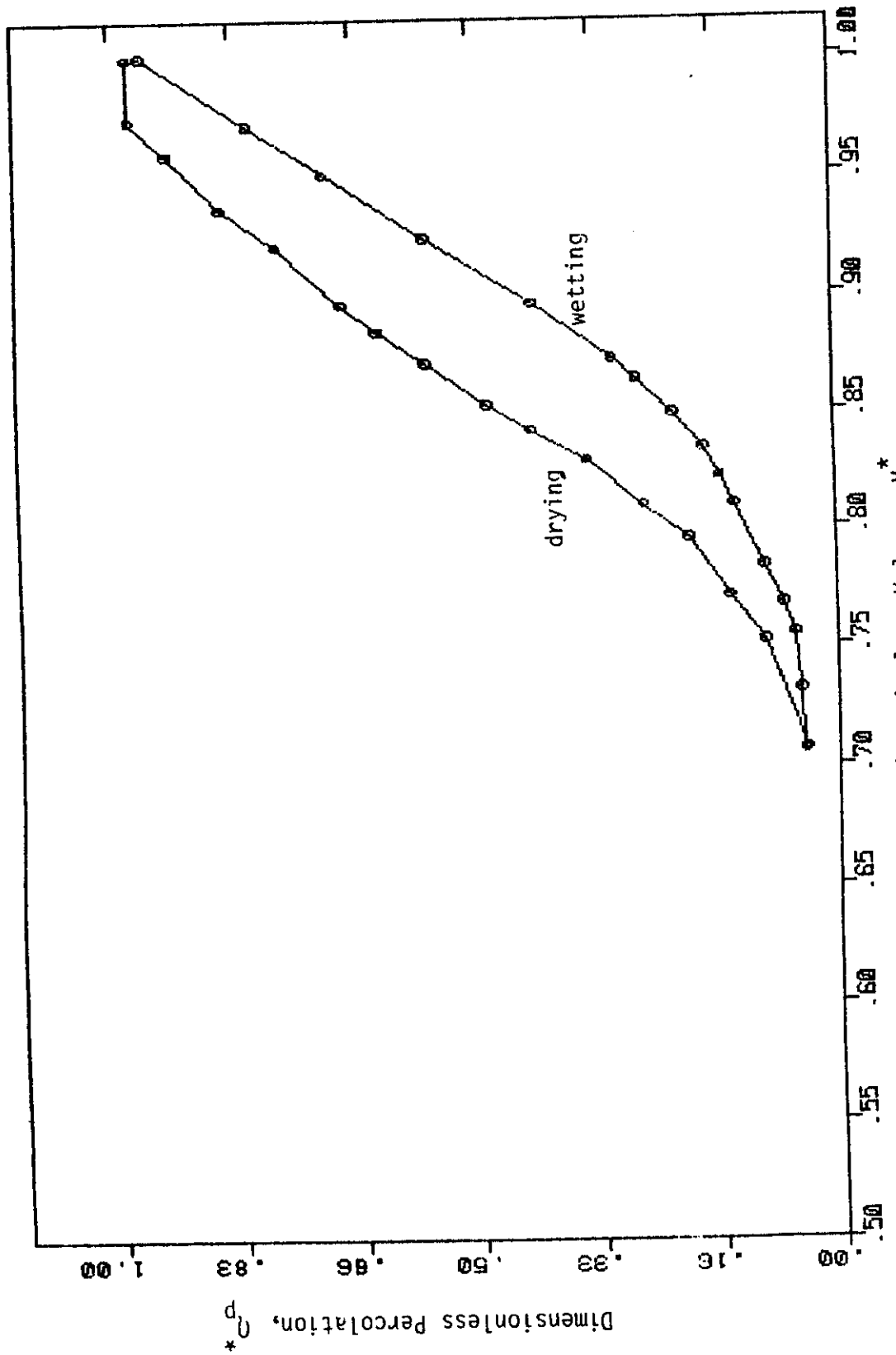

Figure 10. Relationship between Q_p^* and V^* for simulation 7: D=10m, $q=2K_{clay}$, uniform clay profile.

simulation 5(Figure 8) where $q^* = 0.5$. Comparing the Q_p^* vs. V^* relation in Figure 4 to that in Figure 8 indicates a slight dependence on relative application rate, but no drastic differences are seen.

The influence of evaporation from the soil surface or evapotranspiration (extraction of moisture directly from the soil profile) on the Q_p^* vs. V^* relationship for the loam soil is illustrated by the results of simulations 1, 8, and 9 (Figures 4, 11, and 12). It is expected that evaporation or evapotranspiration would have an influence on the boundary drying curve of the Q_p^* vs. V^* relationship. However, comparing the relations illustrated in Figure 4, 11, and 12 demonstrates that even a high evaporative demand of 12 mm/day has insignificant influence on the resulting boundary drying curve of the Q_p^* vs. V^* relationship.

The influence of the depth to the water table on the Q_p^* vs. V^* relationship is illustrated in Figures 4 and 13(simulations 1 and 10). In simulation 1 the water table was at a depth of 10 meters and in simulation 10 the water table was at a 1 meter depth. Comparison of these two results indicate that water table depth has insignificant influence on the Q_p^* vs. V^* relationship. The influence of soil layering on the Q_p^* vs. V^* relationship was tested in simulations 1, 11-15(Figures 4, 14-18). Simulation 1 consists of a uniform profile of loam soil. Simulations 11,12, and 13 have one, two, and four layers of clay, respectively, contained within the one meter profile of loam. Each layer of clay is 5 centimeters thick. In simulation 12 the layers are adjacent to each other and form a single layer 10 cm thick. In

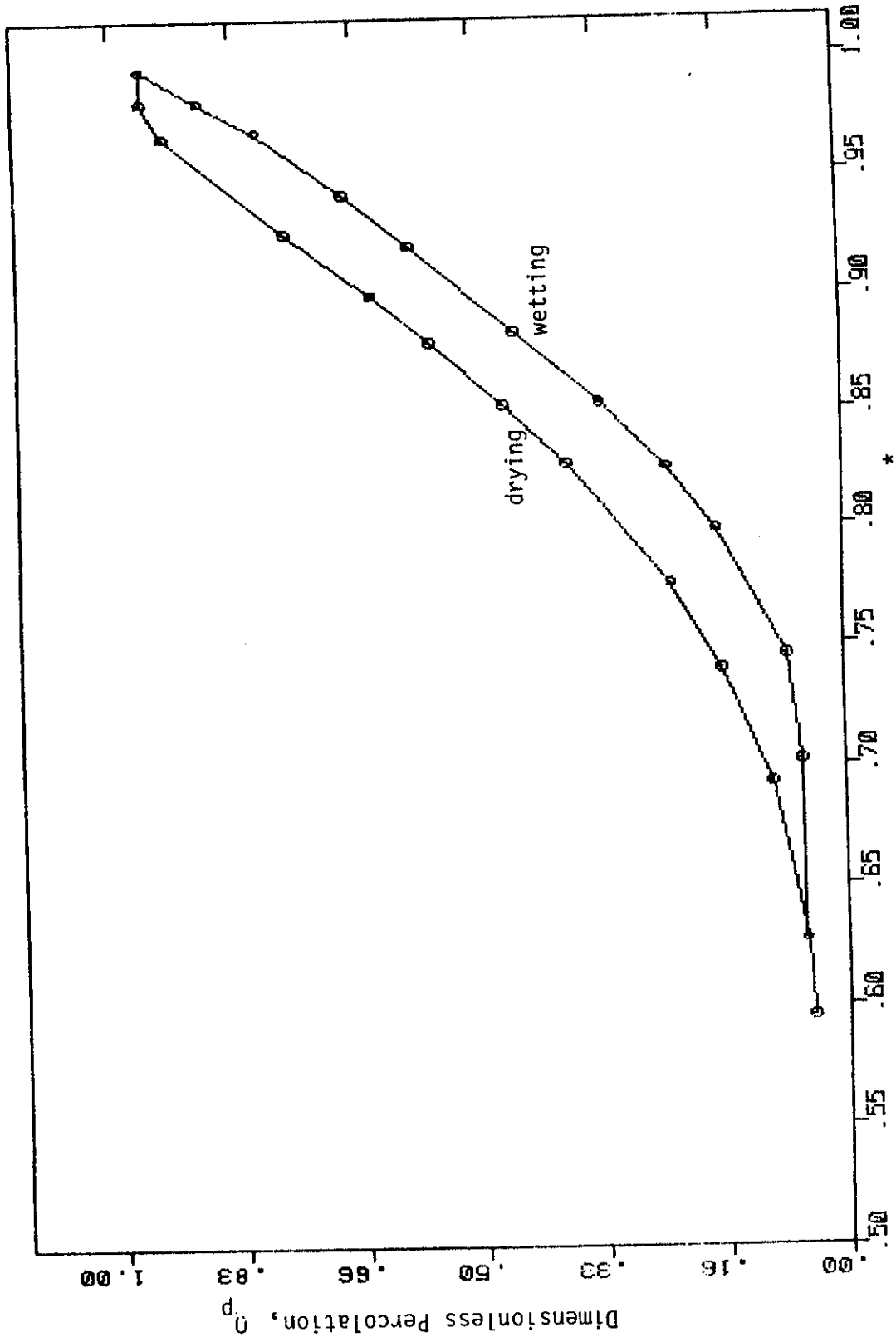

Figure 11. Relationship between Q_p^* and V^* for simulation 8: D=10m, $q=K_{loam}$, uniform loam profile with a soil evaporation rate of 12 mm/day.

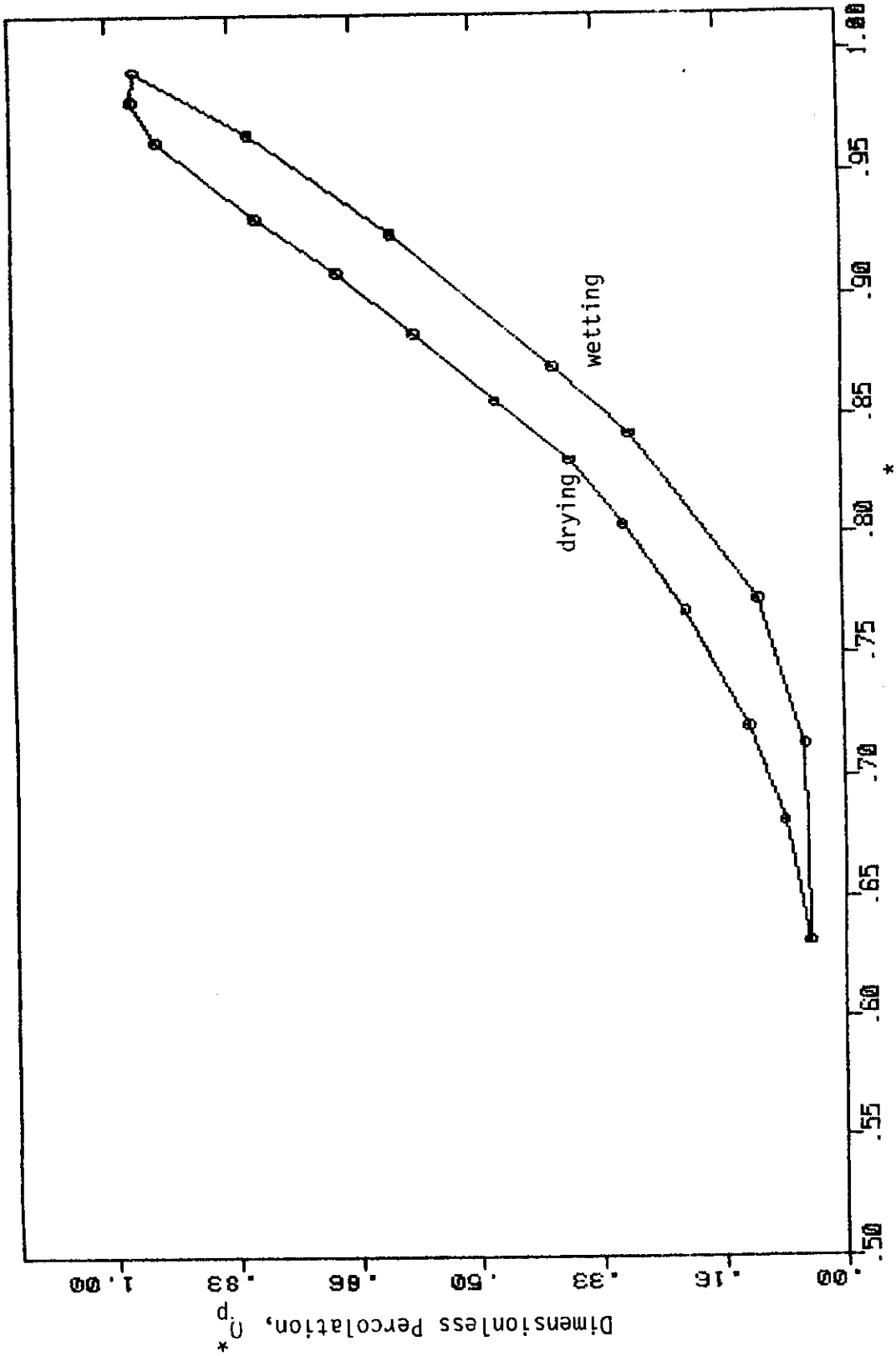

Figure 12. Relationship between Q_p^* and V^* for simulation 9: D=10m, $q=K_{loam}$, uniform loam profile with a transpiration rate of 12 mm/day.

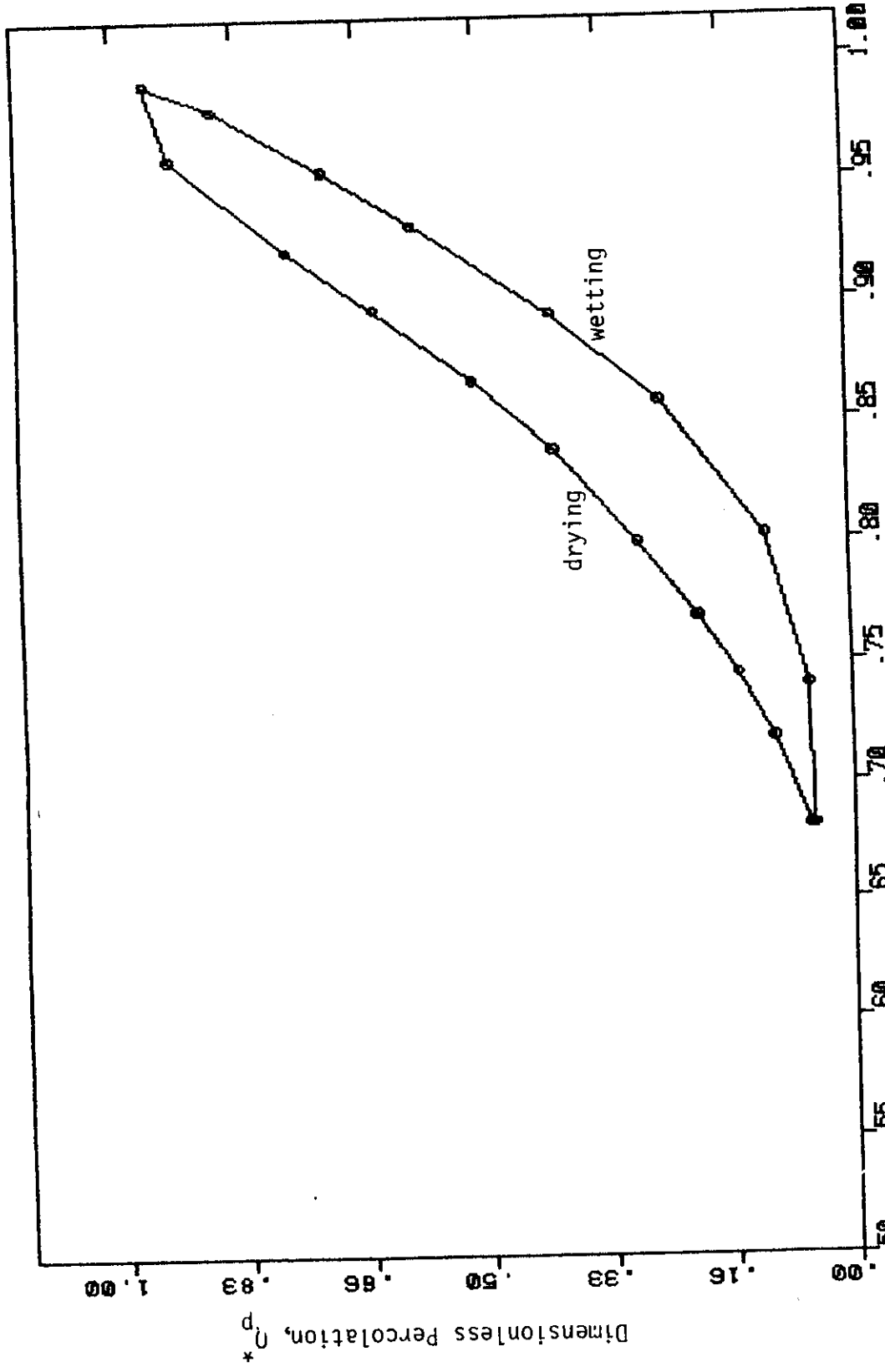

Figure 13. Relationship between Q_p^* and V^* for simulation 10: D=1m, $q=K_{loam}$, uniform loam profile.

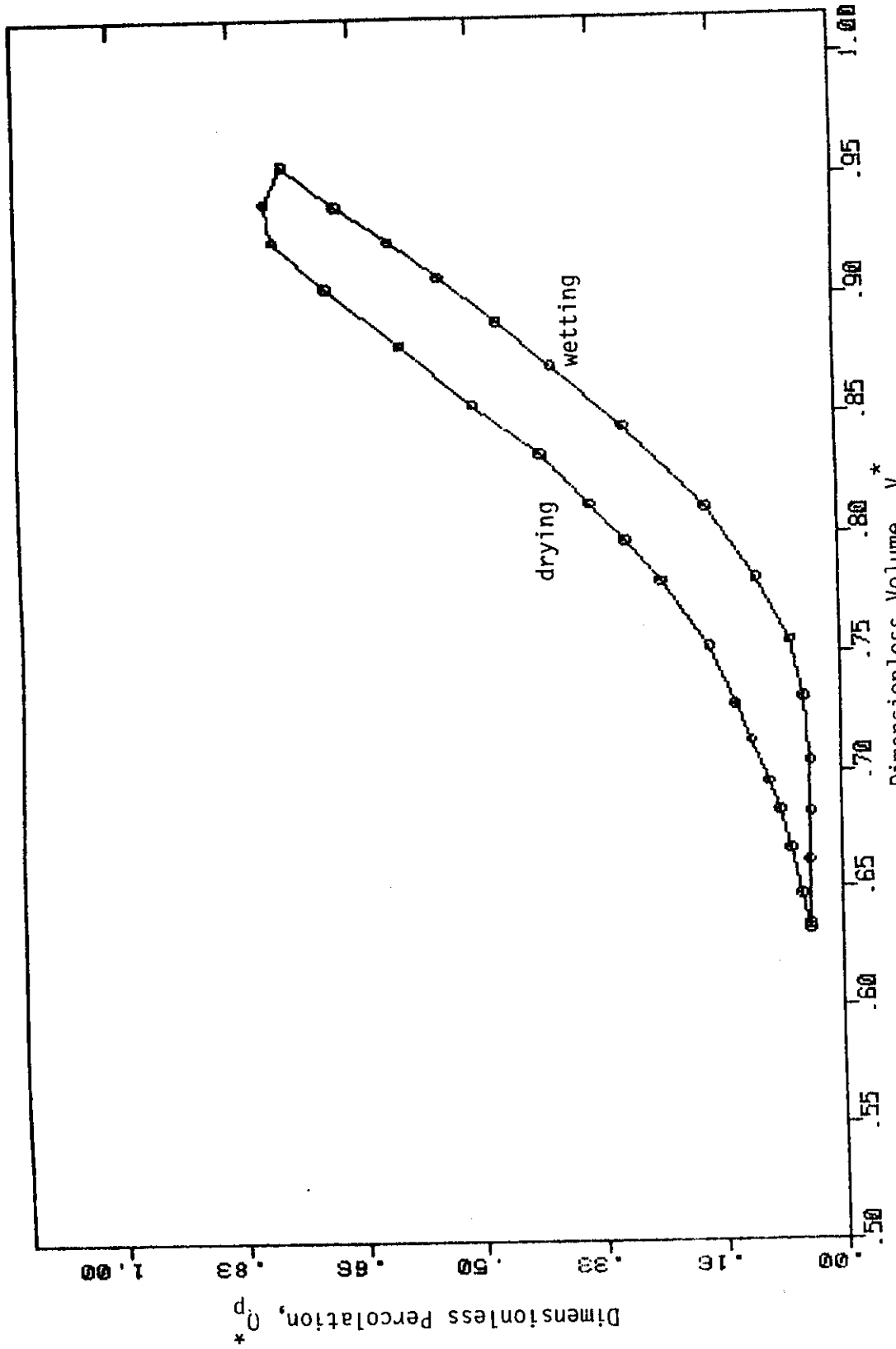

Figure 14. Relationship between Q_p^* and V^* for simulation 11: D=10m, $q=K_s^e$ loam soil with a single 5 cm thick layer of clay located at a depth of 45 cm in the loam profile.

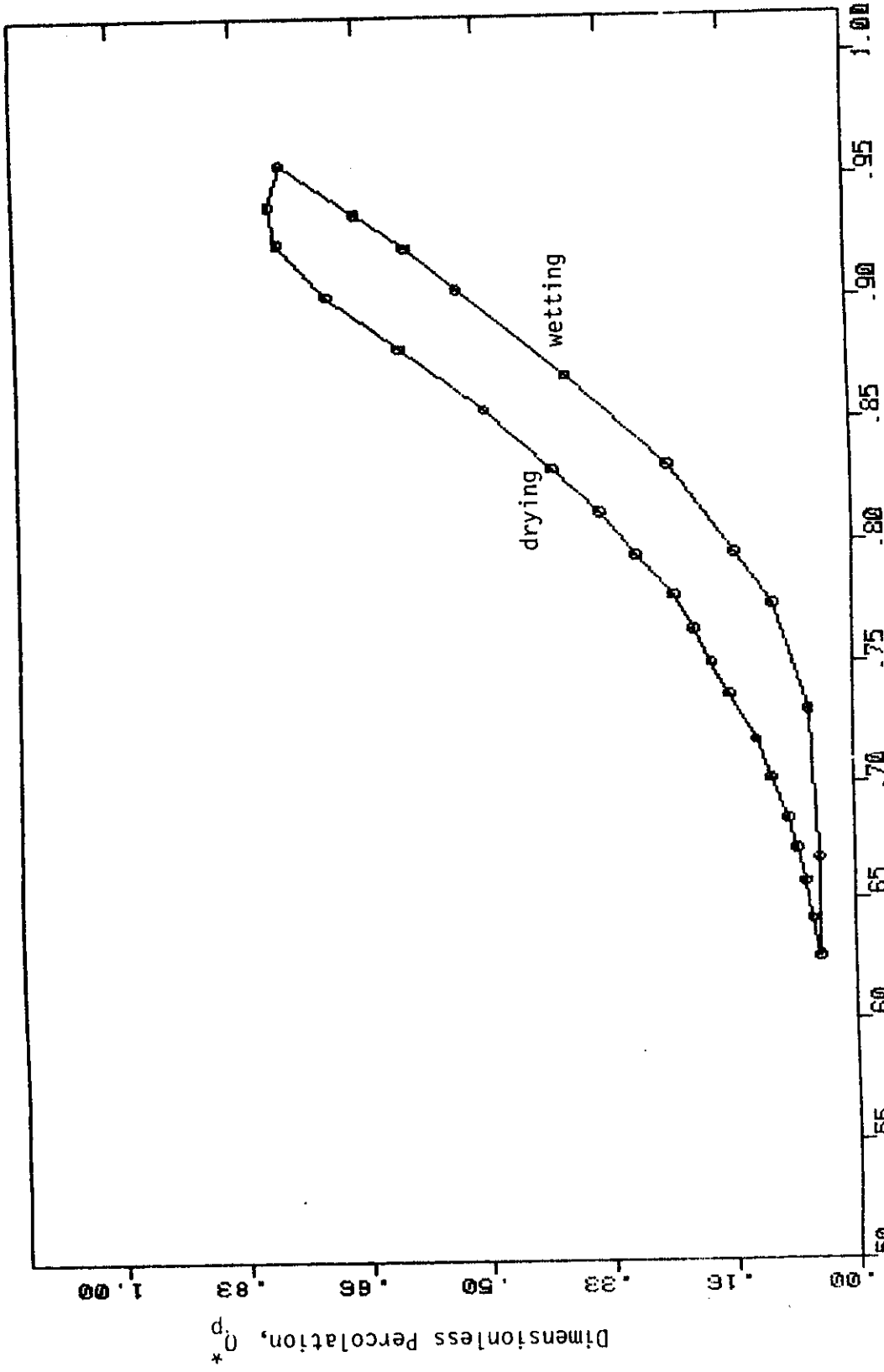

Figure 15. Relationship between Q_p^* and V^* for simulation 12: D=10m, $q=K_s^e$ loam soil with a 10 cm thick clay layer located at a depth of 25 cm in the loam profile.

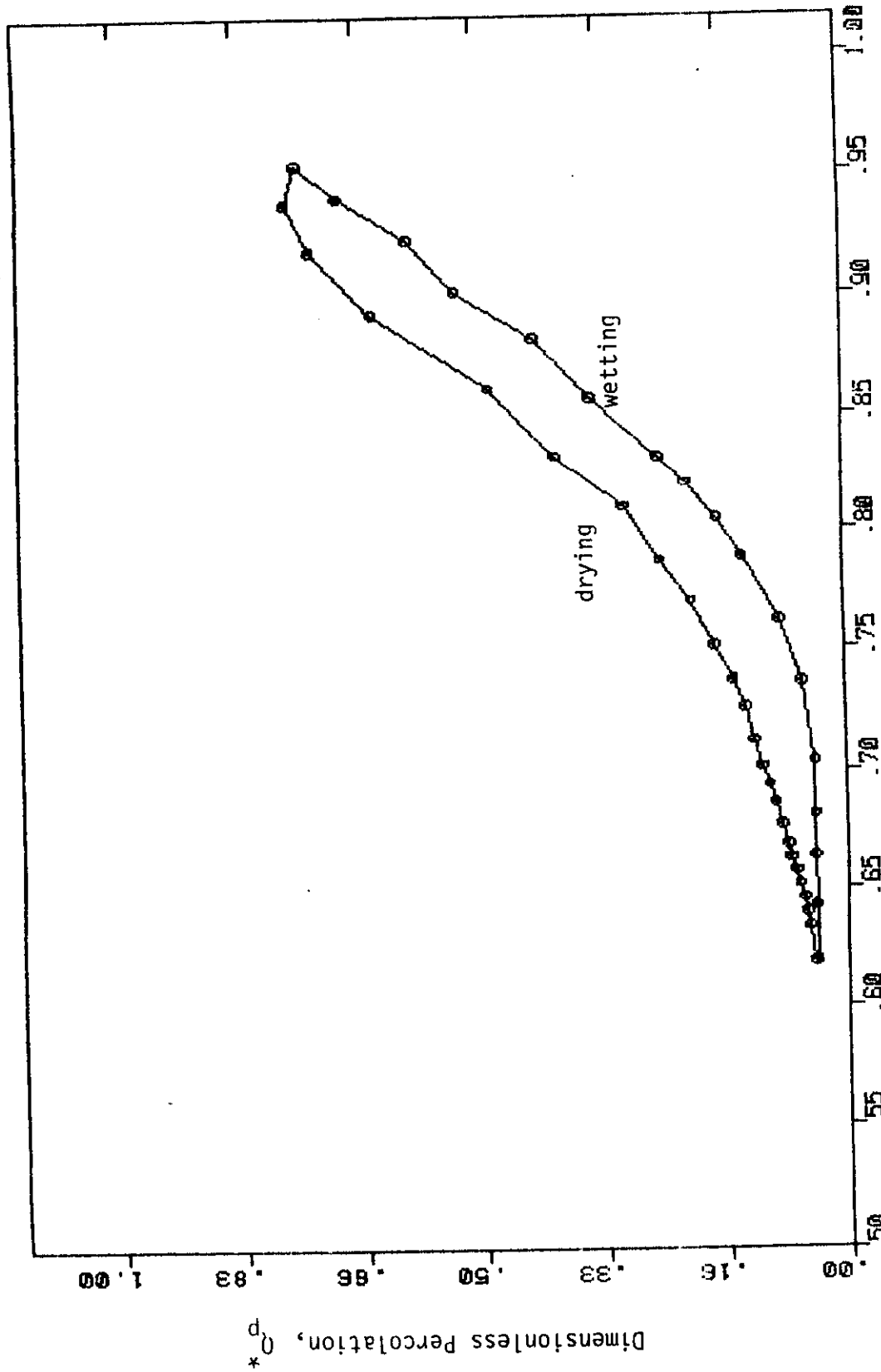

Figure 16. Relationship between Q_p^* and V^* for simulation 13: D=10m, $q=K_s^e$ and loam soil with 5 cm thick clay layers located at depths of 25, 45, 70 and 90 cm in the loam profile.

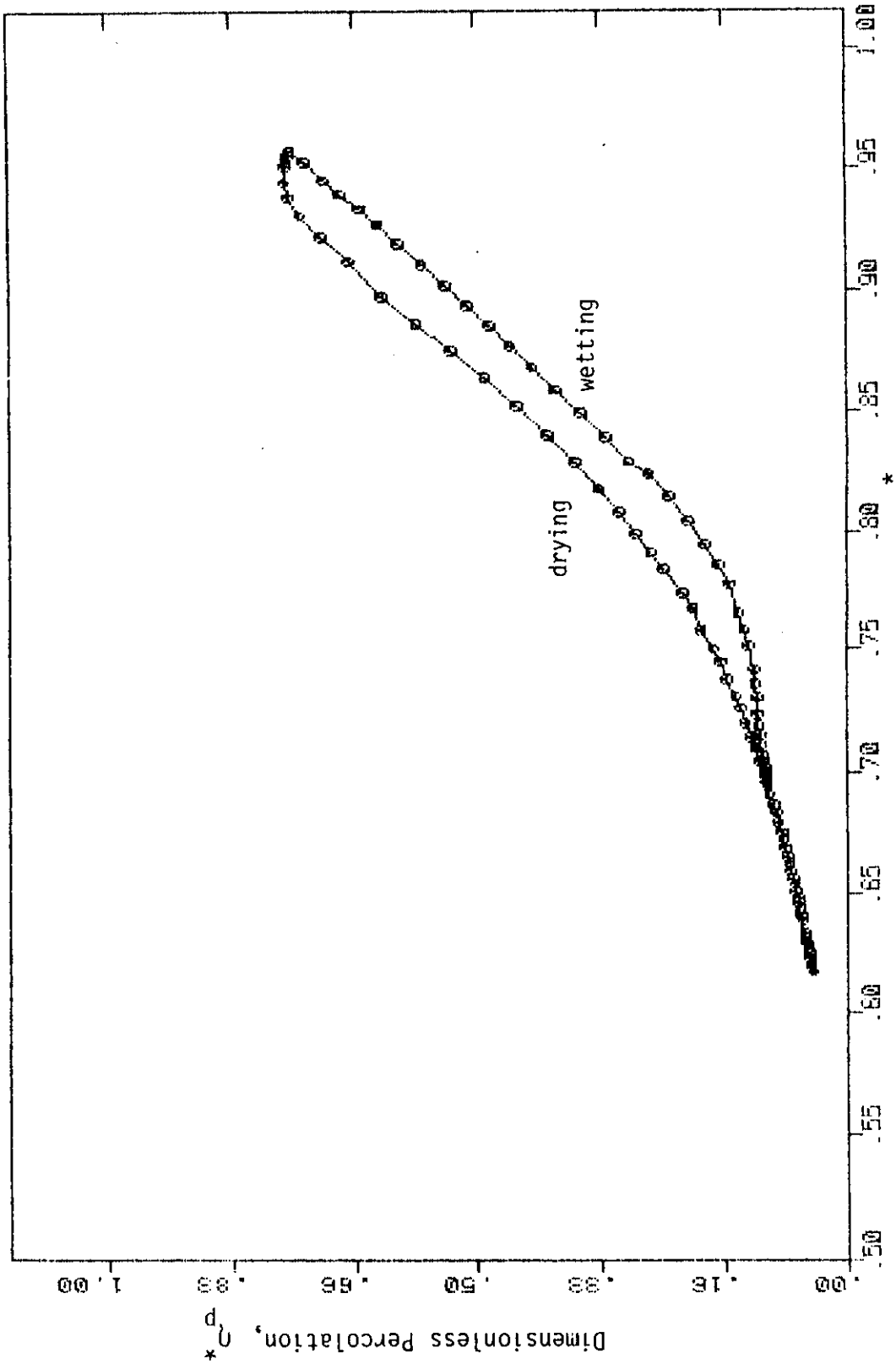

Figure 17. Relationship between Q_p^* and V^* for simulation 14: D=10m, $q=K_s^e$ loam soil with a 10 cm layer of clay at a depth of 45 cm and a 25 cm layer of sand at a depth of 70 cm in the loam profile.

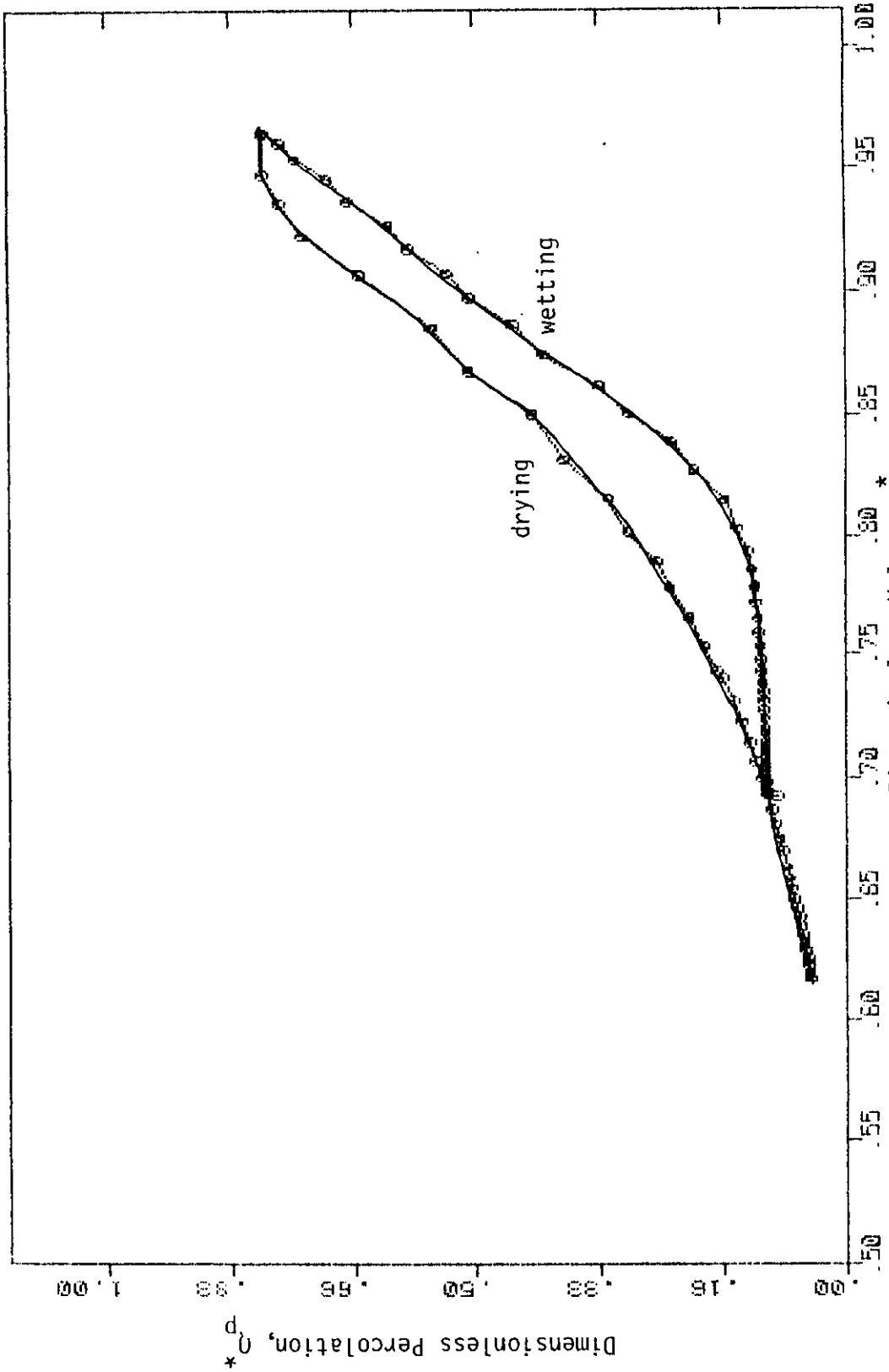

Figure 18. Relationship between Q_p^* and V^* for simulation 15: D=10m, $q=2K_s^e$ loam soil with a 10 cm layer of clay at a depth of 45 cm and a 25 cm layer of sand at a depth of 70 cm in the loam profile.

simulation 13 the layers are separated from each other by a 15 cm layer of loam. The results illustrated in Figures 4 and 14-16 demonstrate that at least for the simulations performed here the clay layers had no influence on the resulting Q_p^* vs. V^* relationship observed in Figure 4. In simulations 14 and 15 the 1 meter profile was composed of a 10 cm layer of clay, a 25 cm layer of sand, and a 65 cm layer of loam. Simulation 14 had the application rate equal to the equivalent saturated hydraulic conductivity of the profile and in simulation 15 the application rate was twice the equivalent saturated hydraulic conductivity of the profile. Comparison of these two simulations indicates that the application rate has only a slight influence on the width of the Q_p^* vs. V^* loop. The effect is seen to be similar to the effect seen earlier in comparing Figures 4 and 7. In addition, comparison of Figures 4 and 17 indicates that the presence of the clay and sand layers does influence the width of the Q_p^* vs. V^* loop but otherwise the relations are very similar.

In a water balance study Black et al.(1969) examined the relationship between deep percolation flux rates and the volume of moisture stored in the soil profile. The soil considered in their study was a Plainfield sand and a lysimeter was used to measure the moisture balance. They used a water balance model in which the percolation rate was set equal to that hydraulic conductivity associated with the average water content of the soil profile lying above the point of specified percolation flux. The water balance model was applied to a three month period in 1967 and the predicted moisture storage over the period was found to be within 0.3 cm of the measured storage. The

drainage rate as predicted by the water balance model was also found to be quite close to the drainage rate measured with the lysimeter.

The findings of this study lend support to the work of Black et al.(1969) except that it was found here that the relationship between percolation and stored moisture is not unique but forms a hysteretic loop. The fact that this loop exists will have some influence on the accuracy of water balance predictions. However, the results of Black et al.(1969) indicate that the assumption of a unique relationship between percolation rate and soil moisture storage is not severe. Further simulation studies will have to be performed to test the accuracy of this assumption for various soil and meteorological conditions.

4.2 TWO-DIMENSIONAL CASE

The results of the simulations for the two-dimensional problem are illustrated in Figures 19-43 in the same order as given in Table 3.

A particular feature of many of the simulations to be shown is that on the wetting cycle the Q_s^* vs. V^* relationship is not perfectly smooth in all cases, but many times exhibits a waviness. This waviness appears to be due to the fact that the node points used to represent the seepage surface of the slope soil surface are rather distant and the transient growth of the seepage surface is not well represented in this way. The seepage surface has to "jump" from node to node to lengthen and the "jumps" are manifested as waves in the Q_s^* vs. V^* relationship. This same phenomenon was observed to occur in a study by Beven (1977).

Simulations 1 and 2 are illustrated in Figures 19 and 20 and demonstrate that the parameter β has little influence on the Q_s^* vs. V^* relationship as long as the value of $a^{1/\beta}$ is held constant. This result is consistent with the findings by Verma and Brutsaert (1971) in the analysis of the recession for large confined aquifer discharge into streams and by Nieber (1982) in the analysis of the rising hydrograph for subsurface return flow from hillslopes. In each simulation the major wetting curve is quite close to the major drying curve. However, in cases where drainage occurs prior to reaching complete saturation the drying curve drops significantly below the major drying curve.

The influence of the rainfall intensity on the Q_s^* vs. V^* relations is illustrated through comparison of the results from simulations 1, 3, and 4 (Figures 19, 21, and 22). The major drying curve is not influenced by the rainfall intensity but the major wetting curve is influenced by the rainfall intensity. In essence, as the rainfall intensity increases relative to the saturated hydraulic conductivity of the soil the major wetting curve deviates further away from the major drying curve. The major wetting curves for simulations 3 and 4 are nearly the same so it is expected that for even higher relative rainfall intensities the major wetting curve will fall close to the one for simulation 4. The maximum difference between the major wetting curves for simulations 1 and 4 is approximately 0.16 Q_s^*. This difference is not so extreme that in some cases one might wish to use only one of the curves to represent all rainfall intensities.

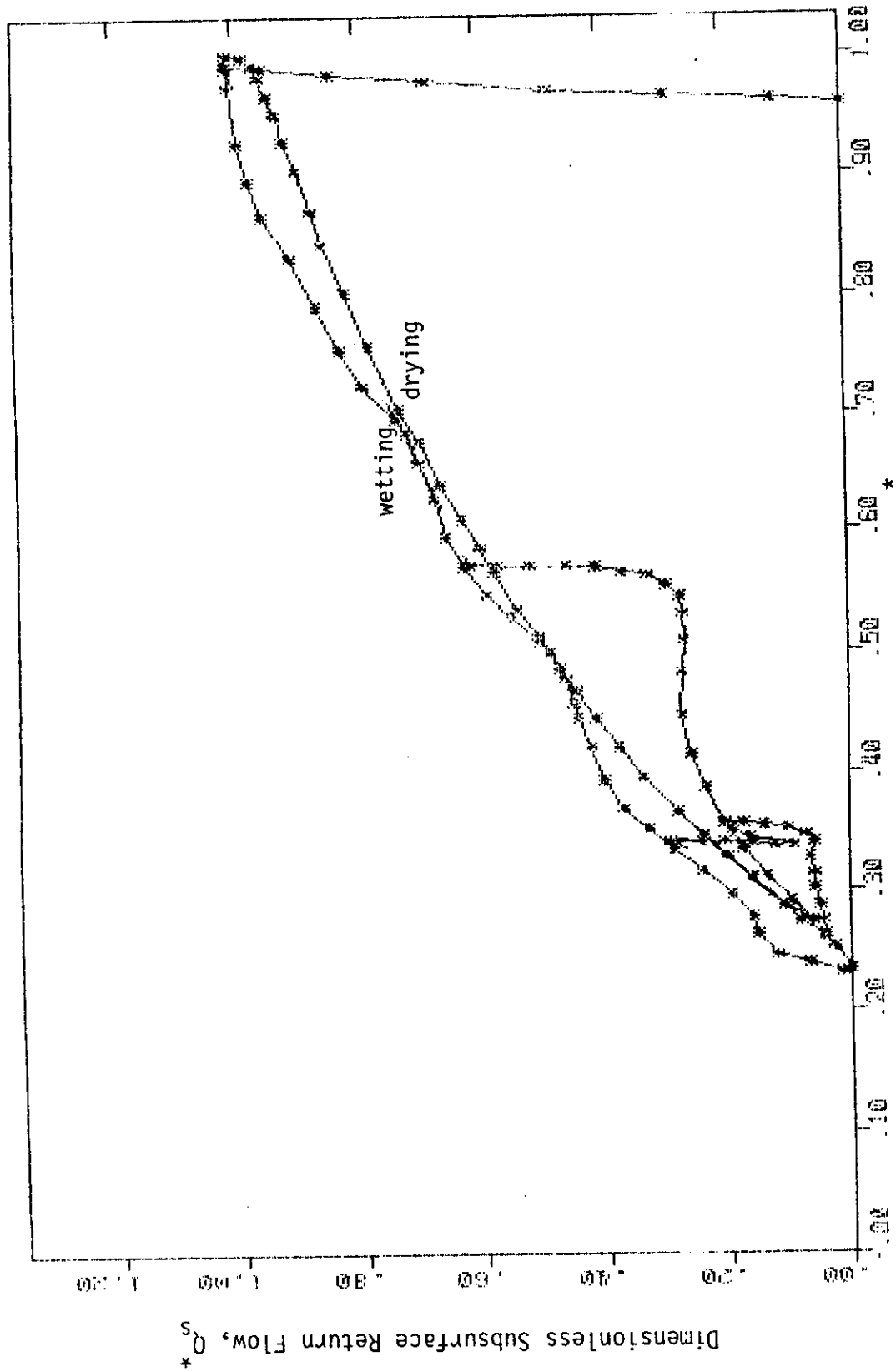

Figure 19. Relationship between Q_s^* and V^* for simulation 1: L^*=20, γ=15 degrees, $\alpha^{1/\beta}$=0.233, β=3.0, N=3.0, q^*=0.10, and a homogeneous soil.

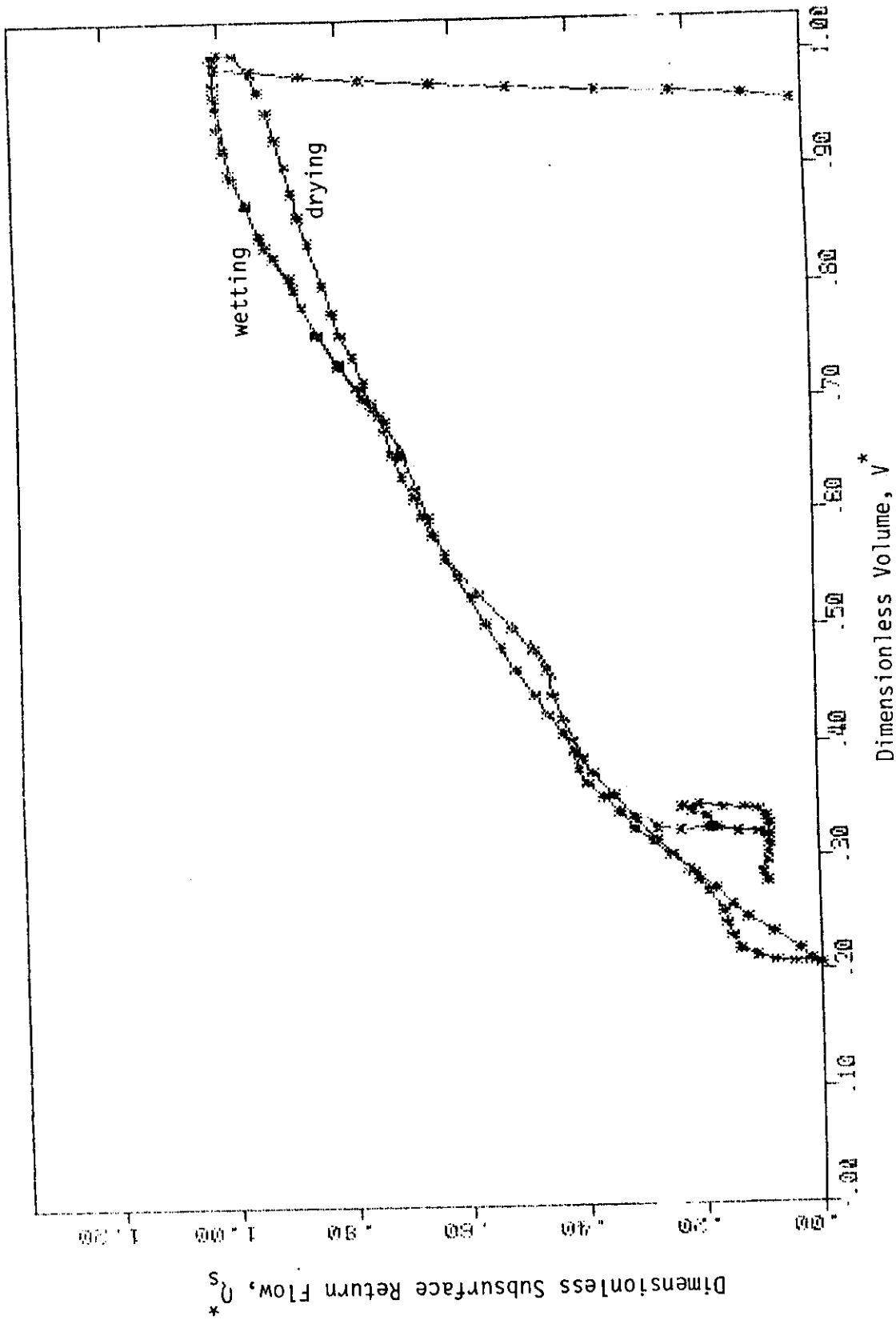

Figure 20. Relationship between Q_s^* and V^* for simulation 2: L^*=20, γ=15 degrees, $\alpha^{1/\beta}$=0.233, β=5.0, N=3.0, q^*=0.10, and homogeneous soil.

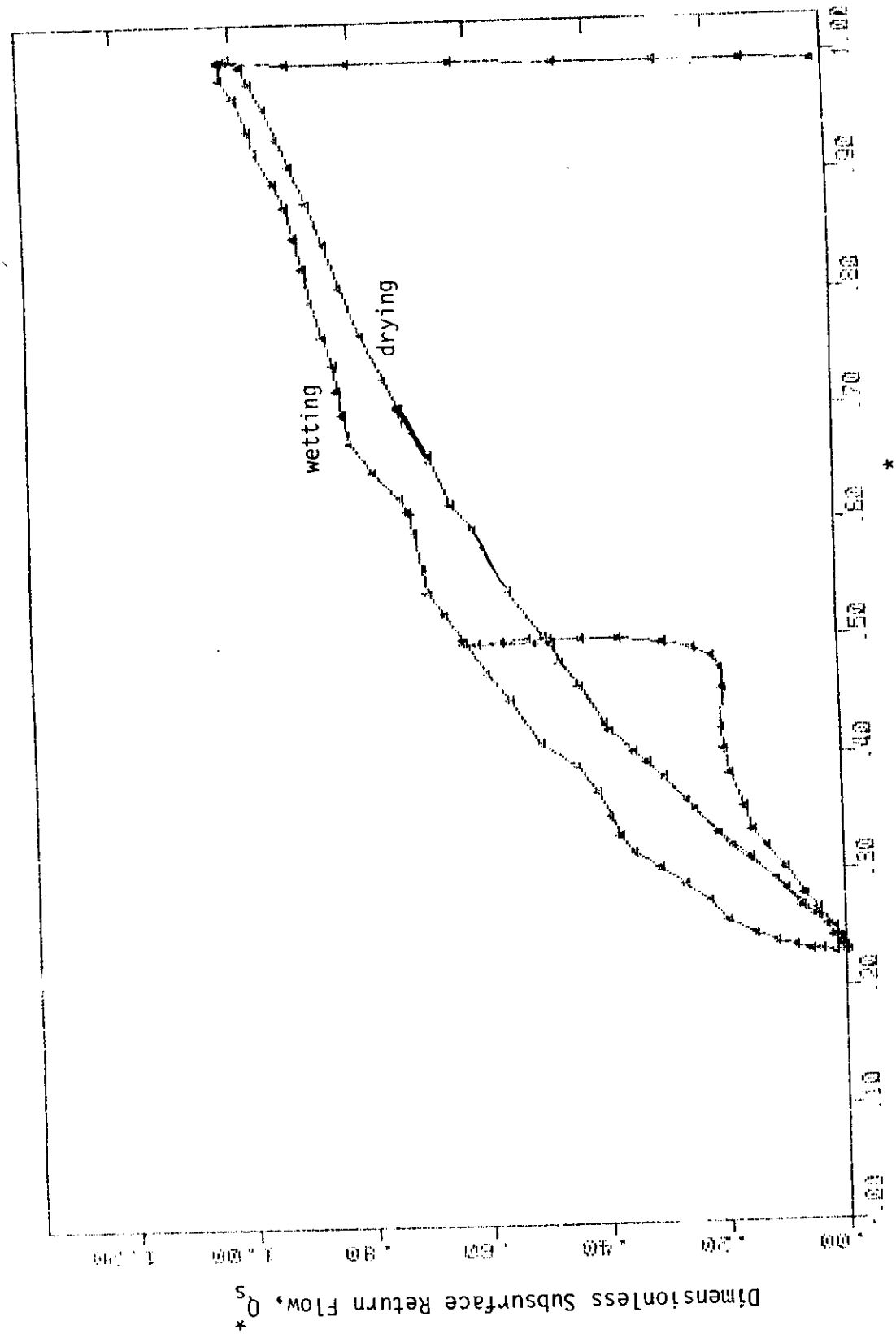

Figure 21. Relationship between Q_s^* and V^* for simulation 3: $L^*=20$, $\gamma=15$ degrees, $\alpha^{1/\beta}=0.233$, $\beta=3.0$, $N=3.0$, $q_s^*=0.50$, and homogeneous soil.

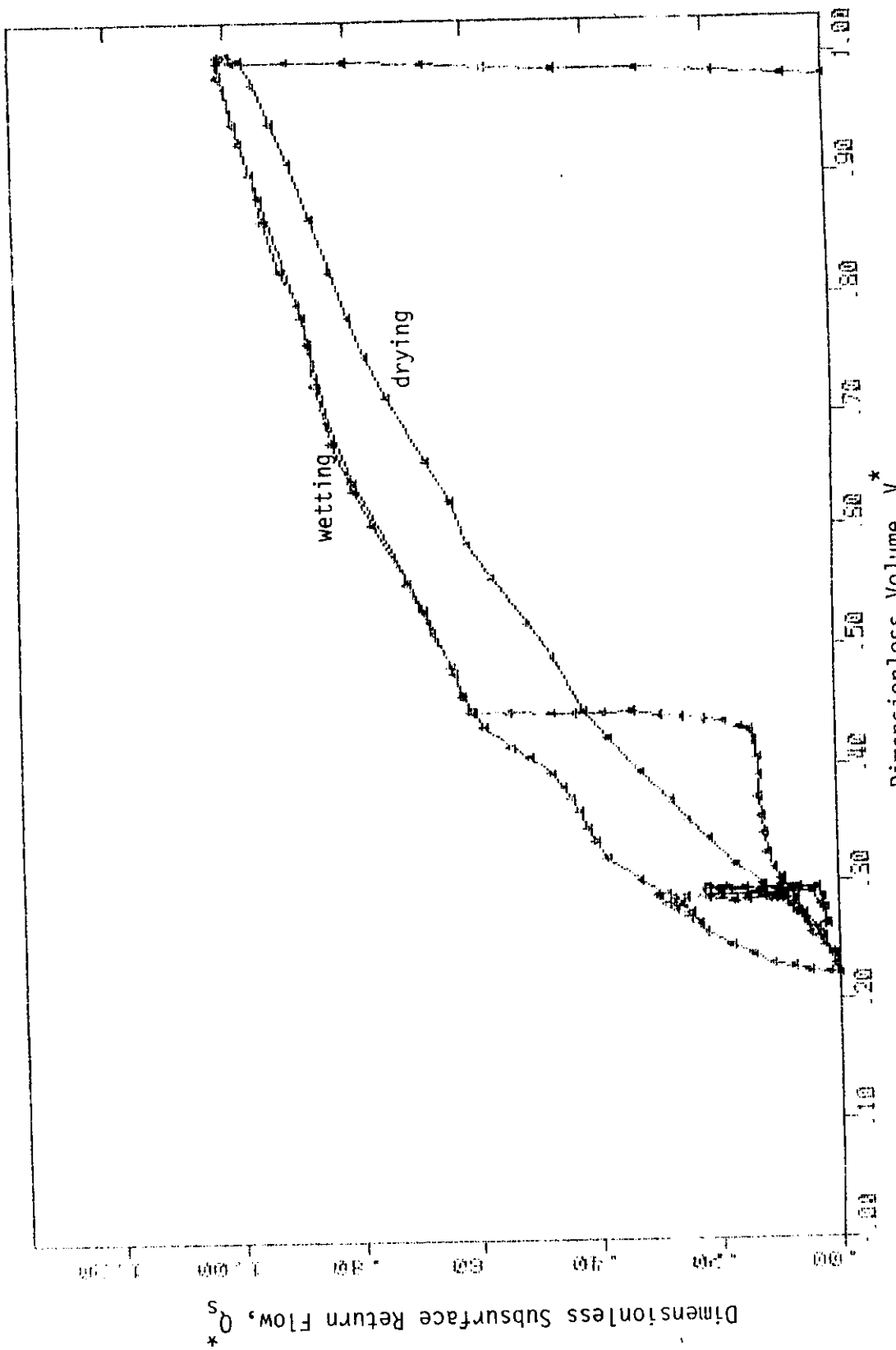

Figure 22. Relationship between Q_s^* and V^* for simulation 4: L^*=20, γ=15 degrees, $\alpha^{1/\beta}$=0.233, β=3.0, N=3.0, q^*=1.0, and homogeneous soil.

The influence of the length-depth ratio L^* on the Q_s^* vs. V^* relations is illustrated by the comparison of results from simulations 1, 5, 6, and 7 (Figure 19, 23-25). Comparison of the results demonstrates that the L^* parameter has a significant influence on the Q_s^* vs. V^* relationship. For the L^* value of 10 (Figure 23) the major wetting curve is significantly above the major drying curve but as L^* increases the major wetting curve approaches the major drying curve (as in Figure 19) and then crosses the major drying curve in two points (as in Figure 24 and 25). The waviness in the wetting cycle curve becomes quite large when L^* equals 50(Figure 25). The main drying and wetting curves cover an increasingly larger portion of the Q_s^* vs. V^* domain as the L^* parameter increases. This is expected since as L^* parameter increases an increasingly larger mass of soil becomes available for drainage of soil moisture. The L^* parameter was also found to be significant by Verma and Brutsaert (1971) in the study of aquifer drainage and by Nieber (1982) in the study of the rising side of subsurface return flow hydrographs.

The influence of the soil characteristic is illustrated by the comparison of results of simulations 1, 8, 9, and 10 (Figures 19, 26-28). The soil characteristics were imposed by changing the parameter $\alpha^{1/\beta}$. It is already established that the parameter N has an insignificant influence for all conditions and the parameter β has an insignificant influence for a given $\alpha^{1/\beta}$ value. But Figures 19 and 26-28 demonstrate that the $\alpha^{1/\beta}$ parameter has a significant influence on the Q_s^* vs. V^* relationships. It is observed from this set of results that as the $\alpha^{1/\beta}$ parameter increases the major wetting curve and the

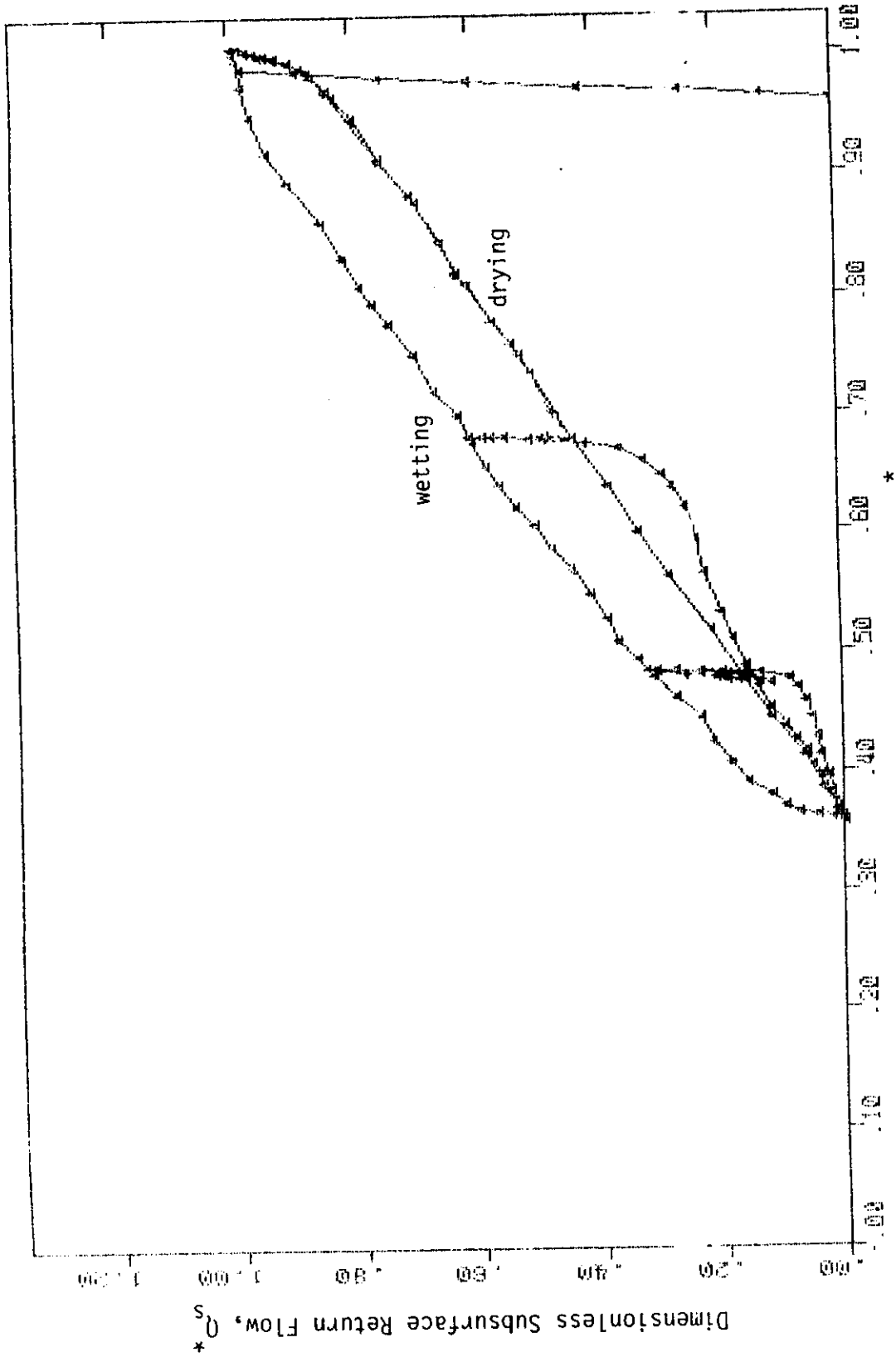

Figure 23. Relationship between Q_s^* and V^* for simulation 5: L^*=10, γ=15 degrees, $\alpha^{1/\beta}$=0.233, β=3.0, N=3.0, q^*=0.10, and homogeneous soil.

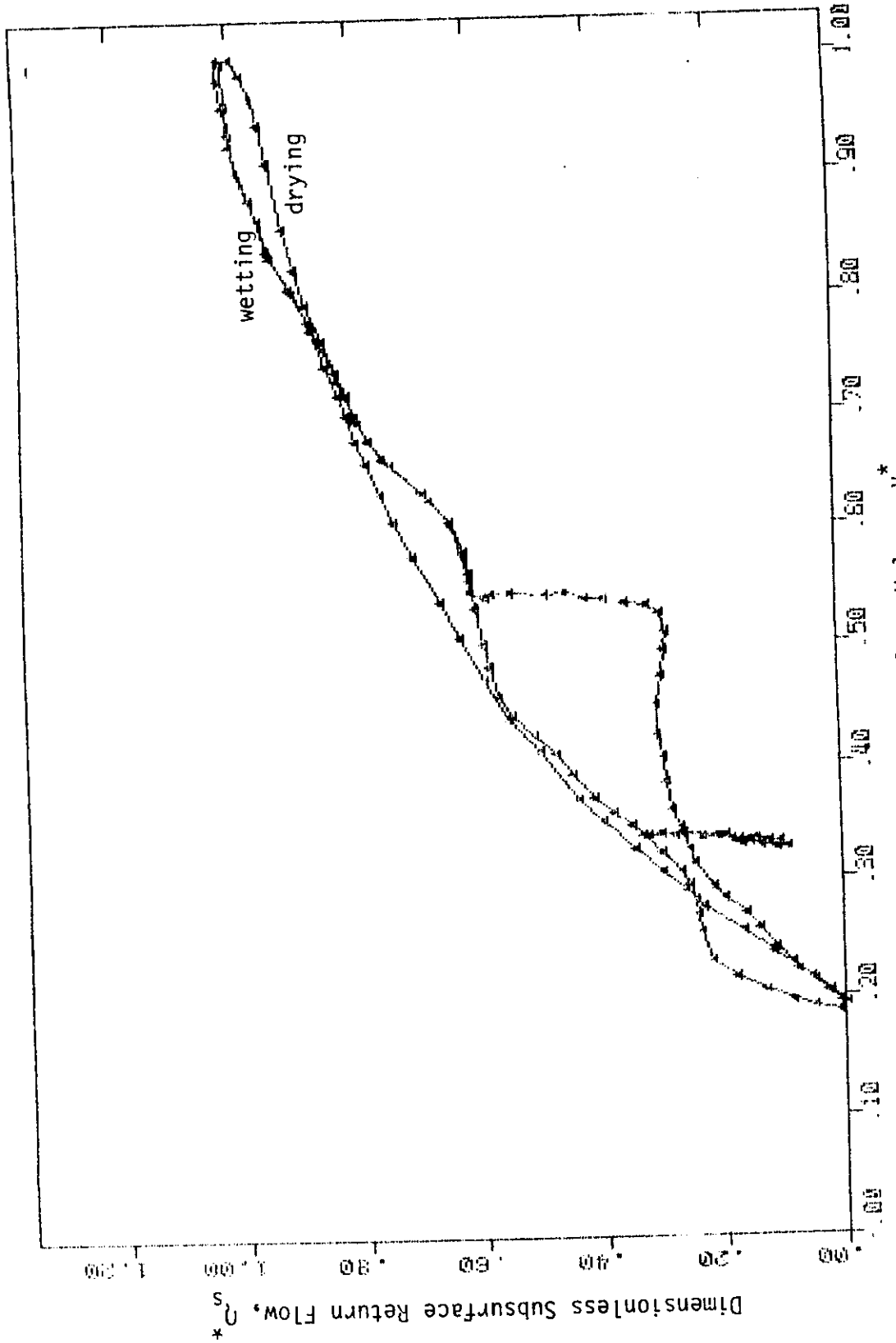

Figure 24. Relationship between Q^*_s and V^* for simulation 6: L^*=30, γ=15 degrees, $\alpha^{1/\beta}$=0.233, β=3.0, N=3.0, q^*=0.10, and homogeneous soil.

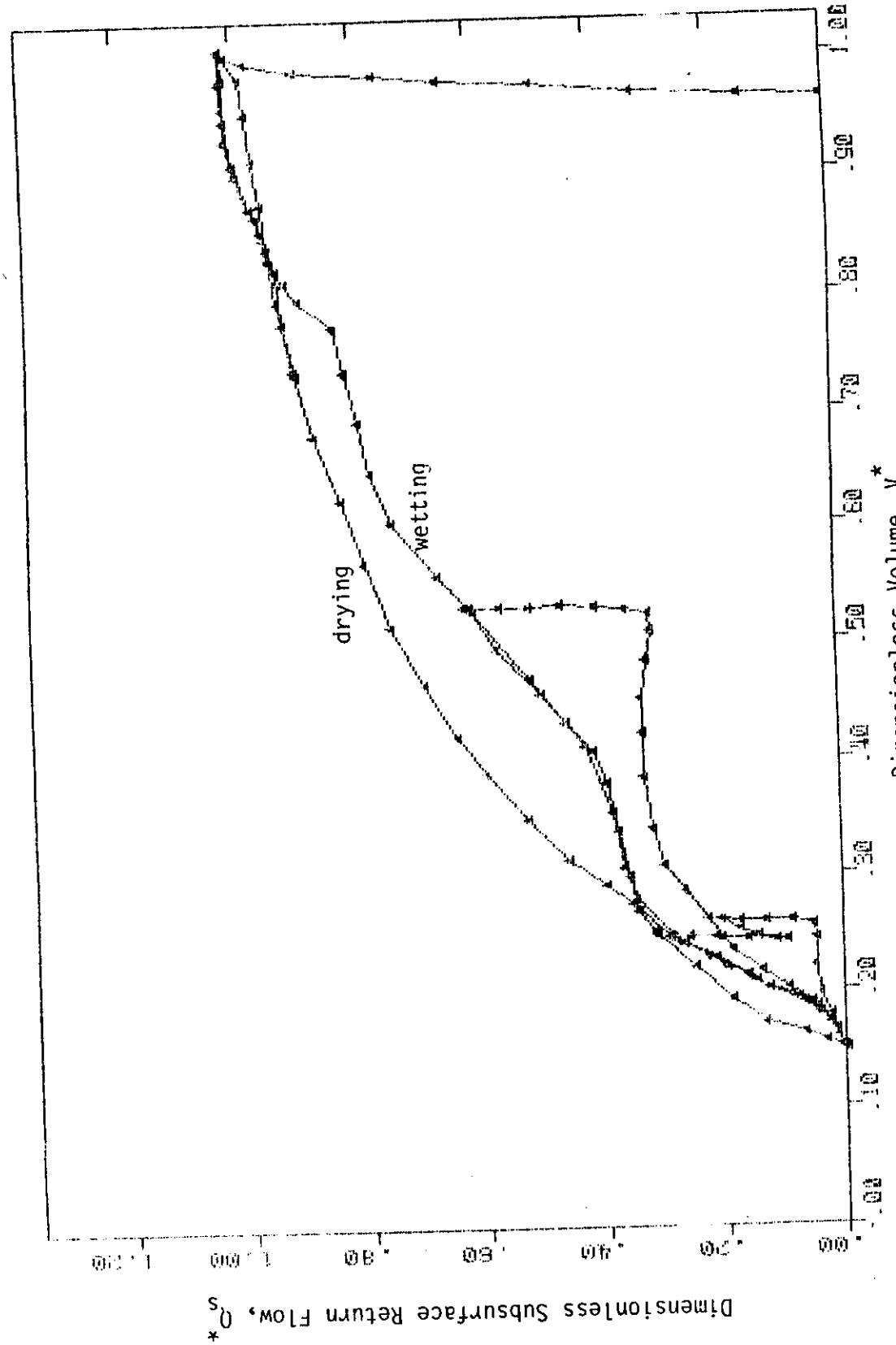

Figure 25. Relationship between Q_s^* and V^* for simulation 7: L^*-50, γ=15 degrees, $\alpha^{1/\beta}$=0.233, β=3.0, N=3.0, q_s^*=0.10, and homogeneous soil.

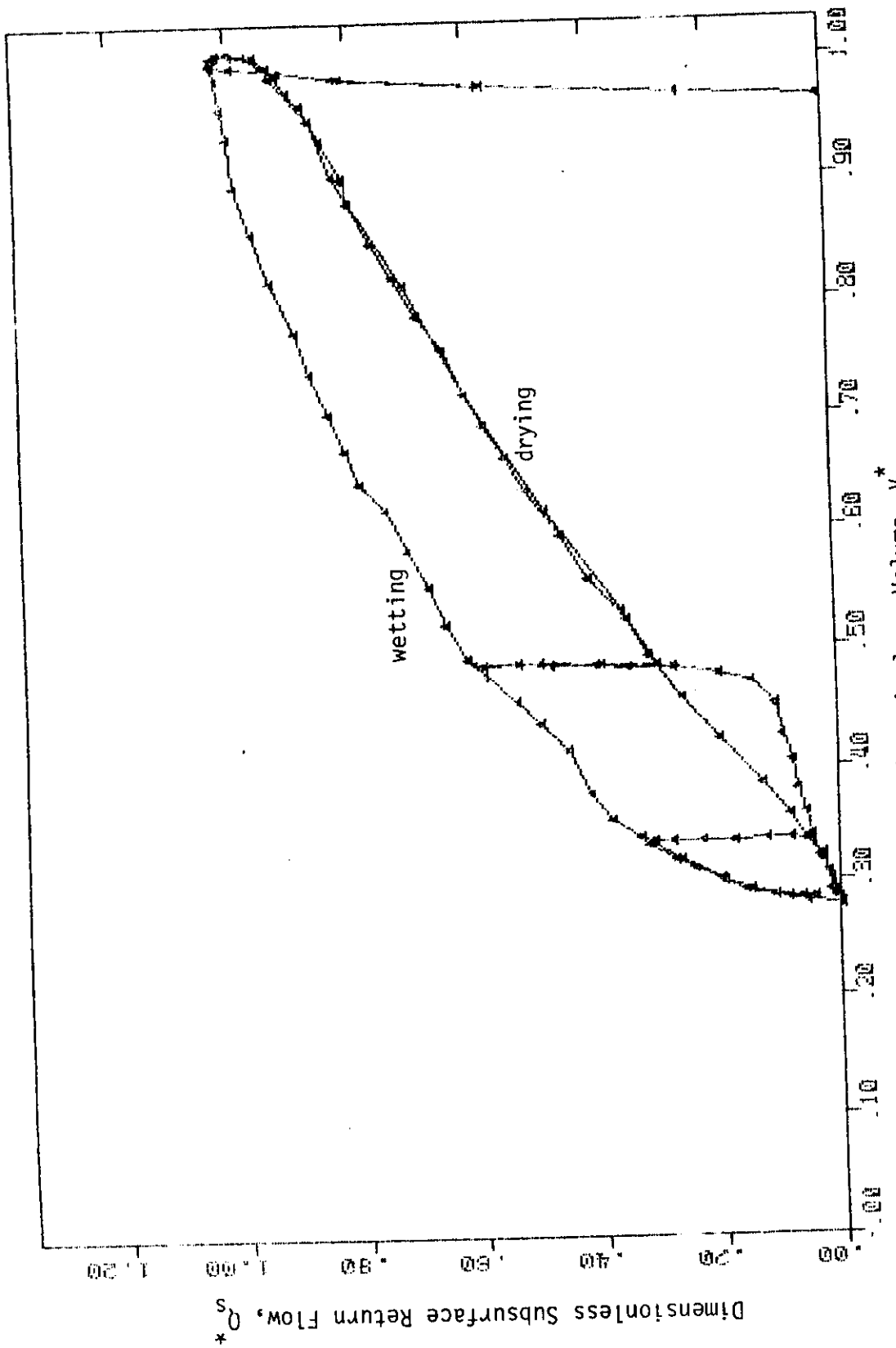

Figure 26. Relationship between Q_s^* and V^* for simulation 8: $L^*=20$, $\gamma=15$ degrees, $\alpha^{1/\beta}=0.464$, $\beta=3.0$, $N=3.0$, $q^*=0.10$, and homogeneous soil.

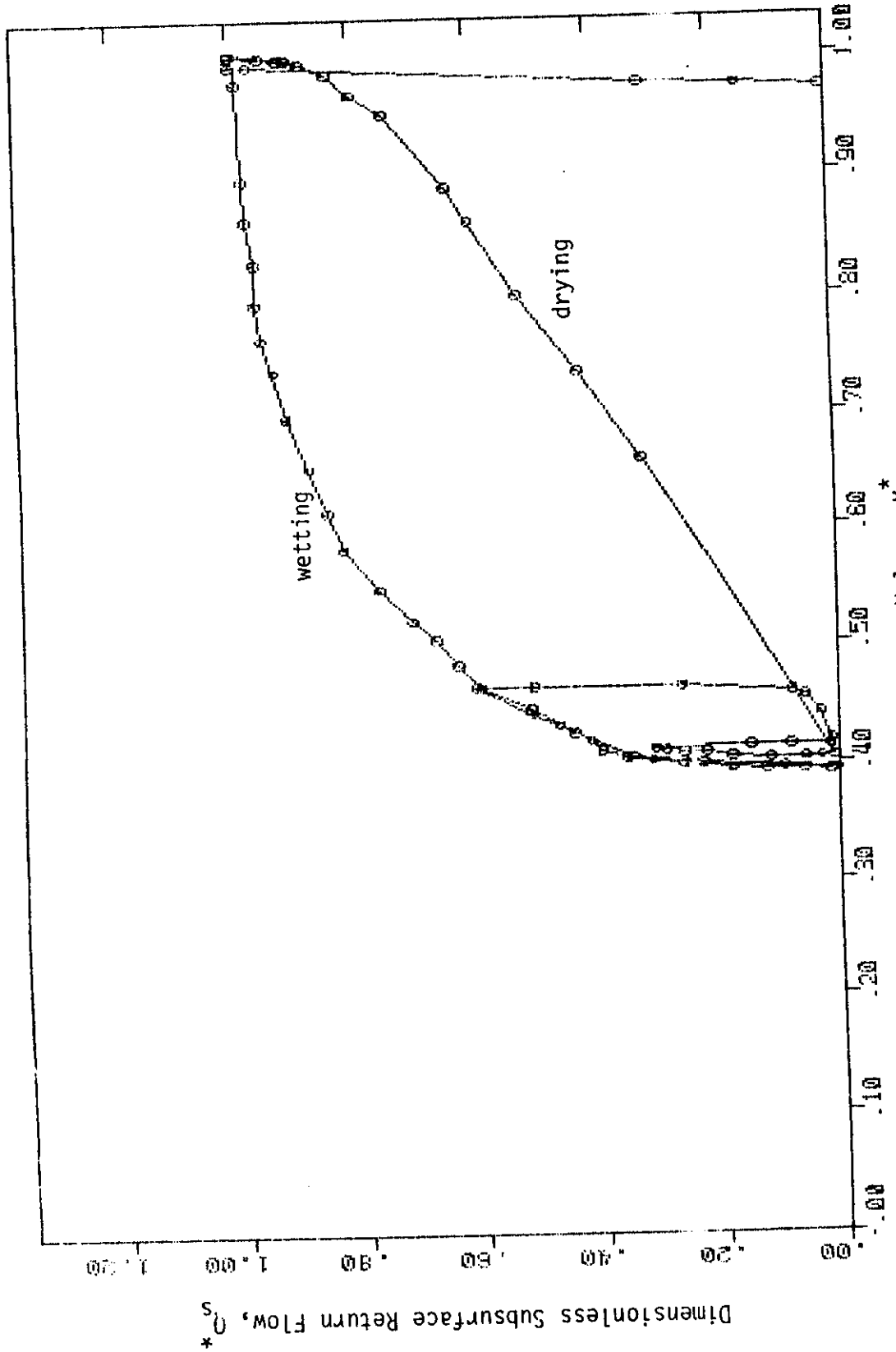

Figure 27. Relationship between Q^*_s and V^* for simulation 9: L^*=20, γ=15 degrees, $\alpha^{1/\beta}$=1.0, β=3.0, N=3.0, q^*=0.10 and homogeneous soil.

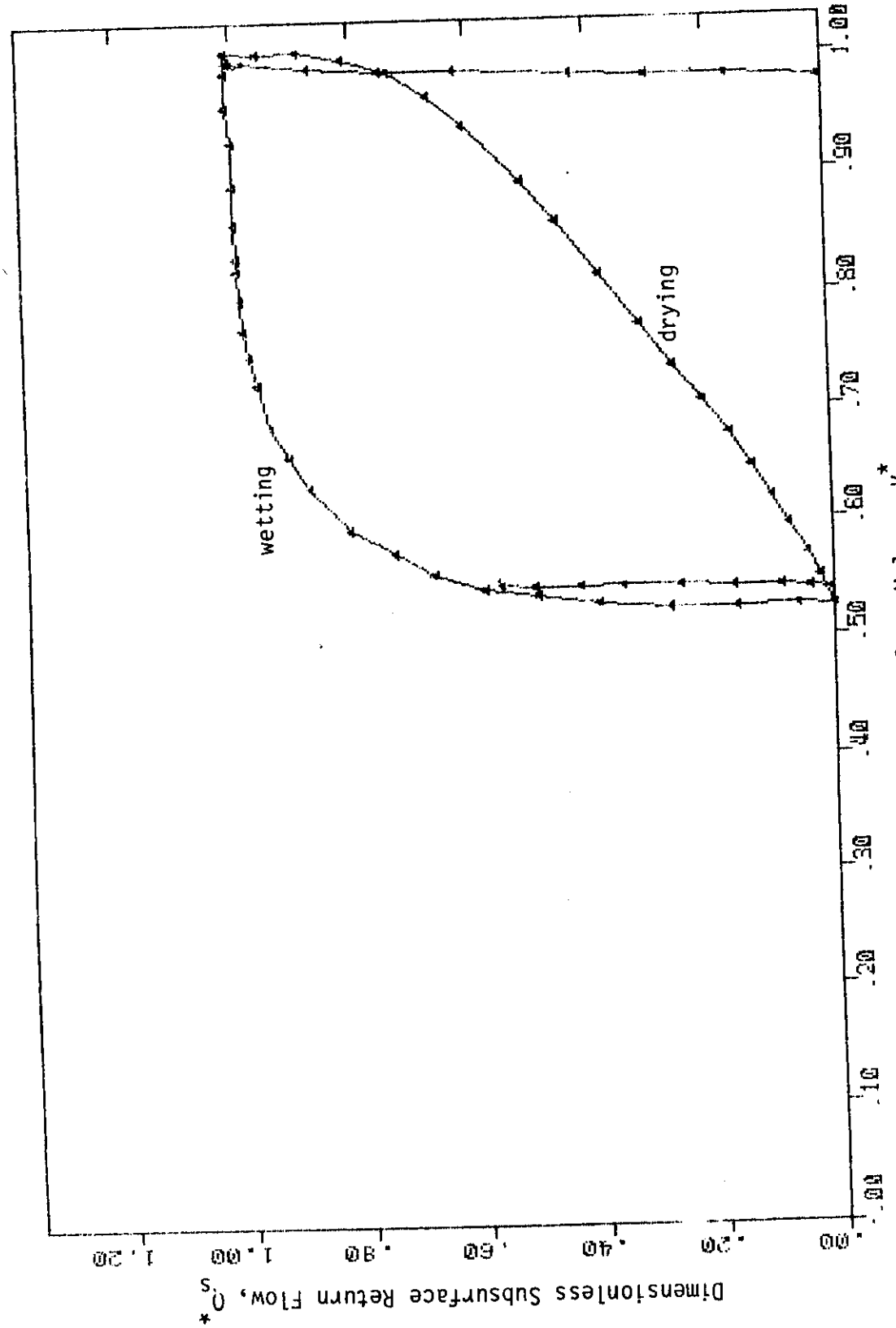

Figure 28. Relationship between Q_s^* and V^* for simulation 10: L^*=20, γ=15 degrees, $\alpha^{1/\beta}$=1.71, β=3.0, N=3.0, q_s^*=0.10, and homogeneous soil.

major drying curve loop becomes wider. It is also apparent that the fraction of total moisture released as subsurface return flow decreases as the $a^{1/\beta}$ parameter increases. As described earlier the $a^{1/\beta}$ parameter is interpreted as the relative measure of the ratio of the capillary fringe thickness to the soil depth. A high value of $a^{1/\beta}$ could correspond to a clay soil with large depth or a gravel with small depth. A small $a^{1/\beta}$ value could correspond to a clay soil with a very large depth (depth large relative to the thickness of the capillary fringe for clay) or a gravel with a medium depth. Figures 19 and 26-28 demonstrate that as the $a^{1/\beta}$ parameter (relative ratio of capillary fringe thickness to soil depth) increases an increasing proportion of soil moisture is held in the soil against drainage. Obviously the $a^{1/\beta}$ parameter is a significant factor in determining the Q_s^* vs. V^* relations.

The influence of slope angle is illustrated by comparison of simulations 1, and 11-13 (Figures 19, 29-31). It is apparent by comparing the results of simulations 1 and 11 (Figures 19 and 29) that the slope can have an effect similar to the $a^{1/\beta}$ parameter. As the slope decreases (correspondingly $a^{1/\beta}$ increases) the major drying and wetting curves of the Q_s^* vs. V^* relationship widen with the major wetting curve moving upward and the major drying curve moving downward. For slopes greater than 15° the major wetting curve is displaced to below the major drying curve as seen from Figures 30 and 31. Obviously slope is an important parameter in determining the form of the Q_s^* vs. V^* relationship. This effect of slope is also seen to be true for the case where the $a^{1/\beta}$ parameter is relatively large as seen from

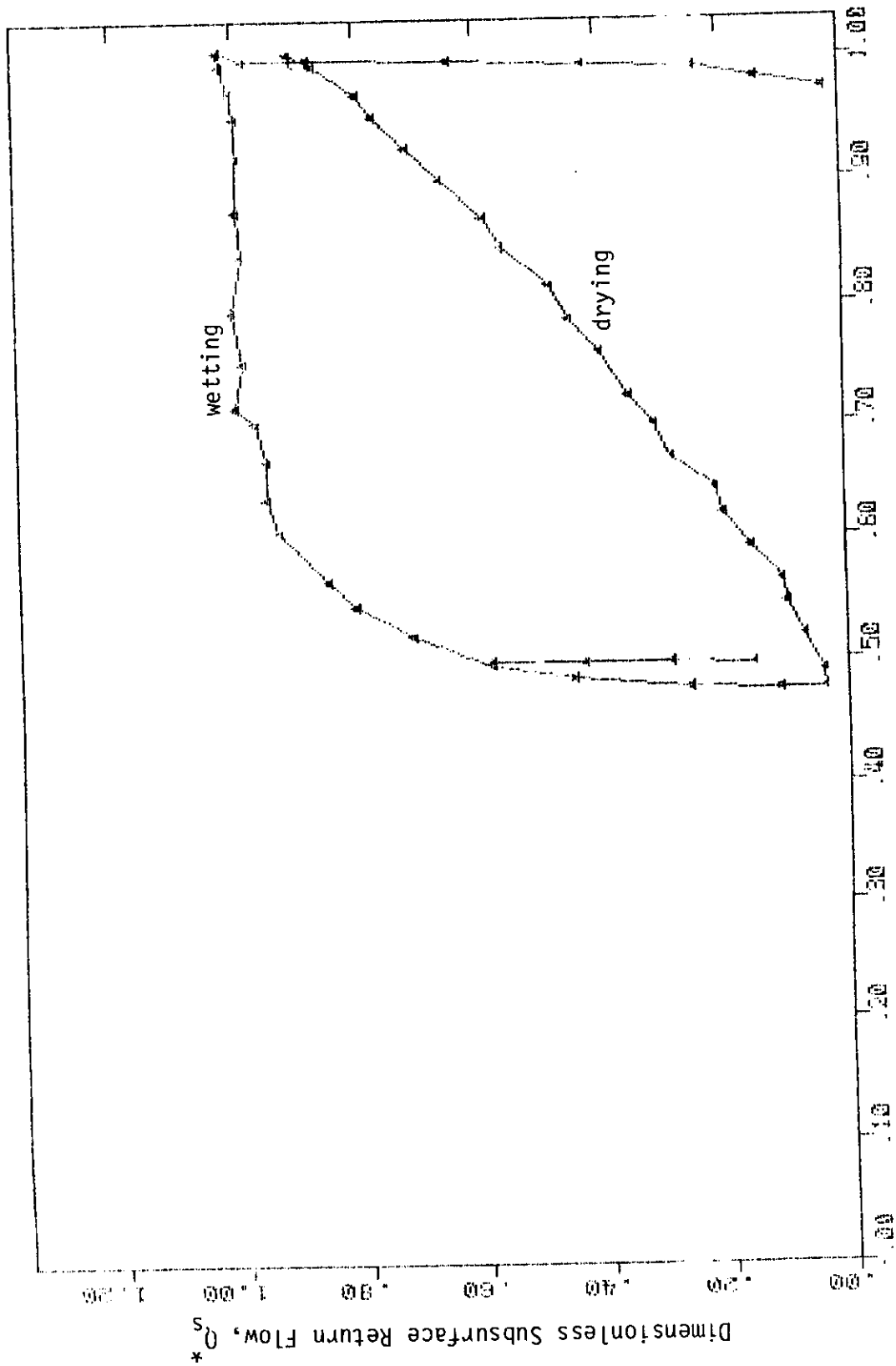

Figure 29. Relationship between Q_s^* and V^* for simulation 11: $L^*=20$, $\gamma=5$ degrees, $\alpha^{1/\beta}=0.233$, $\beta=3.0$, $N=3.0$, $q^*=0.10$, and homogeneous soil.

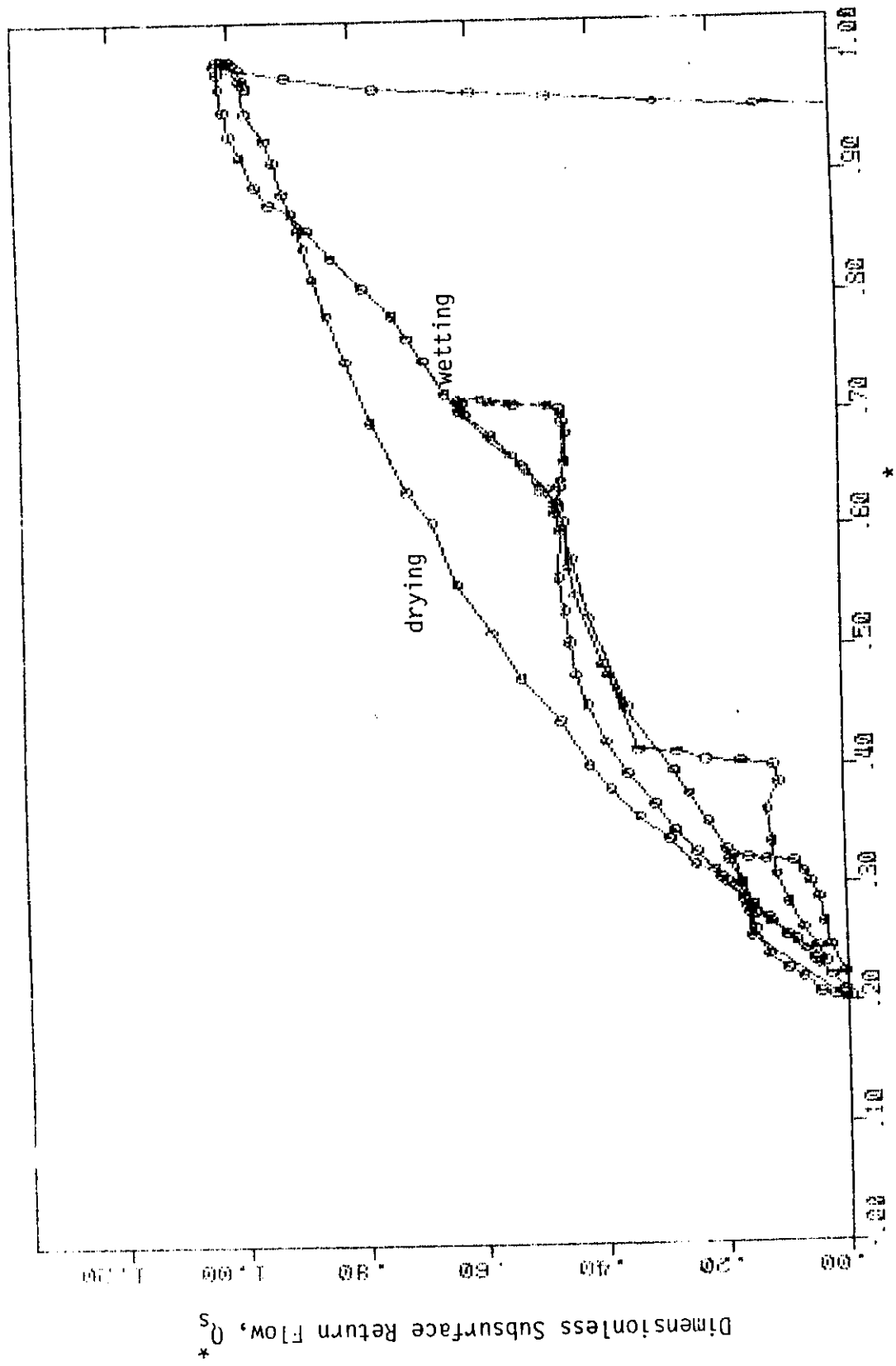

Figure 30. Relationship between Q^*_s and V^* for simulation 12: L^*=20, γ=20 degrees, $\alpha^{1/\beta}$=0.233, β=3.0, N=3.0, q^*=0.10, and homogeneous soil.

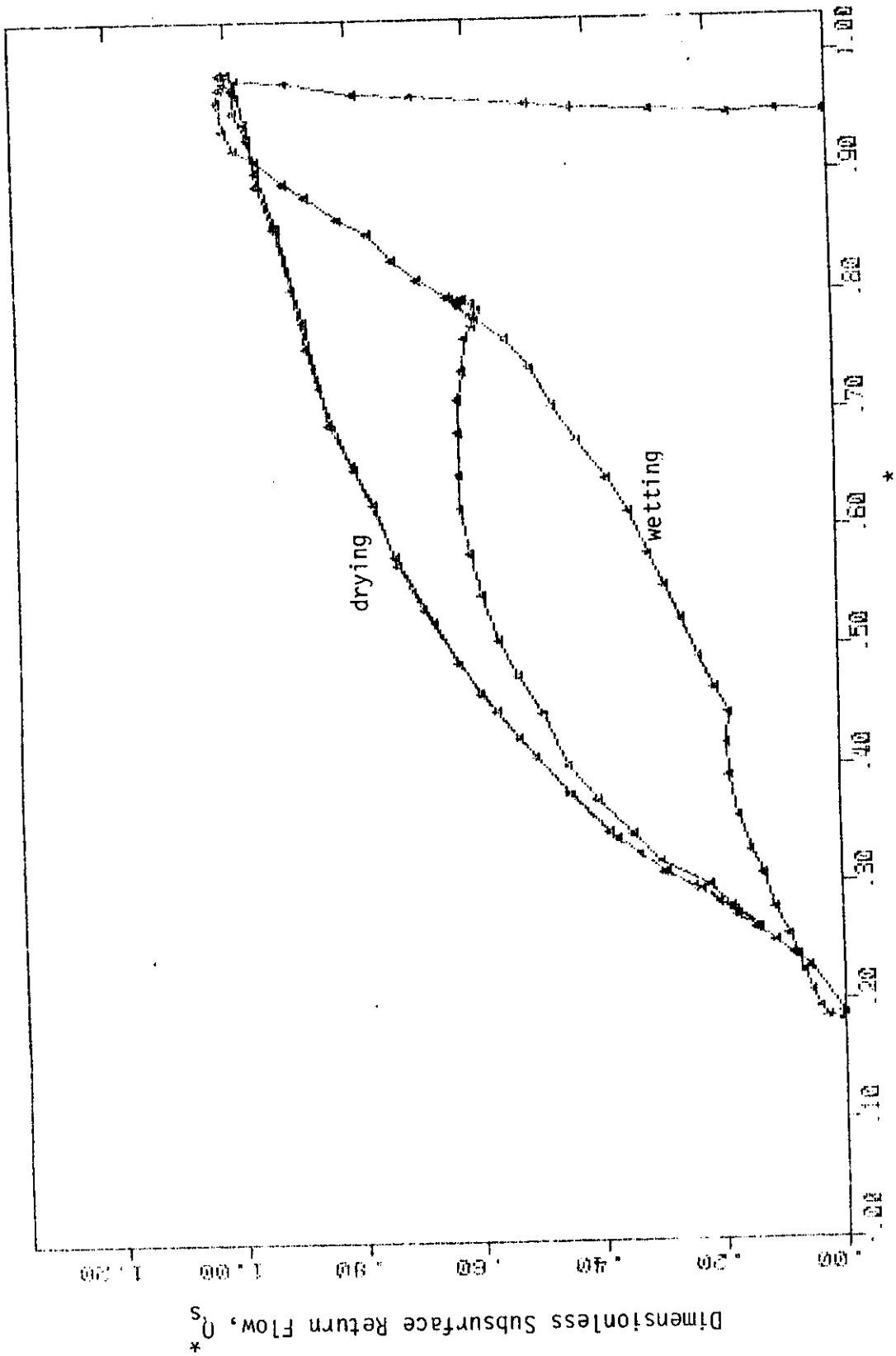

Figure 31. Relationship between Q^*_s and V^* for simulation 13: L^*=20, γ=30 degrees, $\alpha^{1/\beta}$=0.233, β=3.0, N=3.0, q^*=0.10, and homogeneous soil.

comparing the results of simulations 10, 14 and 15 (Figures 28, 32 and 33) It is observed that as the slope angle increases the major wetting and drying curves converge although they never become coincident even for the 30° angle.

The influence of the L^* parameter for conditions of relatively large $a^{1/\beta}$ is demonstrated by comparison of the results from simulations 14, 16, and 17 (Figures 32, 34, and 35). As the L^* parameter increases from 20 to 50 the major wetting and drying curves converge slightly. It appears, though, that the major change that occurs in the Q_s^* vs. V^* relationship is that the relationship stretches over a greater range of the Q_s^* vs. V^* domain.

At a relatively high values of slope angle (30°) and $a^{1/\beta}$ (1.71) the effect of the L^* parameter can be seen by comparing the results of simulations 15, 18, and 19 (Figures 33, 36, and 37). The increase in the L^* parameter causes a slight convergence in the major wetting and drying curves. The most significant effect is that the increase in L^* causes a stretching of the Q_s^* vs. V^* relationship over an increasingly larger portion of the Q_s^* vs. V^* domain.

The errors associated with using a homogeneous soil instead of its equivalent layered soil is illustrated in simulations 20-25. In simulation 20 the layering effect is slight in that the soil constant A increased with depth at the constant rate of 10%. The result of simulation 20 is illustrated in Figure 38 and the equivalent homogeneous case (simulation 21) is illustrated in Figure 39. Comparison of the two results shows the layered case to have a slightly

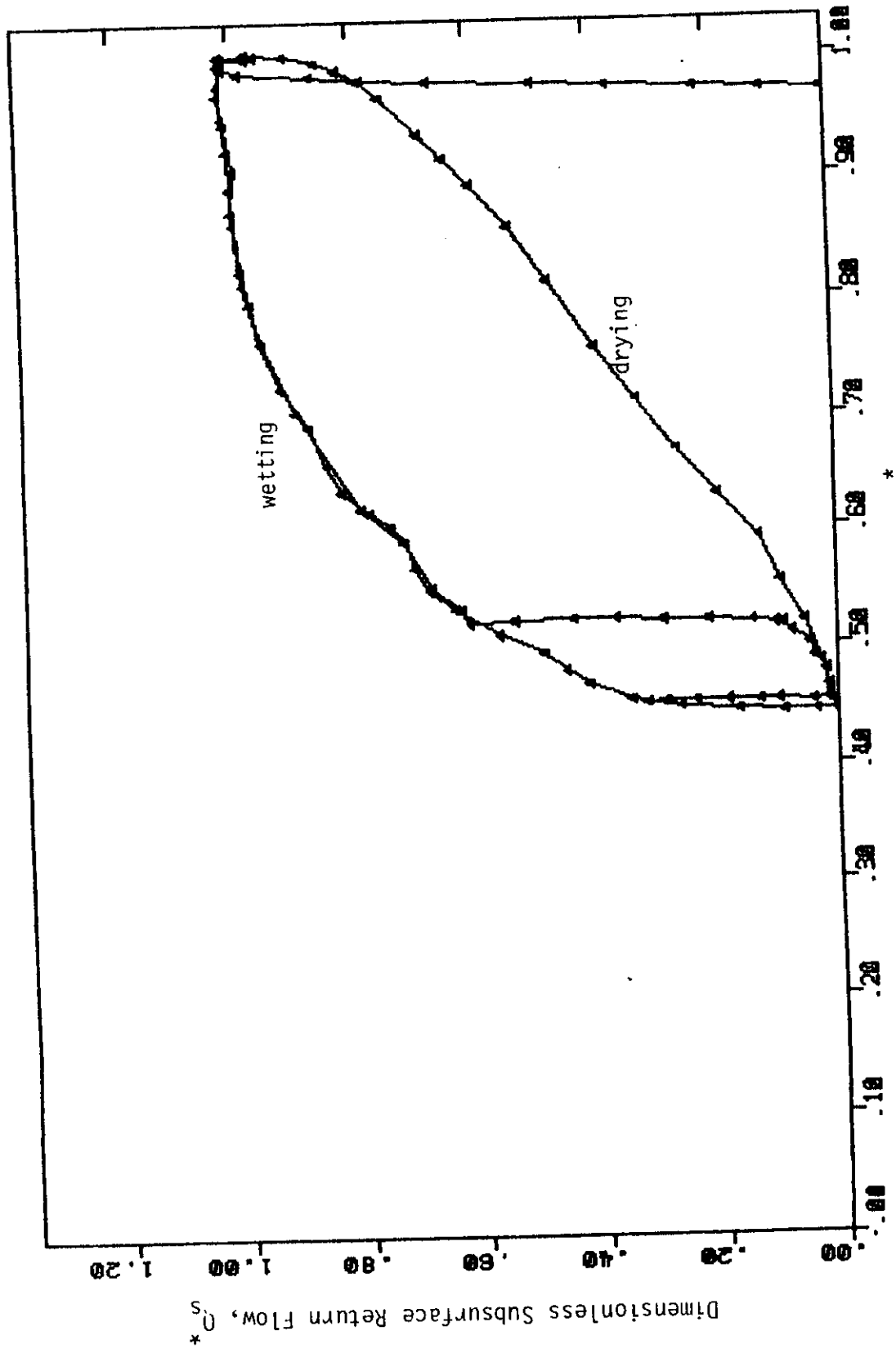

Figure 32. Relationship between Q_s^* and V^* for simulation 14: $L^*=20$, $\gamma=20$ degrees, $\alpha^{1/\beta}=1.71$, $\beta=3.0$, $N=3.0$, $q^*=0.10$, and homogeneous soil.

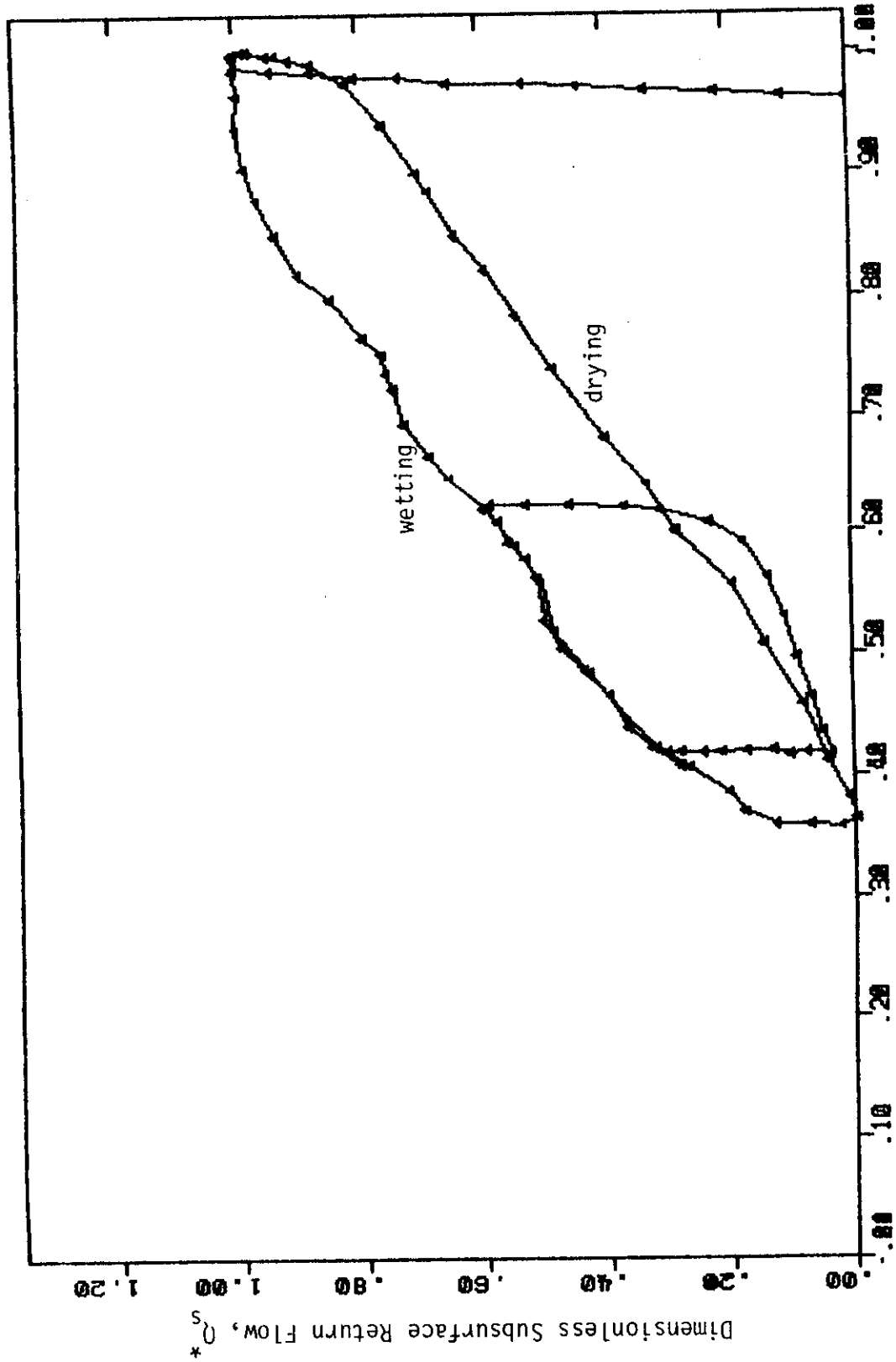

Figure 33. Relationship between Q_s^* and V^* for simulation 15: $L^*=20$, $\gamma=30$ degrees, $\alpha^{1/\beta}=1.71$, $\beta=3.0$, $N=3.0$, $q^*=0.10$, and homogeneous soil.

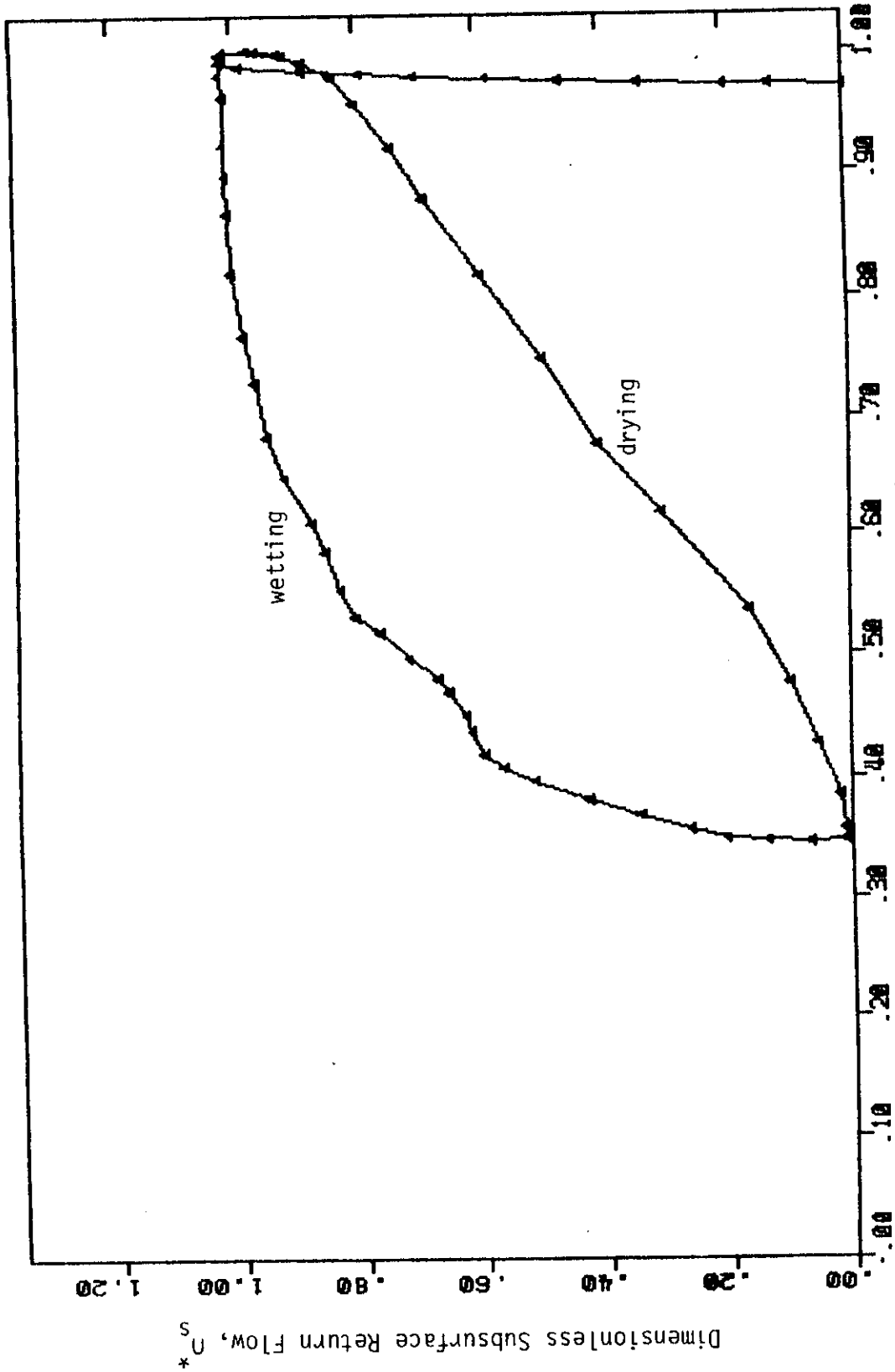

Figure 34. Relationship between Q_s^* and V^* for simulation 16: L^*=30, γ=20 degrees, $\alpha^{1/\beta}$=1.71, β=3.0, N=3.0, q^*=0.10, and homogeneous soil.

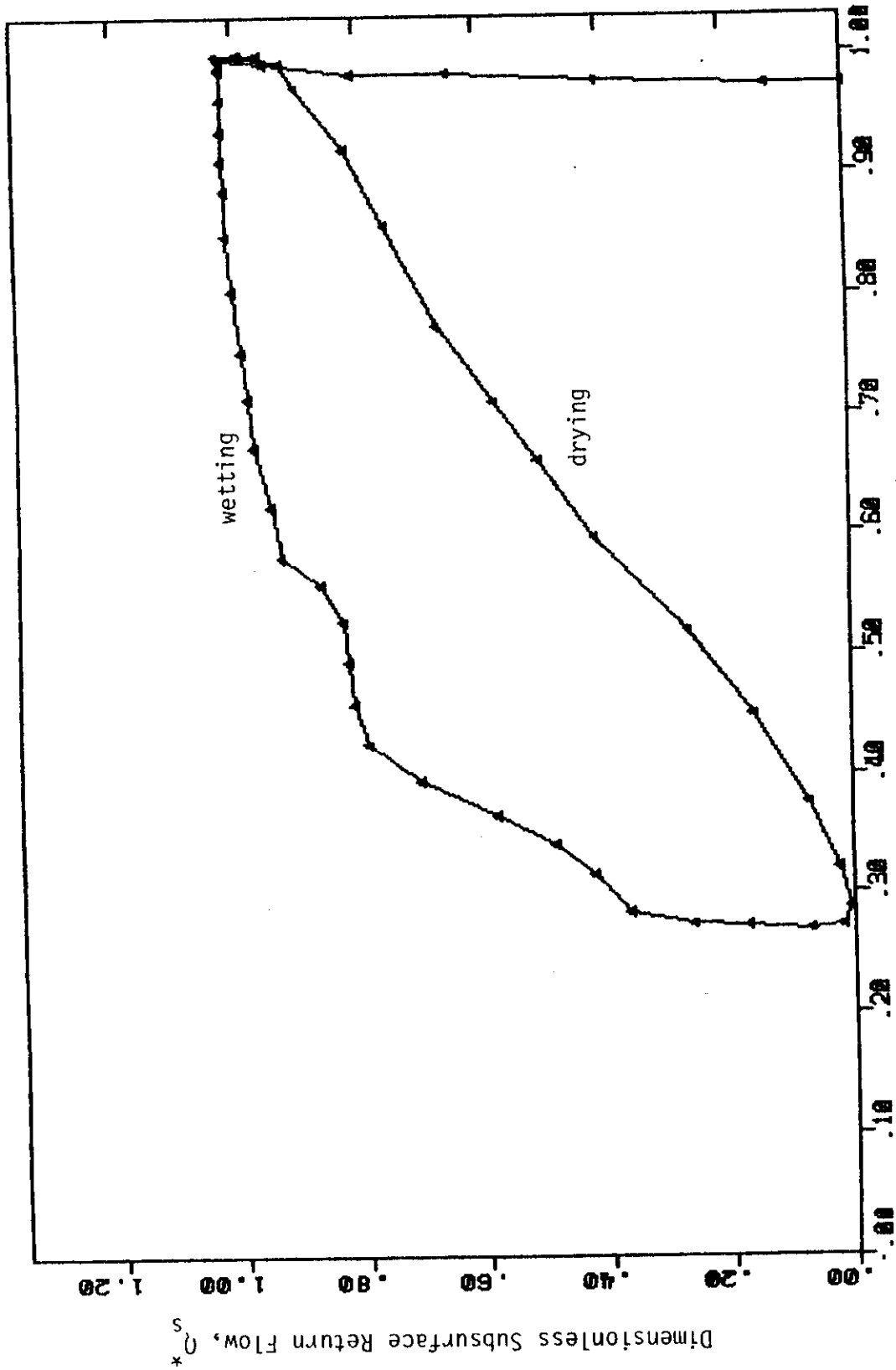

Figure 35. Relationship between Q_s^* and V^* for simulation 17: L^*=50, γ=20 degrees, $\alpha^{1/\beta}$=1.71, β=3.0, N=3.0, q^*=0.10, and homogeneous soil.

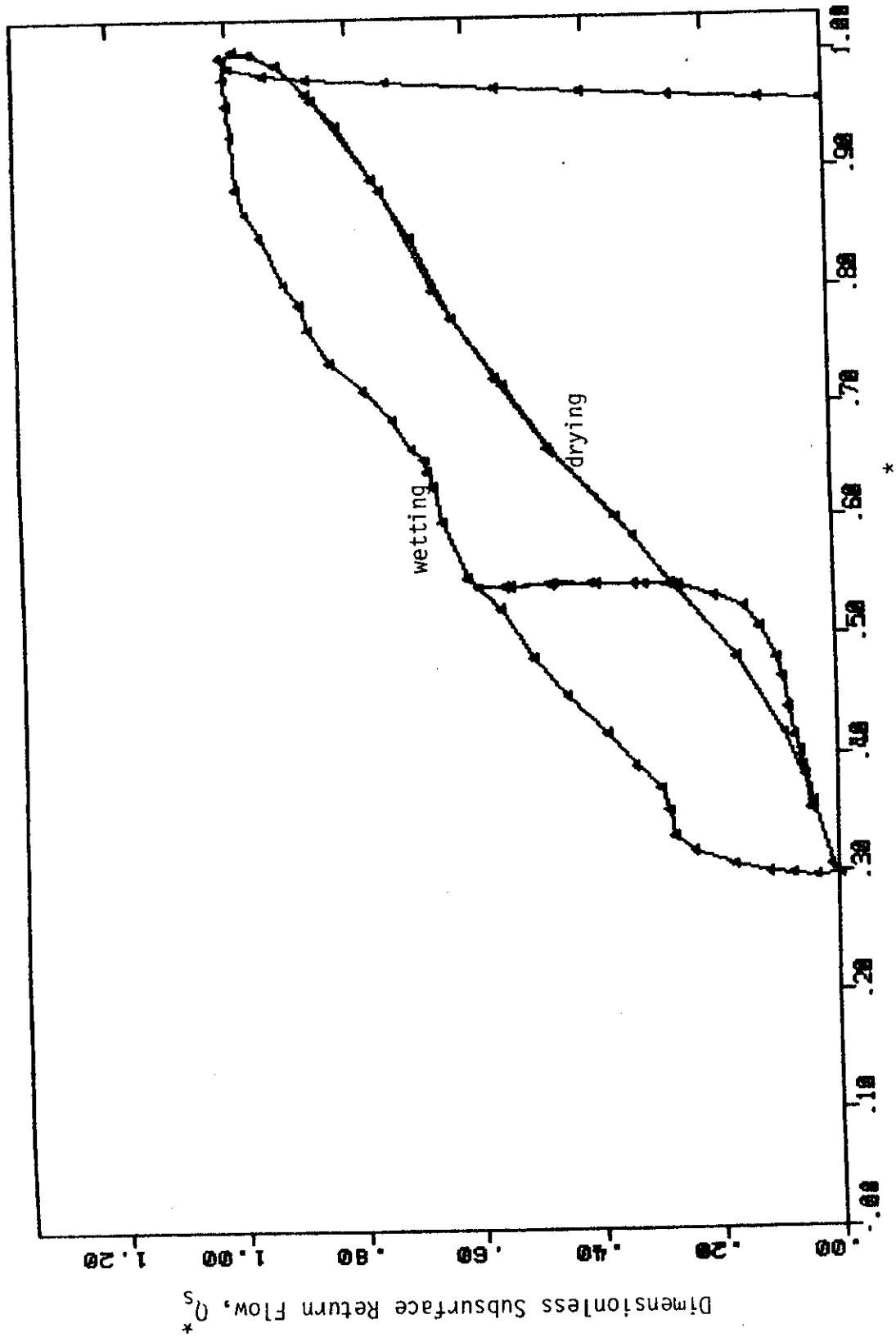

Figure 36. Relationship between Q_s^* and V^* for simulation 18: $L^*=30$, $\gamma=30$ degrees, $\alpha^{1/\beta}=1.71$, $\beta=3.0$, $N=3.0$, $q^*=0.10$, and homogeneous soil.

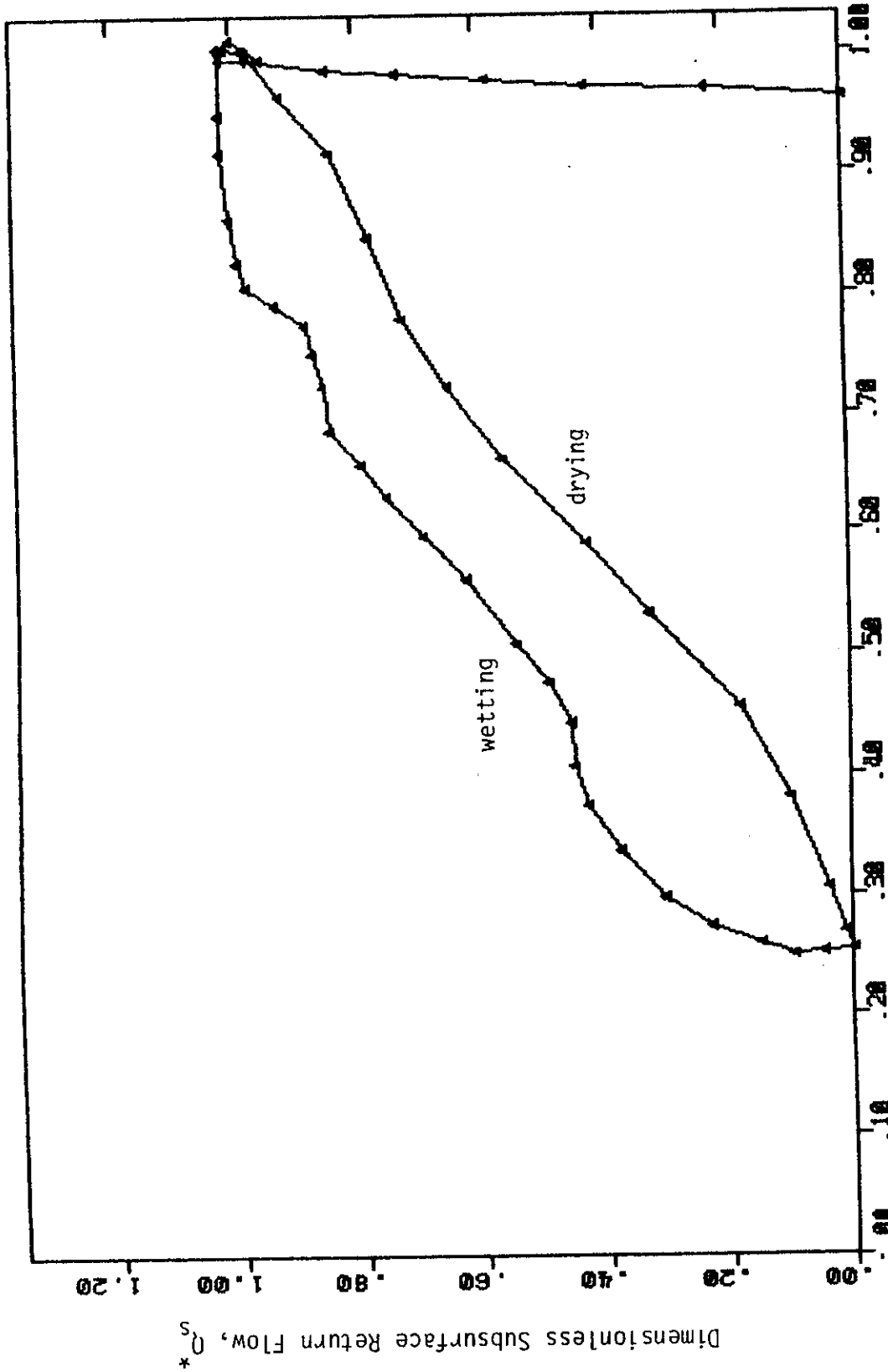

Figure 37. Relationship between Q_s^* and V^* for simulation 19: L^*=50, γ=30 degrees, $\alpha^{1/\beta}$=1.71, β=3.0, N=3.0, q_s^*=0.10, and homogeneous soil.

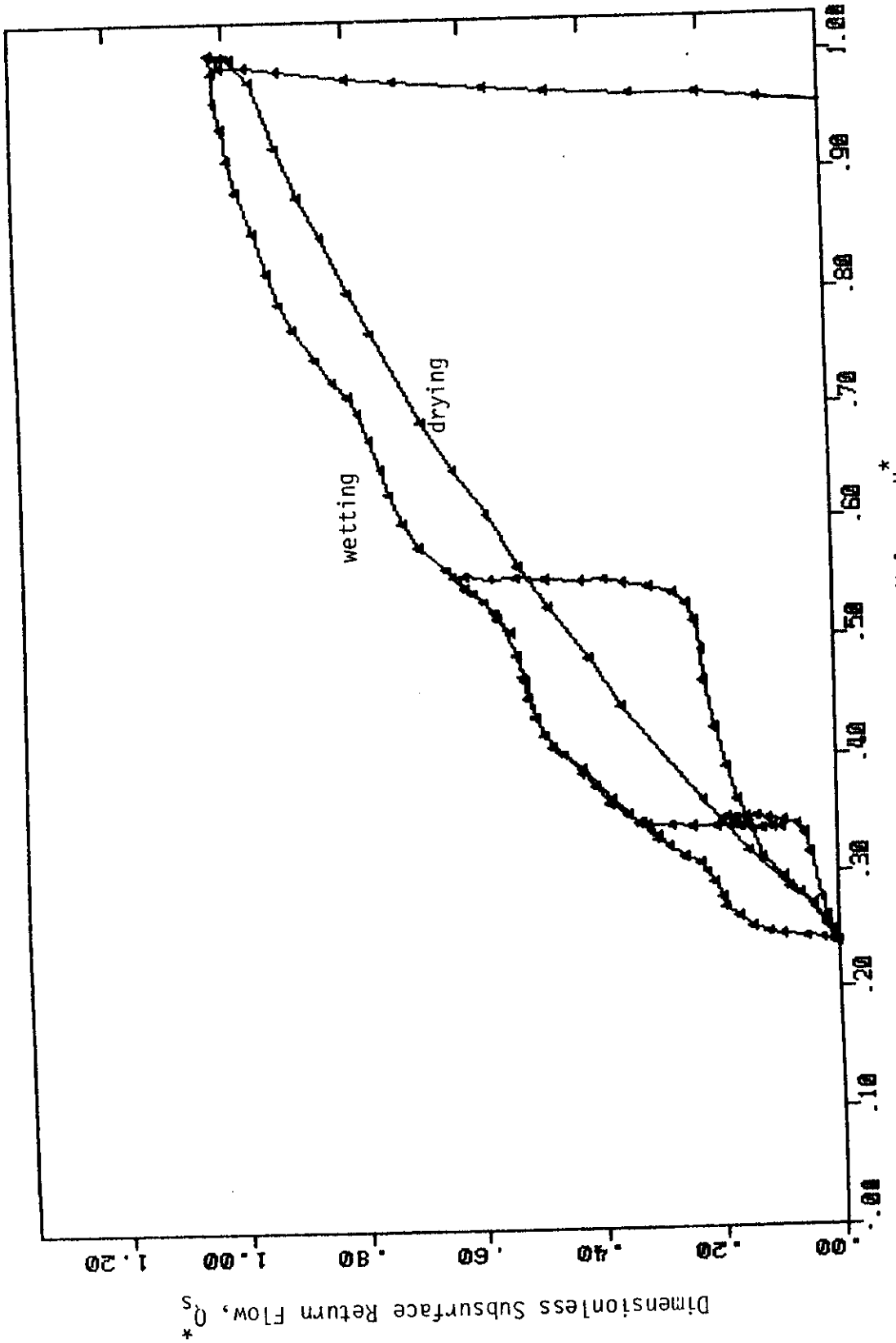

Figure 38. Relationship between Q_s^* and V^* for simulation 20: L^*=20, γ=15 degrees, β=3.0, N=3.0, q^*=0.10, and layered soil (10 layers) with the value of α for each layer being 0.10 greater than the layer immediately above it.

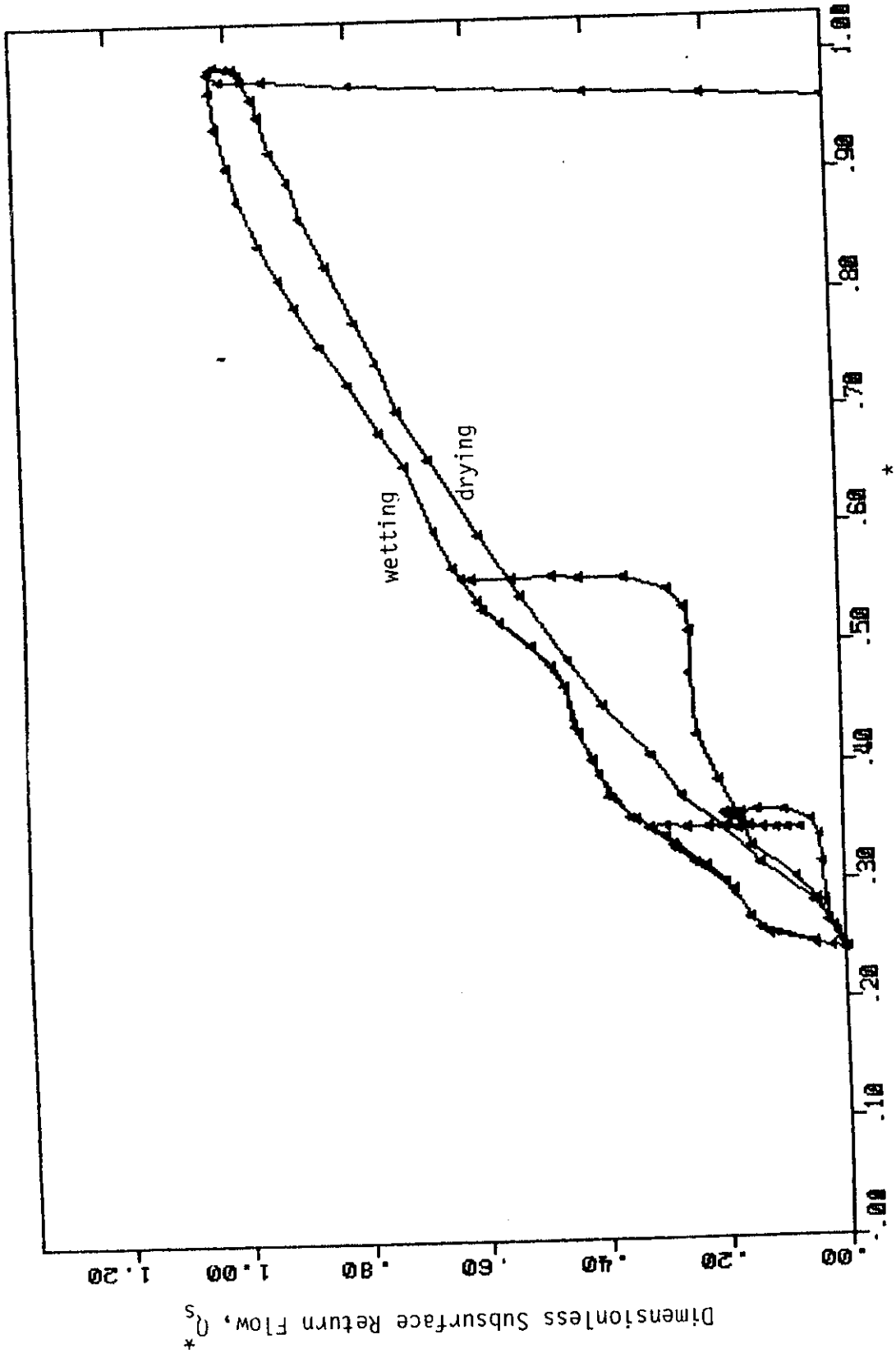

Figure 39. Relationship between Q_s^* and V^* for simulation 21; L^*=20, γ=15 degrees, β=3.0, N=3.0, q^*=0.10, and homogeneous soil with an $\frac{\alpha}{i}^{1/\beta}$ equivalent to the layered condition where the α parameter increased by 0.10 for each deeper layer.

wider Q_s^* vs. V^* loop than the equivalent homogeneous case, but the relationships are otherwise very similar.

For simulations 22 and 23 (Figures 40 and 41) where the A value increased by a constant rate of 20% with depth the layered case has a significantly wide Q_s^* vs. V^* loop than the equivalent homogeneous case. However, the two relationships have similar form. The major difference between the two relationships is in the main drying curve since the main wetting curves hold similar positions on the graph.

Finally, for the condition where the A value increases at a constant rate of 40% with depth into the soil profile (simulations 24 and 25) the results are presented in Figures 42 and 43. The major wetting curves appear to be quite similar here as they were for the 10% and 20% conditions, but the major drying curves deviate from each other even more than observed previously.

It appears that when the soil has significant layering as defined in the conditions imposed for simulations 20, 22, and 24 the use of an equivalent homogeneous case will be accurate enough for the major wetting cycle, but the major drying cycle will be over predicted. The purpose for the comparison of the layered case and its equivalent homogeneous case was to determine whether layering could be eliminated as a parameter in the development of dimensionless curves. Apparently it is not completely possible to do so because of the discrepancy in major drainage curves. It may be that the incorporation of anisotropy in the two-dimensional model would improve the simulation of the layered case with an equivalent homogeneous anisotropic condition. The

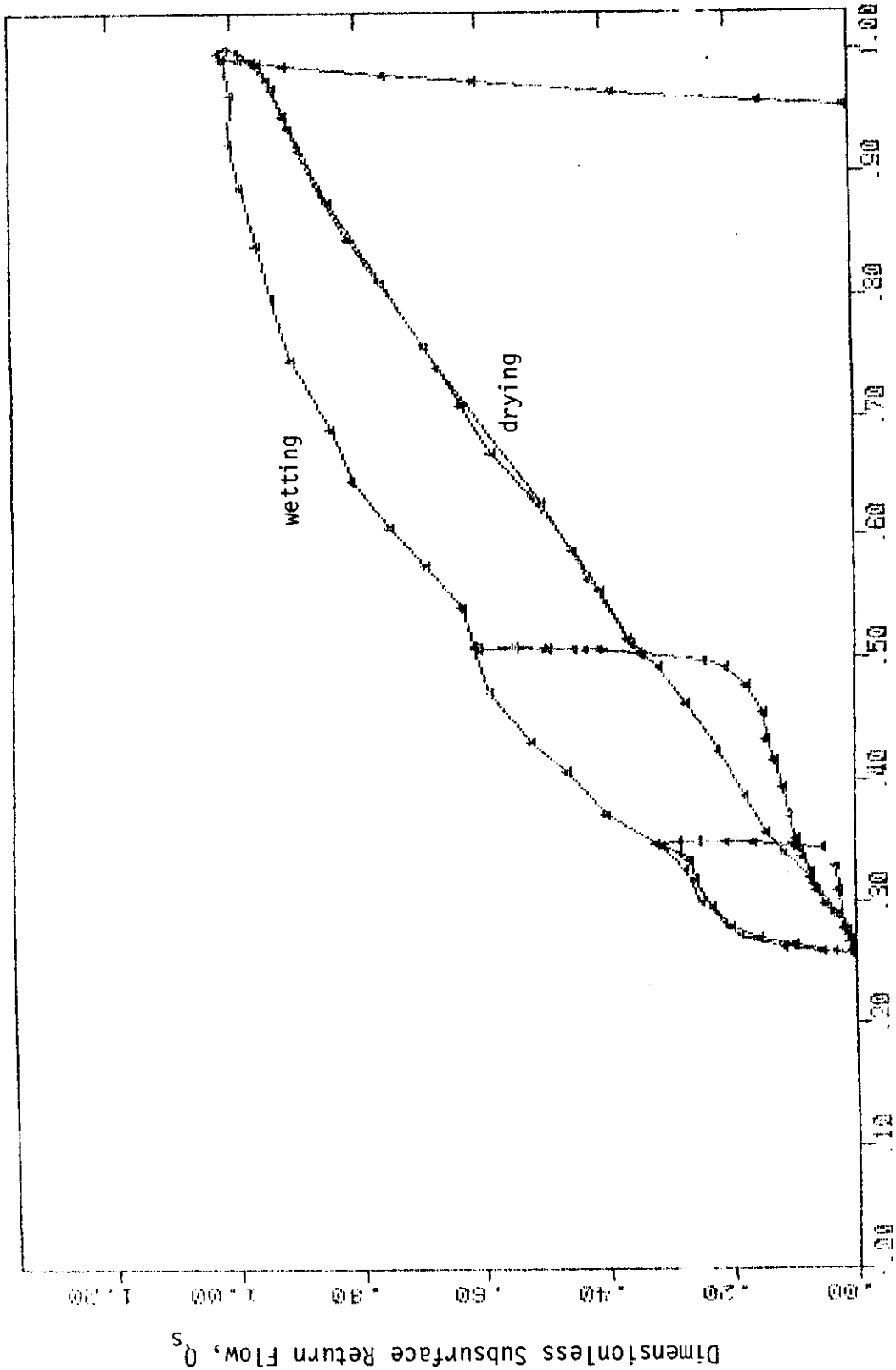

Figure 40. Relationship between Q_s^* and V^* for simulation 22: L^*=20, γ=15 degrees, β=3.0, N=3.0, q^*=0.10, and layered soil (10 layers) with the value of α for each being 0.20 greater than the layer immediately above it.

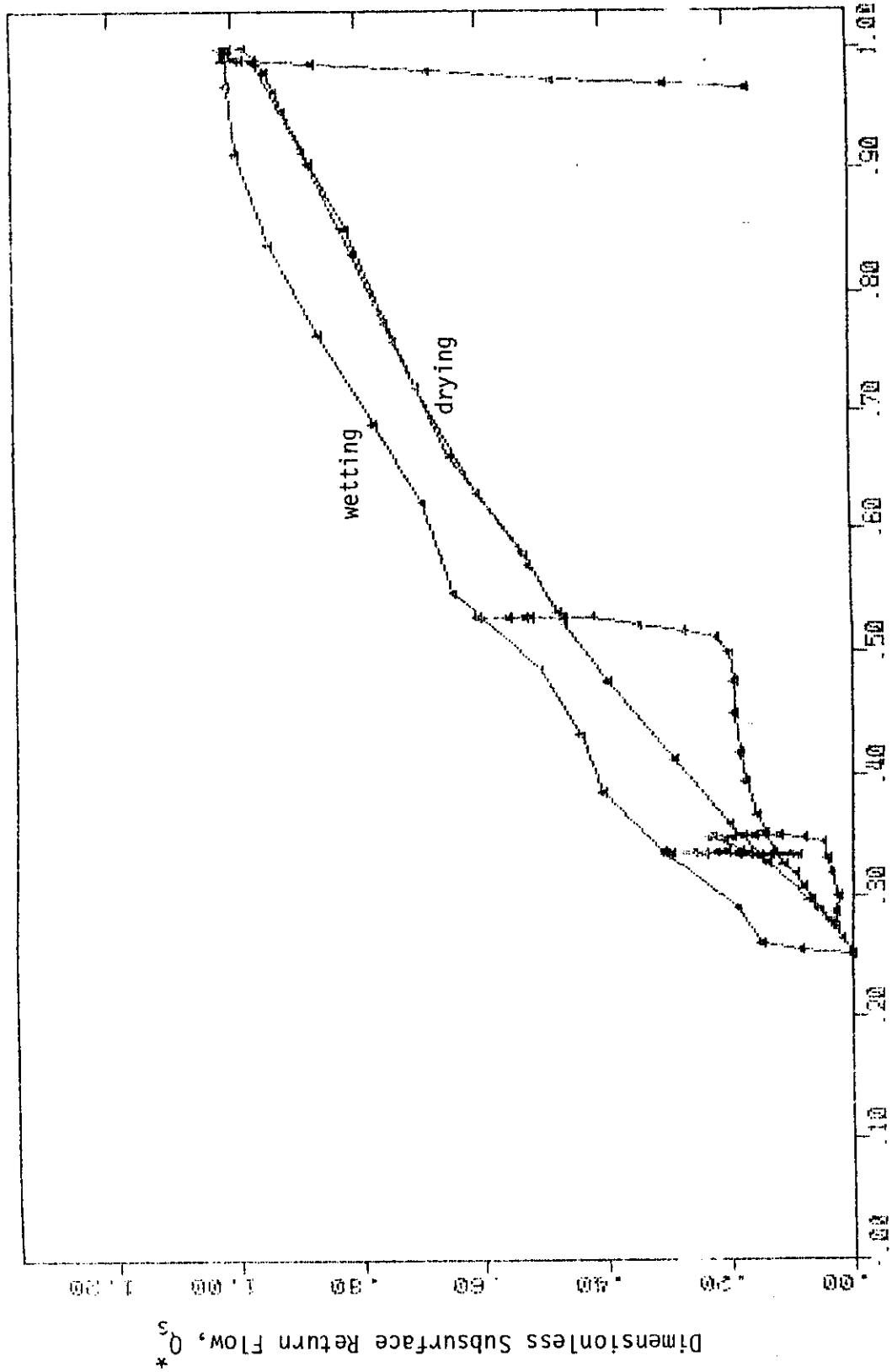

Figure 41. Relationship between Q_s^* and V^* for simulation 23: L^*=20, γ=15 degrees, β =3.0, N=3.0, and homogeneous soil with an $\alpha^{1/\beta}$ equivalent to the layered condition where the α parameter increased by 0.20 for each deeper layer.

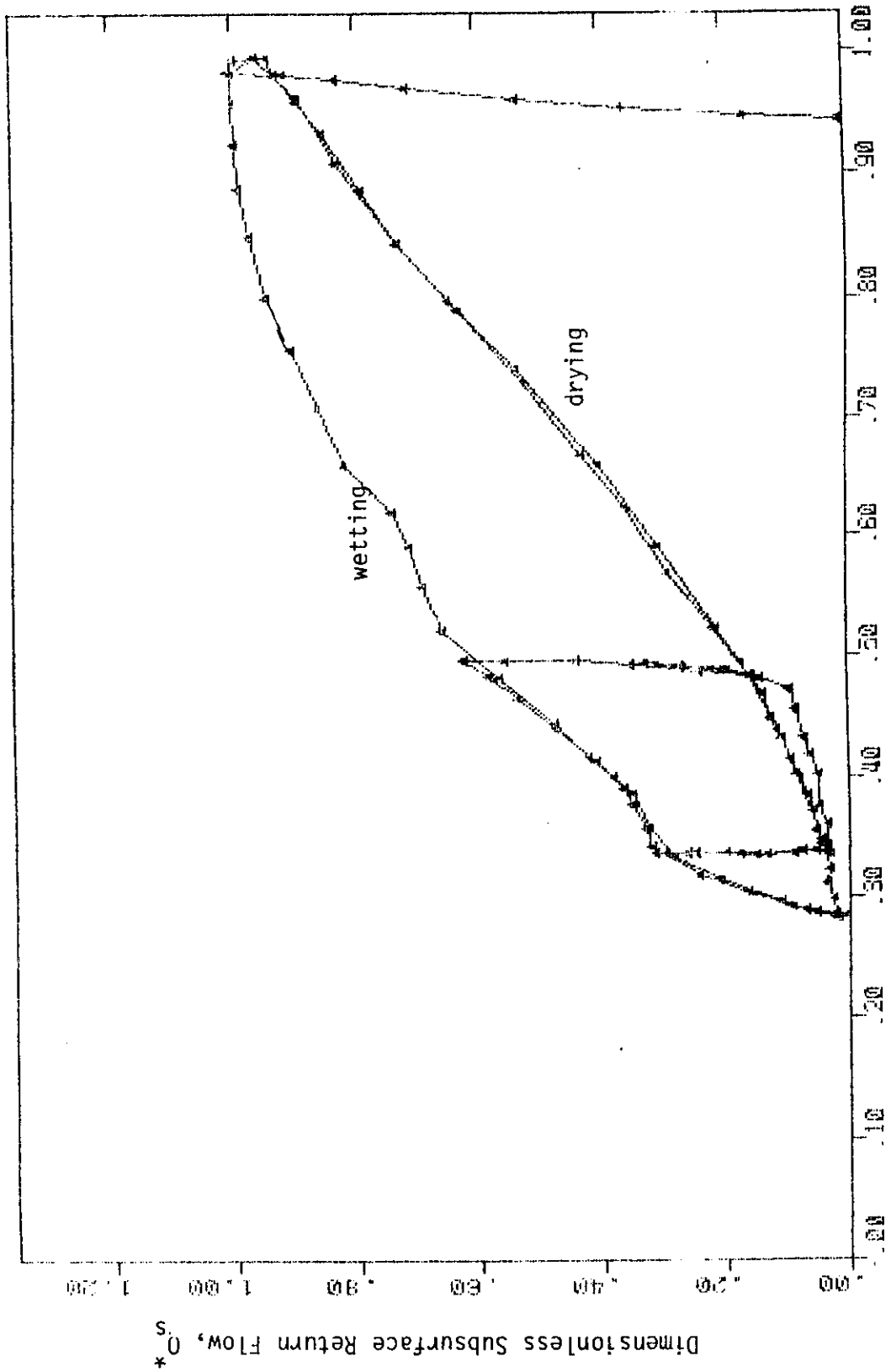

Figure 42. Relationship between Q_s^* and V^* for simulation 24: L^*=20, γ=15 degrees, β=3.0, N=3.0, q^*=0.10, and layered soil (10 layers) with the value of α for each layer being 0.40 greater than the layer immediately above it.

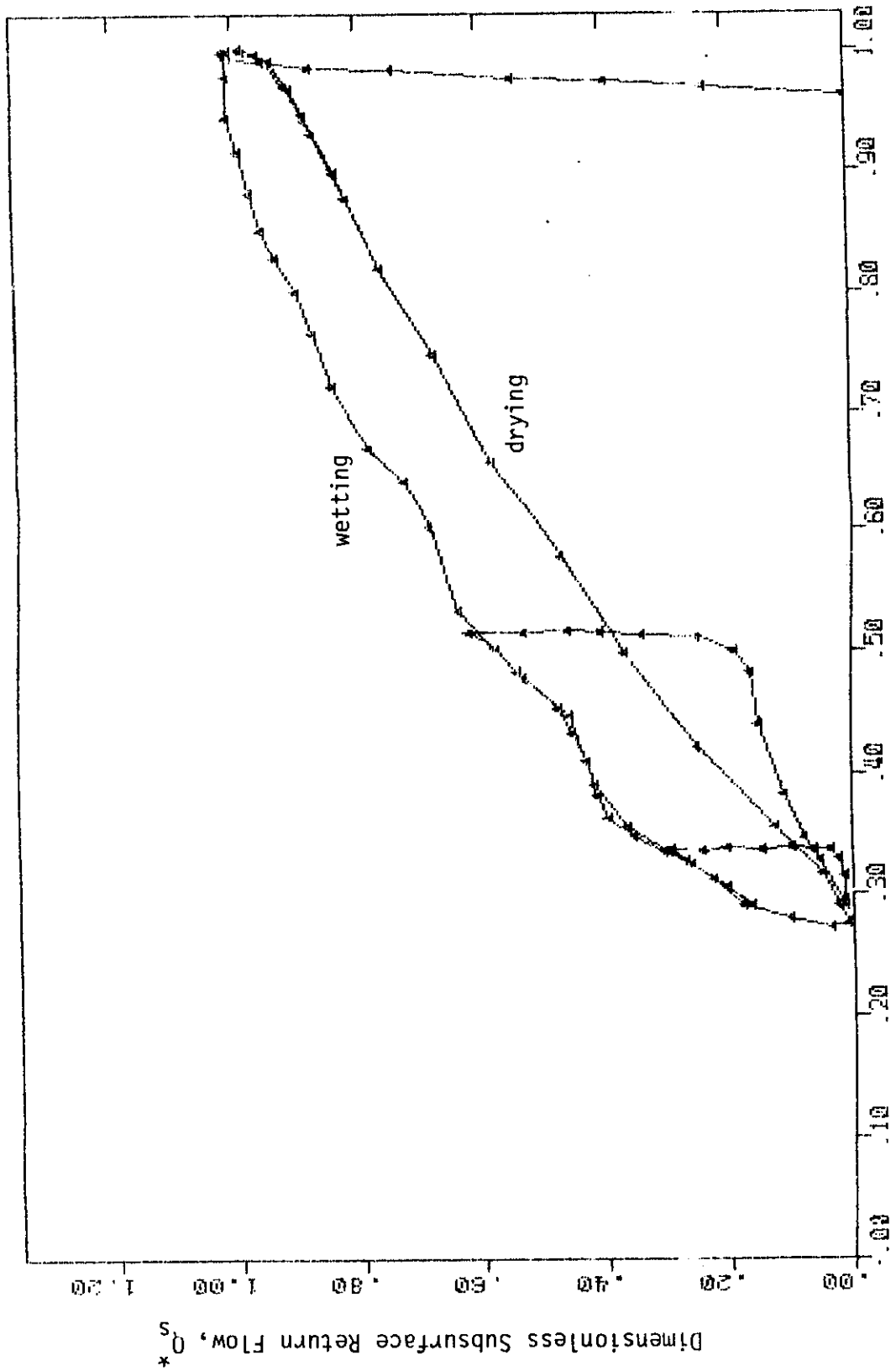

Figure 43. Relationship between Q_s^* and V^* for simulation 25; L^*=20, γ=15 degrees, β=3.0, N=3.0, q^*=0.10, and homogeneous soil with an α/β equivalent to the layered condition where the α parameter increased by 0.40 for each deeper layer.

principal directions of anisotropy would be taken normal to and parallel to the slope.

The results of the two-dimensional solutions presented have demonstrated that there is a set of Q_s^* vs. V^* curves useful in the determination of subsurface return flow controlled by moisture storage. The form of the curves is rather simple and can be readily used in water balance models requiring calculations of the subsurface return flow component of runoff generation.

In a hydrologic modeling study Beven and Kirkby(1979) developed a simple physically-based model of watershed hydrology. In this model the subsurface runoff component was represented by mathematical expressions that considered the variable-source area phenomenon on hillslopes. Required input to this subsurface runoff model was the relationship between subsurface discharge rate and the volume of moisture stored in the soil profile. Beven and Kirkby(1979) presented graphs for the Crimple Beck catchment(Yorkshire, England) which illustrated this relationship. The graphs were derived using watershed discharge measured during rainless periods. The relative volume of moisture stored in the soil profile corresponding to a given discharge rate was estimated from the measured discharges. Due to the lack of resolution of measurements, that is the measurements were on the catchment scale, a hysteresis loop in the subsurface flow-moisture storage relationship was not identified but the form of the curves derived were similar in nature to those presented in this report. It is felt that the subsurface return flow relationships derived in this report could be

useful in deriving the required input for the model presented by Beven and Kirkby(1979) for ungaged catchments. The next step in the research process will be to see whether this can be done for gaged catchments.

Chapter 5

SUMMARY AND CONCLUSIONS

The Richards equation which governs the flow of an incompressible fluid in an incompressible porous medium was used to investigate the characteristics of the percolation process in flat deep soil profiles and the subsurface return flow process in sloping shallow soil profiles. The one-dimensional form of the Richards equations was used for the percolation problem and the two-dimensional form of the Richards equation was used for the subsurface return flow problem. Appropriate boundary and initial conditions were applied for each problem. The governing equations for each case were solved using the finite element method to discretize the space derivatives and the finite difference method was used to discretize the time derivative. The resulting set of nonlinear algebraic equations were solved by the Gaussian elimination procedure with an under-relaxation iterative procedure.

The numerical solution procedure was used in a sensitivity analysis to examine the relationship of percolation(for the one-dimensional problem) and subsurface return flow(for the two-dimensional problem) to the volume of moisture stored in the soil profile. The simulation results were presented in nondimensional form so as to lend their applicability to a wide range of conditions.

The relationship between percolation out of a one meter soil profile and the moisture stored in the one meter depth was found to form a hysteretic loop as expected. The relationship during a wetting cycle was found to lie below the relationship during a drying cycle. It was found that the relationship depended upon soil texture and upon the rate of application of water at the soil surface during the wetting cycle. It was also influenced somewhat by layering of the soil. However, it was influenced little by soil evaportation, evapotranspiration, and the depth to the water table.

The relationship between subsurface return flow and the moisture stored in the soil profile was also found to form a hysteretic loop. The position of the wetting cycle relationship relative to the drying cycle relationship depended on the hillslope conditions. The parameters that were found to have a significant influence on the relationship were the soil textural class, the slope angle, the length of the slope relative to the soil depth, and the intensity of water application. Soil layering was found to be relatively insignificant except for a case where the layering was most severe.

Most comprehensive hydrologic models use fairly simplified representations of the complicated hydrologic processes since it is impossible to acquire the needed information for complicated mathematical formulations when working on a catchment or basin scale of analysis. Generally the information available for calibration of hydrologic models is the input rainfall, the runoff volume, the discharge hydrograph., and some soils and landuse data. Hydrologic

models applied to these conditions will generally have poor resolution(that is they will possess a high degree of parameter lumping) so simple model components will perform just as well as complicated mathematical formulations.

Two important components of the hydrologic cycle are deep percolation and subsurface return flow(interflow). Improvements in the physical representativeness of these components in hydrologic models while maintaining simplicity would be valuable. The results derived in this study indicate that it is possible to characterize these two components in a format appropriate for use in comprehensive hydrologic models. The range of tests that were run to examine the sensitivity of the relationships for the percolation problem and the subsurface return flow problem provide a basis for confidence in the utility of the generated information in modeling these hydrologic processes.

Chapter 6

REFERENCES

1. Becker, E. B., G. F. Carey, and J. T. Oden, 1981. Finite Elements, An Introduction, Prentice-Hall.

2. Beven, K. 1977. Hillslope hydrographs by the finite element method, Earth Surface Processes, 2, 13-28

3. Beven, K.J. and M.J. Kirkby, 1979. A simple, physically based, variable contributing area model of basin hydrology, Hydrologic Sciences Bulletin, 24(1),43-69.

4. Black, T. A., W. R. Gardner, and G. W. Thurtell, 1969. The prediction of evaporation, drainage, and soil water storage for a bare soil, Soil sScience Socity of America Proc., 33(5), 655-660.

5. Brutsaert, W. H., 1982. Evaporation into the Atmosphere; Theory, History, and Applications, D. Reidel Publishing Company, Boston, 299 pp.

6. Colbeck, S. C. 1978. The physical aspects of water flow through snow, IN: V. T. Chow(ed.), Advances in Hydroscience, No. 11, 165-206, Academic Press.

7. Freeze, R. A.,1969. The mechanism of natural groundwater recharge and discharge, 1, One-dimensional, vertical, unsteady, unsaturated flow above a recharging or discharging ground-water flow system, Water Resources Research, 5(1), 153-171.

8. Freeze, R. A.,1972. Role of subsurface flow in generating surface runoff, 2. Upstream source areas, Water Resources Research, 8(5), 1272-1283.

9. Freeze, R. A., 1972. Role of subsurface flow in generating surface runoff, 2. Base flow contributions to channel flow, Water Resources Research, 8(3), 609-623.

10. Gupta, V. K., 1973. A stochastic approach to space-time modekling of rainfall, Tech. Rep. Natur. Resour. Syst., 18, Univ. of Ariz., Tucson

11. Huggett, R. J. , 1975. Soil landscape systems: A model of soil genesis, Geoderma, 13, 1-22.

12. Liggett, J. A. and J. A. Cunge, 1975. Numerical Methods of Solution of the Unsteady Flow Equations, IN: K. Mahmood and V. Yevjevich(eds.), Unsteady Flow in Open Channels, Water Resources Publications, Vol. I, pp. 89-182.

13. Neuman, S. P., 1973. Saturated-unsaturated seepage by finite elements, Journal of the Hydraulics Division, ASCE, 99(HY12), 2233-2250.

14. Nieber, J. L., 1982. Runoff characteristics of uniformly sloped shallow soils, IN: V. P. Singh(ed.), Rainfall-Runoff Relationships, Water Resources Publications, Littleton, Colo., 261-276.

15. Philip, J. R., 1969. Theory of infiltration, IN: V. T. Chow(ed.), Advances in Hydroscience, No. 5, 215-296, Academic Press.

16. Segerlind, L. J. ,1976. Applied Finite Element Analysis, John Wiley and Sons, 422 pp.

17. Sorooshian, S., 1983. Surface water hydrology: On-line estimation, IN: Contributions in Hydrology, U.S. National Report 1979-1982, Proceedings of the Eighteenth General Assembly, International Union of Geodesy and Geophysics, Hamburg, Federal Republic of Germany, August 15-27, 1983.

18. Verma, R. D. and W. Brutsaert, 1971. Similitude criteria for flow from unconfined aquifers, Journal of the Hydraulics Division, ASCE, 97(HY9), 1493-1509.

19. Woolhiser, D. A. and J. A. Liggett, 1967. Unsteady, one-dimensional flow over a plane - The rising hydrograph, Water Resources Research, 3(3), 753-771.

Chapter 7

APPENDIX

Derivation of Finite Element Equations for the One-Dimensional and Two-Dimensional Richards Equation

7.1 ONE-DIMENSIONAL RICHARDS EQUATION

The one-dimensional Richards equation is,

$$L\{\phi\} = C\ \partial\phi/\partial z - \partial/\partial z\ (K\ \partial\phi/\partial z) = 0 \qquad 0 \leq z \leq 1$$

We seek a solution $\phi(z,t) \cong \Phi(z,t)$ such that

$$L\{\Phi\} = \epsilon(z) = \text{residual} \neq 0$$

To make $\epsilon(z)$ vanish in an average sense we use the Galerkin procedure of the method of weighted residuals (Segerlind, 1976). The procedure is stated as

$$G_i = \int_0^1 N_i\ \epsilon(z)\ dz = 0 \qquad i = 1,2,\ldots,M$$

where N_i is the weight function and M is the number of node points. For convenience the integration is performed on discrete element (subdomain) basis, that is,

$$G_i^e = \int_0^{Le} N_i\ \epsilon(z)dz \qquad i=1,2,\ldots,r$$

where r is the number of nodes in element e and Le is the length of element e. It is assumed that

$$G_i = \Sigma_e \, G_i^e = 0 \qquad i = 1,2,\ldots,M$$

Substituting for $\epsilon(z)$ we have

$$G^e_i = \int_0^{Le} N_i \, (C \, \partial\Phi/\partial t - \partial/\partial z \, (K \, \partial\Phi/\partial z)) \, dz$$

The approximation Φ is expressed by the interpolation polynomial

$$\Phi = N_1\Phi_1 + N_2 \, \Phi_2 + \ldots N_r\Phi_r = \underline{N} \, \underline{\Phi}$$

where N_1, N_2, ... , N_r is a set of linearly independent basis functions, and Φ_1, Φ_2, ... , Φ_r is the set of values of Φ at the node points of element e.

For the problem examined here r was chosen to be 2 and so the basis functions are

$$N_1 = 1-z/Le$$

$$N_2 = z/Le$$

The basis functions chosen have C° continuity at element boundaries so the second order derivative appearing in the integral needs to be reduced to first order or else the integral will be undefined. This is desirable for symmetry as well(Becker et al., 1981). This is accomplished through integration by parts, that is,

$$\int_0^{Le} N_i \, \partial/\partial z \, (K \, \partial\Phi/\partial z) \, dz = N_i \, K \, \partial\Phi/\partial z \, I_0^{Le} - \int_0^{Le} K \, \partial N_i/\partial z \, \partial\Phi/\partial z \, dz$$

The result is

$$G^e_i = \int_0^{Le} (N_i \, C \, \partial\Phi/\partial t + K \, \partial N_i/\partial z \, \partial\Phi/\partial z) \, dz - N_i \, K \, \partial\Phi/\partial z \, I_0^{Le}$$

Substituting for Φ in the second term in the integral yields

$$\int_0^{Le} K \, \partial N_i/\partial z \, \partial \underline{N}/\partial z \, \underline{\Phi} \, dz$$

which in matrix form is

$$B^e \, \underline{\Phi} = \begin{vmatrix} \int_0^{Le} (K \, \partial N_1/\partial z \, \partial N_1/\partial z)dz & \int_0^{Le} (K \, \partial N_1/\partial z \, \partial N_2/\partial z)dz \\ \int_0^{Le} (K \, \partial N_2/\partial z \, \partial N_1/\partial z)dz & \int_0^{Le} (K \, \partial N_2/\partial z \, \partial N_2/\partial z)dz \end{vmatrix} \begin{vmatrix} \Phi_1 \\ \Phi_2 \end{vmatrix}$$

The third term in the expression for G_i^e is just the flux rate at the end points of the element and yields for i=1;

$$- N_1 \, K \, \partial\Phi/\partial z \, I_0^{Le} = - (0) \, K \, \partial\Phi/\partial z \, I_{Le} + (1) \, K \, \partial\Phi/\partial z \, I_0 = q^e \, I_0$$

since $K \, \partial\Phi/\partial z = q^e$ at z=0, on element e, and for i=2;

$$- N_2 \, K \, \partial\Phi/\partial z \, I_0^{Le} = - (1) \, K \, \partial\Phi/\partial z \, I_{Le} \; (0) \, K \, \partial\Phi/\partial z \, I_0 = q^e \, I_{Le}$$

since $K \, \partial\Phi/\partial z = -q^e$ at z=Le on element e.

Instead of directly replacing Φ by $\underline{N} \, \underline{\Phi}$ in the time derivative term it is best (Neuman, 1973) for stable results to use,

$$\int_0^{Le} CN_i \, \partial\Phi/\partial t \, dz = \partial\Phi_i/\partial t \int_0^{Le} CN_i \, dz$$

So for the capacitance matrix we get

$$A^e\ \partial\underline{\Phi}/\partial t = \begin{vmatrix} \int_0^{Le} CN_1\, dz & 0 \\ 0 & \int_0^{Le} CN_2\, dz \end{vmatrix} \begin{vmatrix} \partial\Phi_1/\partial t \\ \partial\Phi_2/\partial t \end{vmatrix}$$

Now we have

$$\underline{G}^e = A^e\ \partial\underline{\Phi}/\partial t + B^e\ \underline{\Phi} + \underline{q}$$

Combining contributions from each element e according to the assumption $G_i = \Sigma_e\ G_i^e$ we obtain

$$\underline{G} = A\ \partial\underline{\Phi}/\partial t + B\underline{\Phi} + \underline{Q} = 0 \qquad (A.1)$$

where A is the global capacitance matrix, B is the global conductance matrix and $\underline{Q}$ is the net flux vector. In the vector $\underline{Q}$ all of the terms will in general be zero except for the two at the end points of the global domain (z=0, z=D). The reason is that for node points on the interior the contribution $q_i^e\ I_0$ from element e will cancel with the contribution $q_i^{e-1}\ I_{Le}$ from element (e-1) since they are equal in magnitude but opposite in sign. If however one wishes to incorporate sources or sinks in the computations it is easy to do this by just setting the value of Q_i for node i equal in magnitude to the source or sink and assign the appropriate sign.

Due to the strong dependence of the coefficients C and K on the variable $h(=\phi-z)$ the integrals in A and B are evaluated numerically

rather than analytically. This approach provides for better satisfaction of mass conservation. The typical matrix terms are

$$A_{ii} = \int_0^{Le} CN_i dz = \Sigma_e \, Le \, \Sigma_{s=1}^{b} \, N_i^s \, C_s \, W_s$$

and

$$B_{ij} = \int_0^{Le} K \, \partial N_i/\partial z \, \partial N_j/\partial z \, dz = (-1)^{i+j} \, \Sigma_e \, 1/Le \, \Sigma_{s=1}^{p} \, K_s \, W_s$$

where; N_i^s = value of basis function N_i at Gauss sample point s,

K_s, C_s = values of K and C at Gauss sample point s,

W_s = integration weight associated with Gauss sample point s, and

p = number of Gauss sample points used.

The set of nonlinear ordinary differential equations expressed by equations (A.1) are solved using finite difference discretization for the time domain. A backward difference implicit scheme is used, that is

$$\partial \underline{\Phi}/\partial t \cong (\underline{\Phi}^k - \underline{\Phi}^{k-1}) \, /\Delta t$$

and the result is

$$(A + \theta \Delta t \, B)\underline{\Phi}^k = (A + (\theta-1) \, \Delta t \, B)\underline{\Phi}^k - \Delta t \, \underline{Q}$$

or

$$D \, \underline{\Phi}^k = E \, \underline{\Phi}^{k-1} - \Delta t \, \underline{Q}$$

where θ is a weight chosen between 0 and 1. When θ=0 the scheme is explicit; when θ=1, the scheme is fully implicit; when θ=1/2 the scheme is equivalent to Crank-Nicholson.

7.2 TWO-DIMENSIONAL RICHARDS EQUATION

The two-dimensional Richards equation is given by

$$L\{\phi\} = C\ \partial\phi/\partial t - \nabla \cdot (K\nabla\phi) = 0$$

with boundary conditions,

$$\phi(x,z) = \Omega(x,z)$$

and/or,

$$K\ \partial\phi/\partial n = -q$$

We seek an approximate solution $\phi(x,y) \cong \Phi(x,y)$ and

$$L\{\Phi\} = \epsilon(x,y) = \text{residual} \neq 0.$$

To force the residual $\epsilon(x,y)$ to zero in an average sense over the solution domain we apply the Galerkin procedure of the method of weighted residuals.

$$G_i = \int_V N_i\ \epsilon(x,y)dV = 0 \qquad i = 1, 2, \ldots, M$$

where M is the number of node points and N_i is the weighting function. The integration is performed on a discrete element (subdomain) basis, that is

$$G_i^e = \int_V e\ N_i\ [C\ \partial\Phi/\partial t - \nabla \cdot (K\nabla\Phi)]\ dV^e \qquad i = 1, 2, \ldots, r$$

where r is the number of node points in the element. The second derivative appearing in the integral cannot be handled by the basis functions N_i since they have C° continuity. Thus the second derivative

should be reduced to first order. This reduction is also desirable from the point of view of promoting symmetry (Becker et al., 1981).

The second derivative is reduced using the Gauss divergence theorem by the following steps.

$$N_i \nabla \cdot (K\nabla\Phi) = \nabla \cdot (N_i K\nabla\Phi) - K \nabla N_i \cdot \nabla\Phi$$

Thus,

$$G_i^e = \int_V e (N_i C \partial\Phi/\partial t - \nabla \cdot (N_i K\nabla\Phi) + K\nabla N_i \cdot \nabla\Phi) dV^e$$

By the divergence theorem of Gauss

$$\int_V \nabla \cdot \sigma dV = \int_S \sigma \cdot n dS$$

and choosing $\sigma = N_i K\nabla\Phi$ we get

$$G_i^e = \int_V e (N_i C \partial\Phi/\partial t + K \nabla N_i \cdot \nabla\Phi) dV^e - \int_S e (N_i K\nabla\Phi) \cdot n dS^e \quad (A.2)$$

The function Φ is given by $\underline{N}\ \underline{\Phi} = N_1\Phi_1\ N_2\Phi_2 + \ldots + N_r\Phi_r$, where the Φ_j's are the values of Φ at the node points of element e and the N_j's are the basis functions associated with element e. The second term in the volume integral becomes,

$$\int_V e\ K\nabla N_i \cdot \nabla\Phi\ dV^e = \int_V e (K\nabla N_i \cdot \nabla N)\ \underline{\Phi} dV^e =$$

$$\int_V e\ K (\partial N_i/\partial x\ \partial N_j/\partial x + \partial N_i/\partial y\ \partial N_j/\partial y)\ \phi_j\ dV^e$$

for $i = 1, 2, \ldots, r$; $j = 1, 2, \ldots, r$.

This yields an r x r matrix with the common terms shown. Three node (r=3) linear triangles are used in this study so the matrix will be 3 x 3. The basis function N_i for a linear triangle has the form

$$N_i = a_i + b_i x + c_i y \qquad i = 1, 2, 3$$

where; $a_i = x_{i+1}y_{i+2} - x_{i+2}y_{i+1}$

$b_i = y_{i+1} - y_{i+2}$

$c_i = x_{i+2} - x_{i+1}$

and i varies cyclicly.

The time derivative term is handled using

$$\partial\Phi_i/\partial t = \int_V e\ CN_i\ \partial\Phi/\partial t\ dV^e \ /\ \int_V e\ CN_i\ dV^e$$

since this promotes stable solutions (Neuman, 1973).

The surface integral term is simply the integration along the element boundary of the flux normal to the boundary. The result is that

$$\int_S e\ (N_i\ K\nabla\Phi)\ \cdot n\ dS^e = (q_{i1}\ L_{i1} + q_{i2}\ L_{i2})/2 = Q_i^e$$

where q_{i1}, q_{i2} are the flux rates along two element boundaries connected to node i in element e and L_{i1} and L_{i2} are the lengths of the two element boundaries connected to node i in element e. The result is

$$G_i^e = \Sigma_j A_{ij}^e\ \partial\Phi_j/\partial t + \Sigma_j B_{ij}^e \Phi_j - Q_j^e \qquad i = 1, 2, 3$$

where; $A_{ij}^e = \int_{Ve} CN_i dV^e \qquad i = j$

$$A_{ij}^e = 0 \qquad i \neq j$$

$$B_{ij}^e = \int_V e\ K(\partial N_i/\partial x\ \partial N_j/\partial x + \partial N_i/\partial y\ \partial N_j/\partial y)\ dV^e$$

Performing the matrix operation $G_i = \Sigma_e\ G_i^e = 0$ yields

$$G_i = \Sigma_j A_{ij}\ \partial\Phi_j/\partial t\ \Sigma_j B\Phi_j - Q_j \quad i=1,2,\ldots,M \qquad (A.3)$$

where; $A_{ij} = \Sigma_e \, a_e \, \Sigma_{s=1}^{p} \, C_s \, N_i^s W_s \quad i=j$

$A_{ij} = 0 \qquad i \neq j$

$B_{ij} = \Sigma_e \, ((b_i b_j - c_i c_j))/4a_e \, \Sigma_{s=1}^{p} \, K_s W_s$

$Q_i = \Sigma_e \, (q_{i1} \, L_{i1} + q_{i1} \, L_{i1})/2$

C_s, K_s, N_i^s = values of the coefficients C and K, and basis function N_i at Gauss sample point s,

W_s = weight associated with Gauss sample point s,

a_e = area of element e,

q_{i1}, q_{i2}, L_{i1}, L_{i2} = as defined previously,

$b_n = y_n - y_{n+1}$ n takes on the values 1, 2, 3 cyclicly

$c_n = x_{n+1} - x_n$ cyclicly

x_n, y_n = x and y coordinate locations of the node point n.

Numerical evaluation of the integrals is used instead of analytical integration because it provides for more complete mass conservation for this problem where the coefficients C and K are strongly depemndent on the pressure h.

Equations (A.3) is a nonlinear set of ordinary differential equations. A set of nonlinear algebraic equations is derived by approximating the time derivative with finite differences. A backward difference scheme is used, i.e.

$$\partial \underline{\Phi}/\partial t \cong (\underline{\Phi}^{k} - \underline{\Phi}^{k-1}) \; /\Delta t$$

Substituting and using the time weighting factor θ ($0 \leq \theta \leq 1$) we get

$$(A + \theta \, \Delta t \, B) \, \underline{\Phi}^{k} = (A \, (\theta - 1) \, \Delta t \, B) \, \underline{\Phi}^{k-1} + \Delta t \, \underline{Q}$$

When $\theta = 0$ the scheme is explicit; when $\theta = 1$ the scheme is fully implicit; and when $\theta = 1/2$ the Crank-Nicholson scheme results.